（千葉大学審査学位論文）

Application of stomatal analysis of fossil leaves in the Cenozoic paleoenvironment reconstruction

化石葉の気孔分析の新生代古環境復元への適用

July 2020

WANG Yuqing
王　雨晴

Graduate School of Horticulture
CHIBA UNIVERSITY

Content

List of Figures

List of Tables

List of Equations

Abstract

The atmospheric levels of CO_2, a greenhouse gas, are closely related to global change, and investigation of historical CO_2 levels can help to achieve a better understanding of the global climate change in the deep past. The present global warming is ascribed to increasing levels of atmospheric CO_2 caused by human activity since the industrial revolution. Therefore, knowledge of the role of atmospheric CO_2 in climate changes during the Cenozoic, when climate shifted from icehouse to greenhouse condition, will help to understand our future climate. To date, various methods and proxies have been proposed in paleo-CO_2 reconstruction. Among them, the stomatal parameters I used here, including stomatal index and stomatal density of fossil leaves, are considered as reliable terrestrial proxies to estimate paleo-CO_2 concentration, which have been supported by physiological and functional studies.

At first, I reconstructed the Paleogene atmospheric CO_2 concentrations based on the stomatal index of fossil *Metasequoia* needles. During the Paleogene, the Earth experienced a global greenhouse climate, which was much warmer and more humid than the present. However, unlike for the late Cenozoic, atmospheric CO_2 reconstructions for the Paleogene are still inconsistent. Thus, I reconstructed the levels of atmospheric CO_2 in the early Paleocene, the middle Paleocene and the middle Eocene based on the stomatal index of fossil *Metasequoia* needles collected from four fossil sites in Canada and Japan. I found the atmospheric CO_2 levels during the early and middle Paleocene to be similar to that of the present, and up to twice the present atmospheric CO_2 level was found during the middle Eocene. Our estimated atmospheric CO_2 level supports the hypotheses that the climate changes during the Paleogene cannot be explained merely by atmospheric CO_2 variations, which suggests that atmospheric CO_2 might not have always played a critical role in climate change during these ancient epochs and therefore cannot be a direct analogy for the current global warming.

Unlike the early Cenozoic, the correlation between CO_2 and temperature during the

late Cenozoic has been demonstrated based on different studies. However, limited evidence has been provided by simultaneous investigation of both paleo-temperature and palaeo-CO_2 using the same fossil assemblage. Here, based on the stomatal analyses of *Quercus gilva* from a leaf bed in the Pleistocene Sayama Formation in central Japan, I estimated the palaeo-CO_2 values in an interglacial stage (MIS 57 or 55) at 359±25 ppmv, which is generally higher than the previously reported data from middle early Pleistocene. To understand the climate under this high CO_2 level, I also calculated the mean annual temperature based on the same leaf assemblage using the leaf margin analysis approach. The calculated mean annual temperature was 11.0 °C, suggesting a relatively warm climate during the interglacial stage. Our results revealed a warm environment under high CO_2 level during the early Pleistocene, which demonstrates the vital role of CO_2 in controlling the Early Pleistocene interglacial temperature.

Stomatal analysis of fossil leaves also can be used in estimating the altitudinal transportation range of fossil leaves before their burial, but this kind of study has not been practiced before. The altitudinal range can be clarified by the range of stomatal frequency constituting of a fossil leaf assemblage in that leaf from the highest altitude exhibits the highest stomatal frequency under the lowest atmospheric CO_2 pressure. I detected leaf transport based on stomatal parameter variation of 30 fossilized *Fagus crenata* leaves from the Sayama Formation. Considering the stomatal index variation of fossil *Fagus crenata* leaves, the paleo-CO_2 variation in a warm period of the Pleistocene was estimated as ca. 345-390 ppmv. Based on this paleo-CO_2 variation, the altitudinal transportation range of the Early Pleistocene fossil *Fagus crenata* leaves was estimated at over 1000 m. I presume that leaves of *Fagus crenata* in the fossil assemblage possibly had come from a wide range of altitudes near the fossil site during the Early Pleistocene. This provides an example of altitudinal transportation of plants before their deposition, which suggests a consideration when reconstructing the palaeovegetation and palaeoclimate from fossil assemblages.

Meanwhile, differences of the stomatal parameter variation range among the fossil assemblages from different horizons at a fossil locality indicate the temporal changes of

altitudinal distribution limit of the species. Thus, I proposed a new method to detect changes of altitudinal distribution limit of a plant species based on the stomatal analysis of fossilized leaves. I used the Holocene fossil leaves of *Fagus crenata*, a dominant deciduous tree in the cool temperate zone, from different horizons in a peat bog in Mt. Kurikoma, North Japan. Results of paleo-CO_2 concentration reconstructed from the stomatal analysis indicated paleo-CO_2 of the fossil locality was more variable and higher than the ice core records. This result is possibly influenced by the oceanic CO_2 uptake that increased with the strengthening of Tsushima warm current during the Middle Holocene. The stomatal index variation range of fossil *Fagus crenata* leaves in the Middle Holocene was higher than that of the modern population at a given altitude, indicating transportation of leaves from an altitude higher than the site of fossil deposition. A decreasing trend of the stomatal index variation range between ca. 5000 and ca. 2500 cal BP can possibly be attributed to the downward shift of distribution limit of *Fagus crenata* from an altitude higher than or similar to the present limit to area surrounding the fossil deposition site with climatic deterioration, which is correlated with decreasing East Asian Summer Monsoon intensity and a cooling event around 4000 cal BP.

Keywords

Cenozoic, global warming, leaf margin analysis, paleo-altitude, paleo-CO_2, palaeo-temperature, stomatal analysis, taphonomy

1 Background

1.1 Major methods of paleo-CO_2 reconstruction

Atmospheric carbon dioxide (CO_2), as a primary greenhouse gas in the atmosphere, is considered responsible for the current global warming (Houghton et al., 2001; Royer et al., 2004; Fletcher et al., 2008; Stocker et al., 2013). However, atmospheric CO_2 concentration is predicted to increase continuously after reaching levels of 400 ppmv (parts per million by volume) in 2013 (Meinshausen et al., 2011; Masson-Delmotte et al., 2013). To estimate the impact of different CO_2 concentrations on global environmental systems and achieve solutions for the present global climate change, a better understanding of the correlations between the paleo-atmospheric CO_2 concentration (paleo-CO_2) and the ancient climate becomes crucial.

Three major approaches have been used to obtain the paleo-CO_2 values: composition measurements of air trapped in ice cores (Monnin et al., 2001), geochemical modeling (Berner 1994 and 2006; Berner and Kothavala, 2001) and various proxies recorded in the sediments (reviewed in Beerling et al., 2011). Ice core analysis, considered as the most reliable method, can measure paleo-CO_2 directly but is only applicable to the ages after 0.8 Ma in that the heat from underground bedrock can melt the deepest and oldest ice (Monnin et al., 2001). Geochemical modeling using chemical thermodynamics or/and chemical kinetics to analyze the chemical reactions that affect geologic system can reconstruct paleo-CO_2 for long geological time scales, but it is difficult to improve the precision of CO_2 reconstruction at time scales less than 5 Ma and to distinguish from warming caused by other greenhouse gases such as methane (Berner, 1994; Berner and Kothavala, 2001; Berner, 2006). Several CO_2 proxies were involved to estimate paleo-CO_2, and they are classified into marine and terrestrial proxies. Marine proxies are represented by carbon isotopes from phytoplankton (Freeman and Hayes, 1992; Stott, 1992; Pagani, 1999; Pagani et al., 1999; Pagani et al., 2005) and boron isotopes from

marine calcium carbonate (Pearson and Palmer, 2000; Pearson et al., 2009), which have provided high resolution CO_2 data over a continuous time range, although most of these CO_2 data are concentrated in the late Cenozoic. Terrestrial proxies include carbon isotopes of paleosols, the texture of nahcolite (Lowenstein and Demicco, 2006), carbon isotopes from liverwort fossils (Fletcher et al., 2008), and stomata on the fossil leaves of vascular plants (Kürschner et al., 2001; Smith et al., 2010; Doria et al., 2011; Maxbauer et al., 2014; Wang et al., 2015; Wang et al., 2018a; Wang et al., 2018b), which have been widely used for CO_2 estimation over the entire Cenozoic. However, these CO_2 results exhibit inconsistencies of a large magnitude for the same geological times (Beerling and Royer, 2011), which means that the crosschecking of CO_2 data using different proxies is necessary to reduce the associated uncertainties.

1.2 **Stomatal analysis of fossil leaves**

Stomatal-based atmospheric paleo-CO_2 reconstruction depends on the correlation between the stomatal frequency of terrestrial vascular plant leaves and atmospheric CO_2 level. This method was proposed by Woodward (1987), who found a negative correlation between the stomatal frequency of leaves and atmospheric CO_2 concentration for the first time. He studied herbarium specimens of eight temperate species collected in the past 200 years, and found a reduction of the stomatal density by an average of 40% due to an increase of 60 ppm in atmospheric CO_2 concentration caused by human activities. Then Woodward and Bazzaz (1988) reported that the stomatal frequency also responses to changes in atmospheric CO_2 partial pressure along altitude. The stomatal frequency includes stomatal density (SD) and stomatal index (SI) (Salisbury, 1928): SD refers to the number of stomata contained in unit area (mm^2), while SI is the proportion of stomata to the total number of epidermal cells. Generally, SI is considered as more accurate than SD, because it can compensate the effects of leaf expansion during growth, thus independent of environmental parameters such as temperature, atmospheric humidity and soil

moisture supply (Beerling, 1999).

However, not all plant species present a correlation between stomatal frequencies and atmospheric CO_2 level. C_3 and C4 plants have different responses to atmospheric CO_2 level due to different photosynthetic characteristics (Royer, 2001; Raven and Ramsden, 1988). C_3 plants absorb CO_2 and fix it in sponge tissue and palisade tissue, and the CO_2 concentration in the plant cells always maintains a ratio of about 70% of the atmospheric CO_2 concentration, so the CO_2 concentration in the plant cells will follow the external atmosphere CO_2 concentration changes (Beerling and Woodward, 1996; Ehleringer and Cerling, 1995; Polley et al., 1993). Therefore, the stomata of C_3 plants are very sensitive to changes in atmospheric CO_2 concentration. C_4 plants accumulate the absorbed CO_2 in the vascular sheath, and the endothelium surrounding the vascular sheath prevents CO_2 from penetrating outward, and can accumulate in the vascular sheath to 1000-2000 ppm (Lambers et al., 1998), so the atmospheric CO_2 concentration changes has little effect on C_4 plants, and their stomatal frequency are insensitive to atmospheric CO_2 concentration variation (Raven and Ramsden,1988).

The negative correlation between stomatal frequency and atmospheric CO_2 level was confirmed by using modern materials and applied it to paleo-CO_2 reconstruction from fossil leaves of various taxa which include *Ginkgo* (Retallack, 2001; Beerling and Royer, 2002; Royer, 2003; Retallack, 2009; Smith et al., 2010), *Metasequoia* (Royer et al., 2001b; Doria et al., 2011; Maxbauer et al., 2014; Wang et al., 2015), *Gordonia* (Kürschner et al., 2001), Lauraceae (McElwain, 1998) *Betula* (Wagner et al., 2002; Wagner et al., 1999) and *Salix* (Rundgren and Beerling, 1999). These researches demonstrated that relationship between stomatal frequency and atmospheric CO_2 level is highly species specific. However, plant fossils from the Paleogene might include extinct species and more or less different morphologically from modern taxa.Thus, relict plants such as *Ginkgo* and *Metasequoia*, which have not changed their morphology for a long term since the Mesozoic, have been considered as ideal materials to reconstruct long-term paleo-CO_2 history through the Cenozoic (Retallack, 2001, 2009; Beerling and Royer, 2002;

Royer, 2003; Smith et al., 2010; Royer et al., 2001b; Doria et al., 2011; Maxbauer et al., 2014; Wang et al., 2015). Fossil Ginkgo leaves were used for paleo-CO_2 reconstruction during the Paleogene but data from *Metasequoia* is limited in spite of its common occurrence from the Northern Hemisphere (Lepage, 2005). This study aims to compare the Paleogene *Metasequoia*-based CO_2 results with prior published investigations of stomatal and the other proxy-based data, especially Ginkgo-based ones, and discuss the relationship between CO_2 changes and temperature variation during this period to provide fundamental data for understanding our future climate change.

This species specificity indicates that the relationship between stomatal frequency and atmospheric CO_2 level need to be built based on each living species or nearest living relatives of fossils. Three kinds of method to obtain the relationships has been conducted: (1) use of herbarium specimens collected in different ages because the atmospheric CO_2 concentration has gradually increased from 280 ppm to 400 ppm in the past 150 years (McElwain, 1995); (2) use modern samples collected along the altitude gradient, because the CO_2 partial pressure decreases along atmospheric pressure decrease altitude; (3) use experimental data of plants that grow in climate chambers under different CO_2 level air conditions while other environmental factors are controlled. In this study, I used herbarium of different ages and modern samples collected along altitude to build the relationship between CO_2 level and stomatal frequency of *Fagus crenata* and *Quercus gilva* to apply it to paleo-CO_2 reconstruction.

As mentioned above, stomatal analysis of fossil leaves is assumed to be a reliable method for paleo-CO_2 reconstruction. However, paleoaltitude of the living environment of fossil leaves, which is a factor affecting its accuracy, is occasionally ignored. However, paleo-CO_2 reconstruction is conducted based on an assumption the mother tree of the fossil leaves lived in lowlands close to sea-level. An example is paleo-CO_2 data based on the stomatal frequency of *Quercus guyavifolia* (late Pliocene, south-western China) lower than data estimated from other species, which may due to the paleoaltitude of the habitat of the fossil leaves (Hu et al., 2015), where atmospheric CO_2 is lower. Since reconstructed

CO_2 level are usually considered as sea-level CO_2, when applying stomatal method, it is necessary to choose species that live in lowland. Thus, paleo-CO_2 reconstructed based on the most thermophilous taxon among the fossil assemblage components will be more reliable as these species are believed to inhabit only the lowermost altitude that close to sea-level.

In this study, I found that fossil leaves of *Fagus crenata* from same assemblage demonstrates a variation of stomatal frequency larger than that observed in its modern population at the same altitude. This means that leaves from high altitude under low CO_2 level with high stomatal frequency were transported to the fossil locality. Based on the variation of stomatal frequency, we can calculate the difference of CO_2 level. At a fixed temperature, the decrease in CO_2 level with altitude is predictable (McElwain 2004), thus altitude difference between transported leaves and not transported leaves can be estimated, which can be used as an indicator of paleoaltitude. Considering present available paleoaltitude proxies are limited to hydrogen and oxygen isotopes, air bubbles in basalts and temperature or enthalpy lapse rates with altitude using paleobotanical methods, this new application of stomatal analysis will help a lot in paleoenvironment reconstruction.

1.3 Structure and purpose of this study

This study is consisted by four sub-studies that related to stomatal analysis of fossil leaves, which can be divided into two parts: (1) reconstruction of paleo-CO_2 level of the Cenozoic and analysis its relationship with paleo-temperature; (2) calculation of the variation of stomatal parameters as an indicator of the altitudinal distribution area of a plant species.

In the first part, I used stomatal analysis of *Metasequoia* needles to reconstruct the CO_2 during the Paleocene and Eocene of the early and middle Paleogene. The Earth experienced a significantly warm and humid environment comparable to the present global warming during these periods. Since terrestrial records of CO_2 are still limited

during this period, our research will supply evidences to clarify the Paleogene CO_2 changes, and help reveal the relationship between atmospheric CO_2 and temperature. I also reconstructed paleo-CO_2 level of a interglacial stage in the Pleistocene when conspicuous glacial-interglacial climate changes repeated on a 41-ka cycle. This cycle has been assumed to be coupled with atmospheric CO_2 changes, as demonstrated by the Middle and Late Pleistocene ice core records from the Antarctic. However, limited evidence has been provided by relationships between paleo-CO_2 and paleo-temperature. For this purpose, simultaneous investigation of both paleo-temperature and palaeo-CO_2 by using fossil leaves from the same fossil assemblage is necessary. Thus, I used fossil leaves belonging to an early Pleistocene interglacial stage in the Sayama Formation, central Japan to verify that CO_2 played a critical role in adjusting the Pleistocene glacial-interglacial cycle.

While most of researches of paleo-CO_2 reconstruction have been conducted for materials from the lowland to reconstruct sea-level CO_2 , a potential of altimetry using stomatal parameter has been proposed (Kouwenberg et al., 2007; McElwain, 2004). However, no one has practiced this method into fossil materials. In the second part, I reconstructed the altitudinal transportation of *Fagus crenata* leaves before burial based on stomatal analysis of the fossil leaves in the Early Pleistocene of the Sayama Formation. The detected altitudinal transportation can reveal the distribution range of a plant species in ancient times, and can be a potential paleoaltitude indicator, which is possible to reveal tectonic development in the past.

For another Holocene fossil locality in Mt. Kurikoma, I calculated the stomatal parameter variation range of fossil *Fagus crenata* leaves from fossil assemblages between ca. 5000 and ca. 2500 cal BP as an indicator of the temporal changes of altitudinal distribution limit of the species. Although the distribution change of *Fagus crenata* forests has been investigated using pollen analysis (Kito and Takimoto, 1999; Tsukada, 1982), its altitudinal changes have been difficult to detect based on airborne pollen. Based on the stomatal analysis of these fossil leaves, I evaluated the variation trend of the altitudinal

distribution range of *Fagus crenata*, and discussed the climate factors that constrained the altitudinal distribution of *Fagus crenata* during the Middle to Late Holocene. Altitudinal distribution change of plants under climate change in ancient times can help predict the reaction of plants to climate change in the near future.

2 Basic application of stomatal analysis: reconstruction of sea-level paleo-CO_2 under different paleo-temperature

2.1 The Paleogene CO_2 level reconstructed based on fossil *Metasequoia* needles

2.1.1 Introduction

During the Paleocene and Eocene, grouped as the Paleogene, the Earth experienced a significantly warm and humid environment, and references for the comparison of greenhouse climates are available from the Paleogene (Bowen et al., 2004; Hansen et al., 2008; Beerling and Royer, 2011). The changes in CO_2 level during the Paleogene have been reconstructed via geochemical modeling (Berner, 1994; Berner and Kothavala, 2001; Berner, 2006) and via various proxies (Beerling and Royer, 2011). Plant taxa, such as *Ginkgo* (Retallack, 2001, 2009; Beerling and Royer, 2002; Royer, 2003; Smith et al., 2010), *Metasequoia* (Royer et al., 2001b; Doria et al., 2011; Maxbauer et al., 2014; Wang et al., 2015), *Gordonia* (Kürschner et al., 2001), and Lauraceae (McElwain, 1998) have been investigated to estimate paleo-CO_2 level during the Paleogene, but compared to the late part of the Cenozoic, stomatal-based CO_2 data are still limited for the Paleogene.

In this subsection, I conducted stomatal analysis of fossil *Metasequoia* needles collected from Japan and Canada to estimate CO_2 levels in the early and middle Paleocene and middle Eocene, during which the stomatal-based CO_2 data are still limited. *Metasequoia* Miki *ex* Hu *et* Cheng is a representative plant with evolutionary stasis since the middle Cretaceous. The fossil *Metasequoia* species are generally considered conspecific with the modern species *M. glyptostroboides*, based on morphological and biochemical analyses with its inferred physiology and ecology (LePage et al., 2005). The relationship between SI of modern *Metasequoia* leaves and CO_2 level has been summarized using associated data under experimentally controlled conditions (Royer et

al., 2001b), and the results have been applied to paleo-CO_2 estimation for different ages (Royer et al., 2001b; Doria et al., 2011; Maxbauer et al., 2014; Wang et al., 2015). The extensive and frequent occurrence of *Metasequoia* fossils in time and space (LePage et al., 2005) enables the production of a detailed CO_2 curve comparable with temperature curve throughout the Paleogene without the noise derived from using different kinds of proxies. However, the Paleogene CO_2 reconstruction based on *Metasequoia* needles (Doria et al., 2011; Maxbauer et al., 2014) is still limited compared with *Ginkgo* leaves. To certify the availability of *Metasequoia* fossils for the Paleogene CO_2 reconstruction, I compared the results with prior published investigations of stomatal and the other proxy-based data, and discuss the relationship between CO_2 changes and temperature variation during the period to provide fundamental data for understanding our future climate change.

2.1.2 Materials and methods

2.1.2.1 Fossil locality and geological settings

The well-preserved fossil *Metasequoia* needles used in this study were collected from localities including early Paleocene and middle Eocene strata in northern Japan and the middle Paleocene and middle Eocene strata in arctic Canada (Figure 2.1-1Fig. 2.1-1). Associated ages, geological settings and other information concerning the collected fossil Metasequoia needles can be found in published reports (Tanai, 1979, 1990; Ricketts and Stephenson, 1994; Yang et al., 2005; Hasegawa et al., 2009; Maxbauer et al., 2014; Horiuchi and Uemura, 2017) and are summarized in Table 2.1-1. Voucher specimens are housed in the Xishuangbanna Tropical Botanical Garden, Chinese Academy of Sciences.

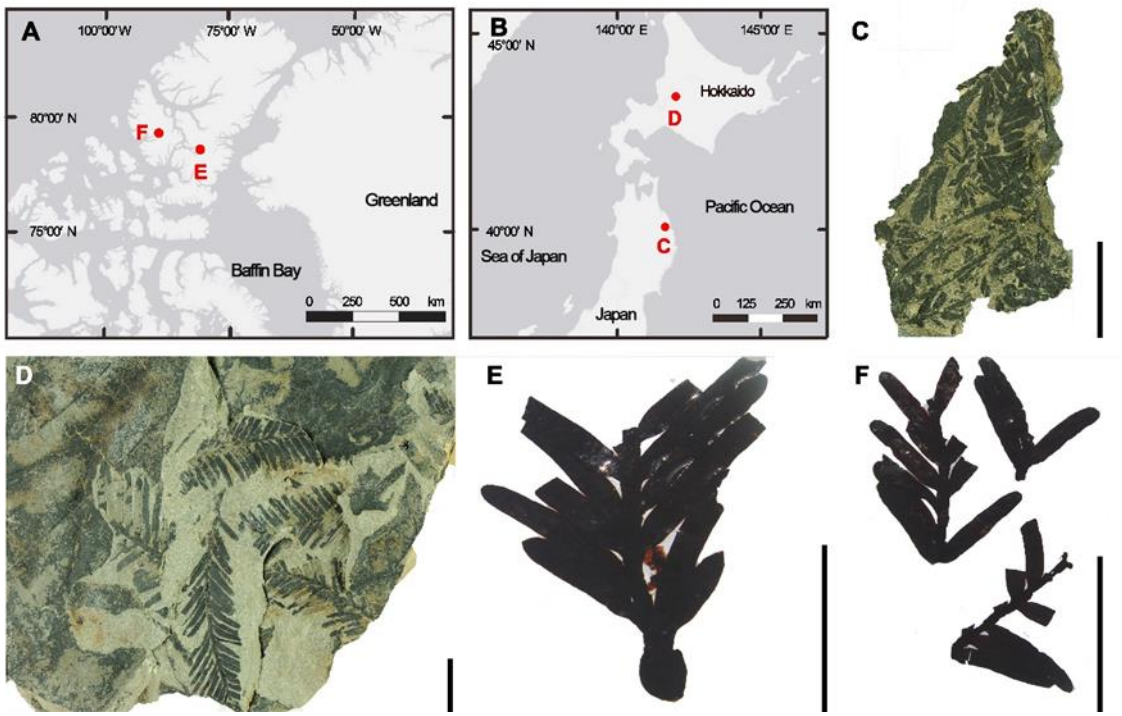

Figure 2.1-1 Geological settings (A and B) of fossil *Metasequoia* needles (C-F). C: Minato Formation, Kuji City, Japan (early Paleocene); D: Bibai Formation, Bibai City, Japan (middle Eocene); E: Iceberg Bay Formation, Ellesmere Island, Canada (middle Paleocene); F Buchanan Lake Formation, Axel Heiberg Island, Canada (middle Eocene). Bar = 1 cm.

Table 2.1-1 Information of *Metasequoia* samples used for reconstructing CO_2 level.

Fossil site	Geologic setting	Epoch (Age)	Dating method	Latitude	Longitude	Reference
Minato, Kuji city, Iwate Prefecture, Japan	Minato Formation, Noda Group,	early Paleocene (64.3–62.5 Ma)	Fission track dating	40°07'30"N	141°50'15"E	Horiuchi et al., 2017
Iceberg Bay, Stenkul Fiord, Ellesmere Island, Canadian Arctic Archipelago	Iceberg Bay Formation,	middle Paleocene（ca. 60 Ma）	Stratigraphic study	77°20′58″N	83°26'08"W	Ricketts and Stephenson, 1994; Yang et al., 2005
Buchanan Lake, Axel Heiberg Island, Canadian Arctic Archipelago	Upper Coal Member of the Buchanan Lake Formation,	middle Eocene (47.9–37.8 Ma)	Stratigraphic study	79°54′55.8″ N	89°01′26.8″ W	Maxbauer et al., 2014
Bibai, Bibai City, central Hokkaido,Japan	Bibai Formation, Ishikari Group,	middle Eocene (41–40 Ma)	Fission track dating	43°15' N	141°50' E	Tanai, 1979, 1990; Hasegawa et al., 2009

2.1.2.2 Cuticle preparation

The fossil needles were treated with 10%–25% hydrochloric acid (HCl) for 2 hours, 40% hydrofluoric acid (HF) for 12 hours, and 10%–25% HCl for at least 1 hour to remove the adhering sediments. After the materials were rinsed with distilled water, the middle third of the needles was cut for cuticle preparation. The needle fragments were macerated with a 3%–5% sodium hypochlorite (NaClO) solution to remove any remnants of leaf tissue other than the cuticular membrane based on the nature of the leaves. After rinsing with distilled water, the cuticular membranes were stained with 1% safranin O and mounted in glycerol for observation and photographing under the transmitted light microscope (Zeiss Axio Imager A2 with Zeiss AxioCam MRc camera), or directly mounted on aluminum stubs for SEM imagery (Zeiss EVO LS10).

2.1.2.3 Stomatal index and the calculation of paleo-CO_2

Image J (1.43μ, Wayne Rasband, http://rsb.info.nih.gov/ij/) was used to count the number of stomatal complexes (stomatal pore with bounding guard cells) and epidermal cells from photos of cuticular membranes taken with light or electron microscopes (Figure 2.1-2). The field-of-view for stomatal analysis is over 0.03 mm^2 for all images. SI was calculated using Equation 2.1-1 (Salisbury, 1928).

$$\mathrm{SI} = \frac{\text{stomatal number}}{\text{epidermal cell number} + \text{stomatal number}}$$

Equation 2.1-1

The nonlinear inverse relationship between the SI of *Metasequoia* and CO_2 levels (Equation 2.1-2)was taken from Royer et al. (2001b).

$$[CO_2]\mathrm{atm} = \frac{\mathrm{SI} - 6.672}{0.003883 \times \mathrm{SI} - 0.02897}$$

Equation 2.1-2

2.1.3 Results

The SI and calculated CO_2 from the prepared cuticular membranes are listed in Table 2.1-2. Our data show that CO_2 was 308±23 ppmv at ca. 63.4 Ma in the early Paleocene, and 370±27 ppmv at ca. 60 Ma in the middle Paleocene. In the middle Eocene, CO_2 increased to over 473±121 ppmv at 47.9–37.8 Ma, based on materials from the Iceberg Bay Formation. The materials from the Bibai Formation (middle Eocene) show the lowest SI among all *Metasequoia* fossils used in this research, indicating a high CO_2 of 706±321 ppmv at 41–40 Ma.

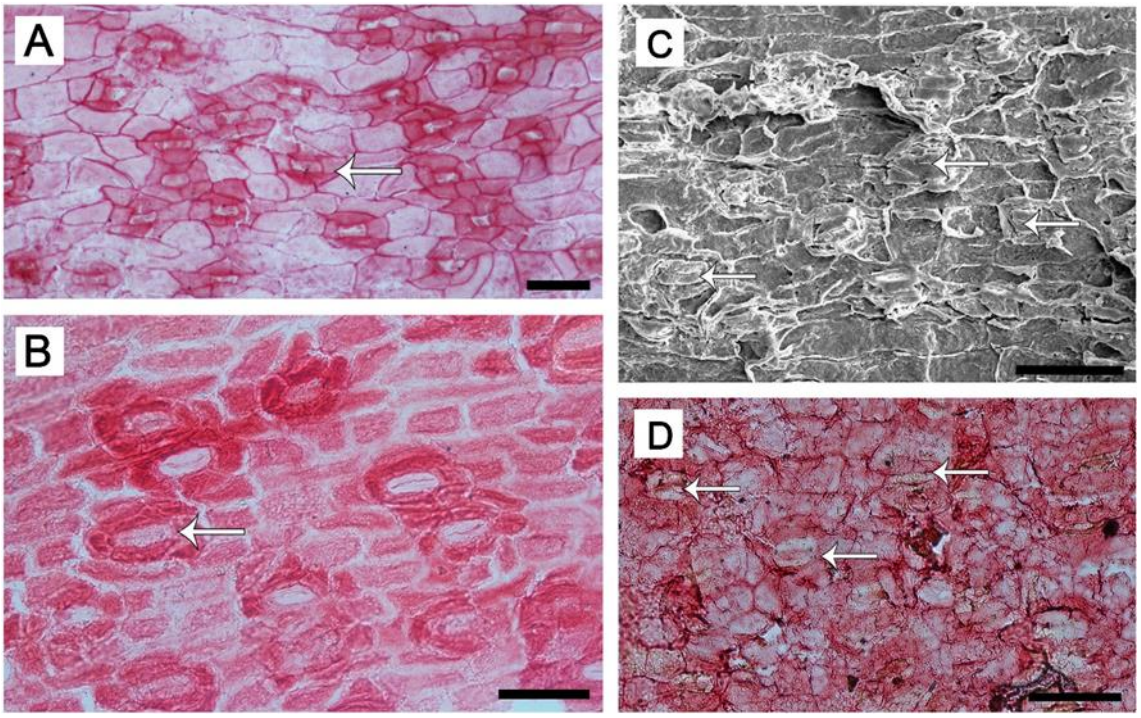

Figure 2.1-2 Microphotographs of lower cuticles of *Metasequoia* needles from A: Iceberg Bay Formation, Ellesmere Island, Canada (middle Paleocene), B: Minato Formation, Kuji City, Japan (early Paleocene), C: Buchanan Lake Formation, Axel Heiberg Island, Canada (middle Eocene), and D: Bibai Formation, Bibai City, Japan (middle Eocene). The white arrows indicate stomata. (C) was obtained by SEM while all the others were obtained by light microscopy. Bar = 50 μm.

Table 2.1-2 SI of fossil *Metasequoia* needles and the corresponding CO_2 estimates.

Fossil site	Epoch	Age (Ma)	Number of fossil needles (no.)	SI (%)	CO_2 (ppmv)
Minato	late Paleocene	64.3–62.5	10	12.08±1.60	308±23
Ellesmere Island	middle Paleocene	ca. 60	9	9.35±0.41	370±27
Axel Heiberg Island	middle Eocene	47.9–37.8	12	8.87±1.06	473±121
Bibai	middle Eocene	41–40	9	8.21±0.63	706±321

2.1.4 Discussion

2.1.4.1 CO_2 level during the Paleocene

Only *Ginkgo* leaves have been used as yet for stomatal index-based CO_2 reconstruction for the Paleocene, and the data have provided a continuous record of variations in CO_2 between ca. 54 Ma and ca. 65 Ma (Royer et al., 2001b; Beerling and Royer, 2002; Royer, 2003; Beerling et al., 2009). However, the stomatal CO_2 record between 64 Ma and 59 Ma was based only on one datum at 61.5 Ma (Royer, 2003). The fossil *Ginkgo* leaves indicate that CO_2 was at 330–470 ppmv during 65–64 Ma, after which it dropped to 317 ppmv at 61 Ma and then increased again to 530–570 ppmv at 59 Ma (Royer, 2003). Subsequently, *Ginkgo*-based CO_2 varied mainly between 300 ppmv and 500 ppmv with a peak of 667 ppmv at 55.8 Ma at the Paleocene–Eocene boundary (Royer et al., 2001a; Beerling et al., 2009). The two *Metasequoia*-based CO_2 level results in this paper, 308 ppmv at ca. 63 Ma and 370 ppmv at ca. 60 Ma, are the oldest CO_2 level data based on the stomatal analysis of *Metasequoia* needles to date. Our data, with small error ranges, completes the sequence of *Ginkgo*-based CO_2 records with the drop in CO_2 values at 63 Ma; and also support the increasing trends in CO_2 found between 61 Ma and 58.5 Ma, as demonstrated in the *Ginkgo*-based CO_2 records (Royer, 2003) (Figure 2.1-3).

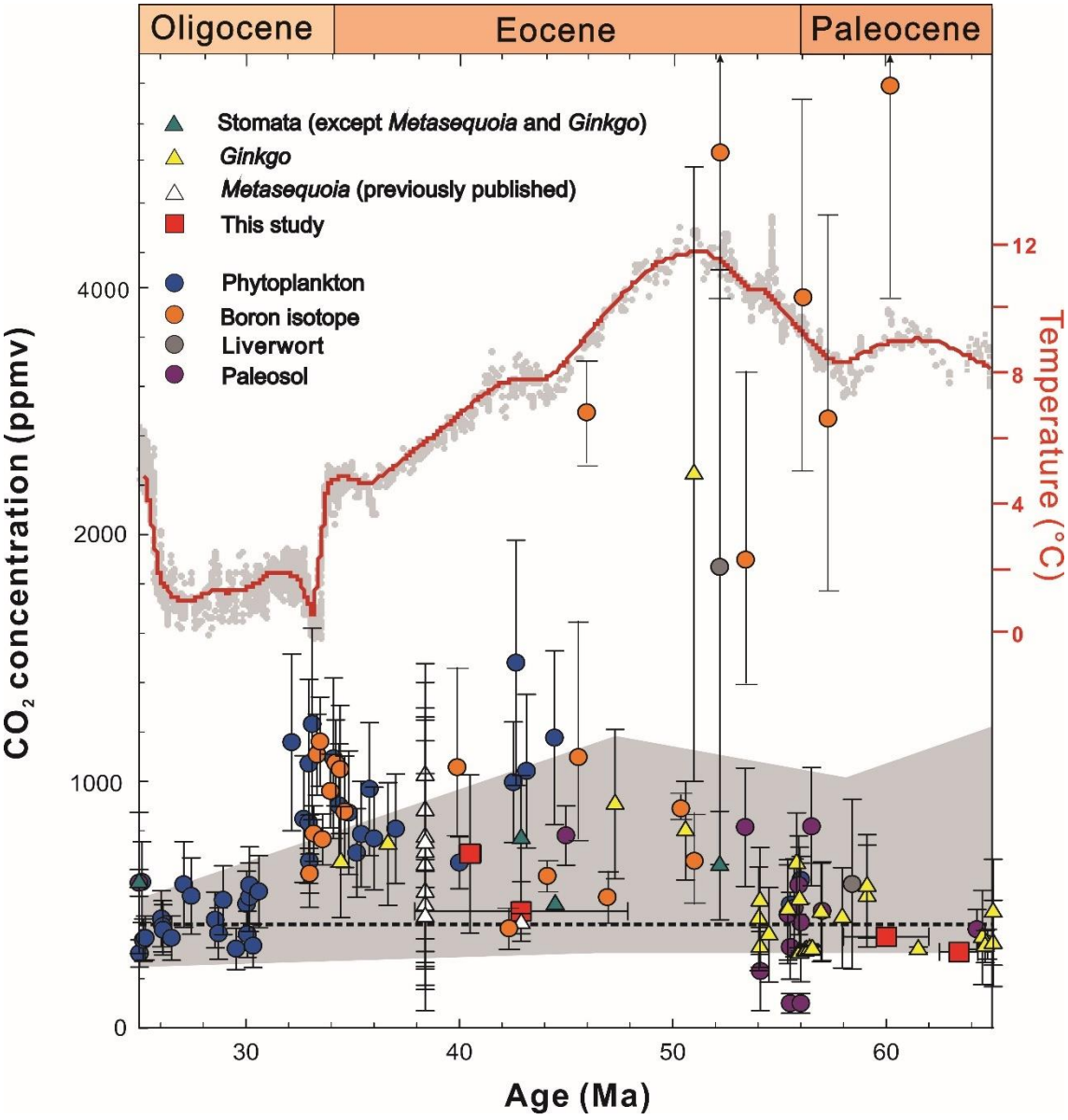

Figure 2.1-3 Atmospheric CO_2 history in the Paleogene, reconstructed by GEOCARB III (grey shade) (Berner and Kothavala, 2001) and different proxies. Including previously published stomatal analyses of *Metasequoia* (Doria et al., 2011; Maxbauer et al., 2014), *Ginkgo* (Retallack, 2001; Beerling and Royer, 2002; Royer, 2003; Beerling et al., 2009; Retallack, 2009; Smith et al., 2010), and other species (McElwain, 1998; Kürschner et al., 2001; Greenwood et al., 2003), liverworts (Fletcher et al., 2008), and analysis of paleosols (Koch et al., 1992; Sinha and Stott, 1994; Ekart et al., 1999; Royer et al., 2001a; Nordt et al., 2002;), phytoplankton (Freeman and Hayes, 1992; Stott, 1992; Pagani, 1999; Pagani

et al., 1999; Pagani et al., 2005), and boron isotopes (Pearson and Palmer, 2000; Pearson et al., 2009). Deep-sea temperatures (Zachos et al., 2001) are shown in the upper panel. The error bars represent the reported uncertainties. The horizontal dashed line indicates the present-day atmospheric CO_2 level (400 ppmv).

Proxies other than stomatal parameters for CO_2 reconstruction during the Paleocene have been derived from alternative terrestrial proxies, including the carbon isotopes of paleosols or liverworts, and marine proxies such as the boron isotopes from marine calcium carbonate or carbon isotopes from phytoplankton (Figure 2.1-3). Paleosol-based CO_2 was estimated as ca. 400 ppmv in the earliest Paleocene (Nordt et al., 2002) and 100–800 ppmv in the late Paleocene and early Eocene, which exhibits wide variations as compared to other proxies (Sinha and Stott, 1994; Royer et al., 2001b). In addition, the isotope analysis of liverworts indicated a CO_2 of 583 ppmv at ca. 58.4 Ma, which is consistent with the *Ginkgo*-based data. However, CO_2 reconstruction based on marine boron isotopes in the late Paleocene and the early Eocene (Pearson and Palmer, 2000) exhibits significantly higher values (> 2000 ppmv) than the data from terrestrial proxies (Sinha and Stott, 1994; Royer et al., 2001b; Royer, 2003), along with considerable fluctuations. However, this boron isotope method is based on the assumption that the boron isotopic composition of the ocean remains at nearly constant levels throughout time, without changes due to biological processes or differences in temperature, which has not been proved for the Paleocene (Royer et al., 2001a).

Contrary to the current view that global warming is associated with the CO_2 levels, the paleotemperature during the Paleocene was much higher than what it is today, according to marine isotope data (Zachos et al., 2001). The early and middle Paleocene fossil floras also indicate a higher temperature than that today at mid and high latitudes, according to their physiognomic characters and the fact that the Nearest Living Relatives of these species are also distributed in areas with warmer temperatures (Spicer and Parrish, 1990). The appearance of crocodilians during the Paleocene (Markwick, 1998) in the

United States is further proof of a warm environment. Considering the evidence for a warm climate during the early and middle Paleocene, if our stomatal CO_2 reconstruction is correct, factors besides CO_2 are necessary to explain the global warmth during this period. The lower Paleocene CO_2 of this study indicates that the warm climate in the early and middle Paleocene is not comparable to the present global warming because the effect from CO_2 on the increasing global temperature was less apparent than it is in the present. Although the Paleocene–Eocene Thermal Maximum (PETM) has been confirmed to be associated with the release of methane (Dickens et al., 1997; Higgins and Schrag, 2006; Pancost et al., 2007; Winguth et al., 2010), our CO_2 data is from an earlier period. Thus, instead of methane, factors like paleogeography, enhanced meridional heat transport, and high latitude vegetation feedbacks may help to explain this warm period (Royer et al., 2001b).

2.1.4.2 Higher CO_2 level than today during the middle Eocene

The Earth during the middle Eocene also experienced a long-term period of global warmth, with higher temperatures than those of today, and a decreasing trend in temperature after the early Eocene climatic optimum (Hansen et al., 2008; Bohaty et al., 2009; Wolfe et al., 2017). The stomatal data from this period generally exhibits CO_2 values higher than the present level CO_2 (ca. 400 ppmv), although the data are limited compared with that from the Paleocene. High levels of CO_2 were represented in *Ginkgo* fossils, which indicated CO_2 levels of 907 ppmv at ca. 47.3 Ma (Retallack, 2009). Stomatal analysis of fossil *Gordonia* (Kürschner et al., 2001) and Lauraceous (McElwain, 1998) leaves present a CO_2 level of 500–800 ppmv during 44.5–42.9 Ma. Our CO_2 level data (473±121 ppmv) at 47.9–37.8 Ma in the middle Eocene is lower than that found in these published studies. At the same fossil locality in Axel Heiberg Island, fossil *Metasequoia* needles have previously been used in CO_2 estimations by stomatal analysis (471 ppmv) and carbon isotope analysis based on the plant gas-exchange model (441 ppmv) (Maxbauer et al., 2014). The consistency between their results and the present

study indicates that fossil *Metasequoia* leaves are reliable for use in CO_2 estimation, and the CO_2 levels presented by this taxon do not vary among researchers or according to differences in methods.

Other stomatal data from the middle Eocene found in this study estimated CO_2 levels of 706±321 ppmv at 41–40 Ma, which is higher than the CO_2 estimation of 47.9–37.8 Ma. However, this value is within the range of values estimated by the stomatal analysis of *Metasequoia* needles from ten fossil-bearing layers in a fossil locality in northwestern Canada, which indicated a series of CO_2 data from ca. 1000 ppmv to ca. 400 ppmv at 38.4 Ma, with a decreasing trend.

Compared with the Paleocene CO_2 data, middle Eocene CO_2 estimated both by stomatal and the other proxies vary over a short time-span. The boron isotope data documented changes in CO_2 from ca. 400 ppmv at ca. 43 Ma to over 1000 ppmv at 39 Ma (Pearson and Palmer, 2000), although boron-based CO_2 data from the middle Eocene generally give lower values than those found in the early Eocene, which vary between 400 ppmv and 2500 ppmv (Pearson and Palmer, 2000). Meanwhile, the CO_2 based on the isotope analysis of phytoplankton also indicated a fluctuation in CO_2 values between ca. 1200 and ca. 650 ppmv during the period from 44 Ma to 40 Ma, although the precision of this method decreases when CO_2 rises to above 750 ppmv (Kump and Arthur, 1999; Royer et al., 2001a).

Different proxies indicate higher CO_2 levels during the middle Eocene, but the relationship between CO_2 and global warming in this age has not been clarified due to the inconsistent results of CO_2. Plant fossils have recorded a warm climate during the Eocene as well, for example, the northern limit for distribution of a frost intolerant palm was 20° latitude further north than it is currently in North America (Greenwood and Wing, 1995). Multiple climate proxies also demonstrate an Arctic environment with winter temperatures at or just above freezing and summer temperatures of ≥ 20 °C during the early–middle Eocene (Eberle and Greenwood, 2012). During this warm period, a decrease in temperature since the middle Eocene was detected in marine oxygen isotopes (Zachos

et al., 2001), which cannot be explained by the CO_2 variation based on stomatal or other proxy data. Thus, other factors, such as complex feedbacks initiated by tectonic alterations to the ocean basins (Shellito et al., 2009), increased polar stratospheric clouds (Sloan and Pollard, 1998), and increased latent heat transport (Ufnar et al., 2004) may be complementary warming mechanisms besides CO_2 level increases. However, our understanding of the climate change mechanisms during this greenhouse period is still far from clear.

2.1.4.3 Advantages of fossil Metasequoia needles in paleo-CO_2 estimation

Metasequoia fossils have been reported in more than 500 localities in the Northern Hemisphere, belonging to various ages from the Cretaceous to the Pleistocene (LePage et al., 2005). This very wide and frequent occurrence of *Metasequoia* fossils in time and space allows the production of an evolutionary curve in CO_2 throughout the whole Cenozoic from use of these fossil needles alone, without the noise derived from using different kinds of proxies. Although several *Metasequoia*-based CO_2 records from the Cenozoic have been published to date (Royer et al., 2001b; Doria et al., 2011; Maxbauer et al., 2014; Wang et al., 2015), the *Metasequoia*-based CO_2 data from the Paleogene are still insufficient compared with data from *Ginkgo*. This may be ascribed to its fragile cuticle as compared to *Ginkgo*. However, development of fluorescence microscopes, laser scan microscopes and electron scanning microscopes enables much easier observation of such delicate cuticles.

This research demonstrated that the mechanisms that caused the Paleogene climate change were significantly complex, and that variations in CO_2 played a less important role than today. Thus, studies concerning climate changes during the Neogene and Quaternary will be more helpful for a better understanding of the present mechanisms leading to global warming. Fossil *Metasequoia* needles from the late Cenozoic are very abundant, especially in Japan, and other materials with continuous and high-resolution stratigraphic settings are available for investigation (LePage et al., 2005). Leaf margin

analysis and stomatal analysis of a Japanese fossil assemblage has implied a coupled relationship between CO_2 and temperature during the Quaternary (Wang et al., 2018b). Compared with the species that were distributed over a wide range of altitudes, such as *Fagus*, *Quercus* and *Ginkgo*, *Metasequoia* is generally limited to floodplains at low altitudes, which can avoid errors in CO_2 estimation caused by the transportation of leaves from higher altitudes before fossilization (Wang et al., 2018a). Since the stomatal index can record rapid CO_2 changes occurring within 100 years (Royer, 2001), *Metasequoia* fossil needles have the potential to provide more detailed information in CO_2 evolutionary history during the Cenozoic.

2.2 Warm climate under high CO_2 level in the early Pleistocene based on the Sayama Formation in central Japan

2.2.1 Introduction

From the latest Pliocene, the climate regime in the Northern Hemisphere changed from warm, ice-free conditions to give rise to an icehouse Earth (Mudelsee and Raymo, 2005; Rohling et al., 2014). The early Pleistocene was characterized by conspicuous glacial-interglacial climate changes on a 41-ka cycle, accompanied by the development of ice sheets in the Northern Hemisphere (Lisiecki and Raymo, 2005). The climatic deterioration during the glacial stages influenced the distribution and composition of terrestrial flora at mid-latitudes in the Northern Hemisphere (van der Hammen et al., 1971; Popescu et al., 2010; Martinetto et al., 2017), and promoted the expansion of boreal vegetation into the lowland areas of central Japan (Momohara, 2016; Yamakawa et al., 2017). However, the warm and oceanic environments during these interglacial stages reappeared in the early Pleistocene, which is apparent from a fossil leaf assemblage of ca. 1.6 Ma in the Sayama Formation on the Pacific side of central Japan (Ito et al., 2017). This warm environment sustained the populations of thermophilous plants and exotic elements that had earlier gone extinct in the other areas of central Japan. Glacial-interglacial cycles are coupled with atmospheric CO_2 changes, as demonstrated by the Middle and Late Pleistocene ice core records from the Antarctic (Jouzel et al., 2007; Lüthi et al., 2008). As increases in the atmospheric CO_2 are also related to present climate changes (Stocker et al., 2013), palaeo-CO_2 reconstruction of the Pleistocene interglacial stages may provide us a better understanding of present global change. However, palaeo-CO_2 and palaeo-temperature in the early Pleistocene have been chiefly reconstructed for marine environments (Hansen et al., 2008; Hönisch et al., 2009; Seki et al., 2010; Tripati et al., 2011), and terrestrial records of this period are scarce compared with those in the middle and late Pleistocene, for which ice core data are available.

This study aims to estimate both palaeo-temperature and palaeo-CO_2 based on a leaf fossil assemblage, belonging to an early Pleistocene interglacial stage (MIS 57 or 55), in the Sayama Formation, central Japan (Ito et al. 2017). I applied SD analysis to fossilized leaves of *Quercus gilva*, which has the highest temperature requirement among the components of the studied fossil assemblage. In addition, I quantitatively reconstructed the palaeo-temperature based on LMA, to investigate the relationship between palaeo-CO_2 and palaeo-temperature in this interglacial interval.

2.2.2 Geological setting

The fossil sampling site (35°46′33″N, 139°22′43″E, 130 m a.s.l.; Figure 2.2-1) is an outcrop of the Sayama Formation exposed in the riverbed of the Osawa River in the Sayama Hills, western Tokyo (Saitama Research Group and Kanto Quaternary Research Group, 1970; Nirei and Takegoshi, 2007). The formation is distributed along the western margin of the Kazusa Group sedimentary basin that consists of continuous sedimentation of deep-to-shallow sea deposits in Chiba Prefecture between 2.4 and 0.5 Ma (Ito and Katsura, 1992). The leaf fossil bed is embedded in a 3-m thick fluvial silt overlain by a 7-m thick marine sediment layer. The horizon of the assemblage is 16 m above the Sayama-garasushitu tephra bed (SYG) and 13 m below the Sayama-gomashio tephra bed (SGO) (Ito et al., 2017). The SYG tephra is correlated with the Tsuike Ash, which is situated between the peaks of MIS 57 and 58 in the Uonuma Group in the Niigata Prefecture (Momohara et al., 2017). The SGO tephra is correlated with the Ob4b-1 tephra that is above the Omn-SK110 tephra (Suzuki et al., 2016), which is correlated with the peak of MIS 54 (Nozaki et al., 2014). Thus, the age of the Sayama fossil leaf bed is constrained to ca. 1.65–1.55 Ma, between MIS 58 and MIS 54 (Sakai and Kurokawa, 2002; Muramatsu, 2008; Suzuki et al., 2011; Momohara et al., 2017).

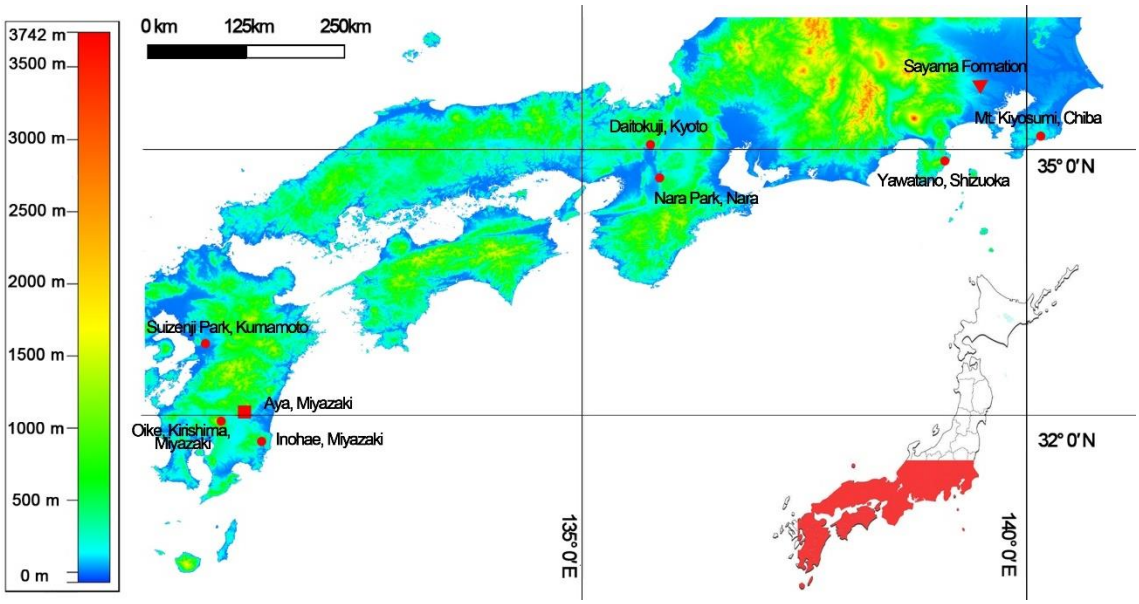

Figure 2.2-1 Map showing the sampling sites for modern leaves (square) and herbarium specimen (square and circle) together with the Sayama Formation (triangle). The original map was downloaded from the Consortium for Spatial Information (CGIAR-CSI; http://www.cgiar-csi.org/).

2.2.3 Materials and methods

2.2.3.1 Palaeo-CO_2 reconstruction

As the relationship between stomatal density and palaeo-CO_2 is species-specific even within a single family (Royer, 2001; Kürschner et al., 2008), it is necessary to select a suitable species among the components of a fossil leaf assemblage as a proxy for sea-level palaeo-CO_2. Among the components of the leaf fossil assemblage, *Quercus gilva* has the highest temperature requirements (Ito et al., 2017). *Quercus gilva* is an evergreen broad-leaved tree that is a major component of warm-temperate evergreen broad-leaf forests in southern China (Flora of China Editorial Committee, 1994) and southwestern Japan (Koike, 1989). I considered that the distribution of *Quercus gilva* is limited to the lowermost altitude, and that the palaeo-CO_2 based on its stomatal density reflects sea-level palaeo-CO_2.

As sun and shade leaves generally exhibit different responses to CO_2 gradient

(Kürschner et al., 1996; Royer et al., 2001b; McElwain, 2004; Kouwenberg et al., 2007), they should be examined separately to establish the correlation between stomatal density and CO_2. However, the lower and interior position of shade leaves in canopy decreases their chances of wind dispersal to places of fossilization (Kürschner et al., 1996), and their thinner mesophyll and cuticles are susceptible to bacterial degradation (Roth and Dilcher, 1978; Spicer, 1981). Thus, the percentage of shade leaves is generally limited in fossil assemblages (Kürschner, 1997; Hu et al., 2015), and I used only sun leaves in this study.

To distinguish the sun and shade leaves, the epidermal anticlinal wall pattern is considered a useful parameter (Watson, 1942; Kürschner, 1997; Wang et al., 2018), but due to the poor preservation condition of our sample fossil materials, it was not possible to determine the epidermal anticlinal wall pattern. However, most of the *Quercus gilva* leaves in this fossil assemblage have coriaceous and thick lamina and are believed to be sun leaves, which are distinguishable from the shade leaves, with thin and light-colored lamina.

2.2.3.2 Stomatal analysis of the extant materials

For palaeo-CO_2 estimation, I needed to construct a relationship between stomatal density (SD) of *Quercus gilva* and atmospheric CO_2 level, based on modern materials and herbarium specimens that were collected when atmospheric CO_2 level was lower than that in the present. Sun leaves of *Quercus gilva* were collected from five trees each at 200 m, 400 m, 518 m, and 590 m a.s.l. in Aya, the southern part of the Miyazaki Prefecture, south Japan (Figure 2.2-1). All the leaves were collected from the surface of sunny sides of the canopies. Ten sun leaves from each of the five trees were collected for stomatal analysis (Poole, 1999; Beerling and Royer, 2002). In addition, herbarium specimens collected between AD 1961 and 1996, which are stored in the Herbarium of Graduate School of Horticulture, Chiba University (MTDO), were examined. I used five sun leaves from each herbarium specimen for cuticle observation.

For each extant leaf, I first removed the hair on the lower epidermis by washing it in water. Then, I applied a clear nail polish on the lower epidermal surface of the area between two adjacent secondary veins along the mid-vein in the center of the lamina. After air drying the nail polish, I removed it from the leaf to get the cast of the lower epidermal surface. I then enclosed it using glycerin on a glass slide and observed it under a transmitted light microscope connected to a digital camera. Thirty cuticular fields from each tree or each herbarium specimen were photographed for SD calculation.

2.2.3.3 Calibration curves between SD and CO_2

I estimated the calibration curves between the SD of *Quercus gilva* and CO_2 based on the extant samples. I calculated the CO_2 of each sampling spots based on Equation 2.2-1 (Jones, 2013):

$$H = -\ln\left(\frac{p2}{p1}\right) \times \frac{R \times T}{MA \times g}$$

Equation 2.2-1

p1: CO_2 (Pa) at sea level

p2: CO_2 (Pa) at the sampling spot

R: gas constant (8.3144 Pa m^3 mol^{-1} K^{-1})

T: average mean annual temperature (K) between the sampling spot and sea level

MA: molecular weight of air (0.028964 kg mol^{-1})

g: acceleration due to gravity (9.8 m s^{-2})

H: elevation (m) of the sampling spot

Accurate T data of each sampling spot were calculated based on National Land Numerical Information (http://nlftp.mlit.go.jp/ksj/) for extant materials and “Mesh 2000 Climatic Values in Japan” (JMA, 2002) for herbarium materials, respectively. The datasets are composed of 1 km mesh data of average altitudes and corresponding monthly mean temperatures based on data from ca. 1000 meteorological stations in Japan between 1980–2010 and 1971–2000, respectively. Temperatures at the altitude of the sampling spots were calculated by linear regression of datasets at different altitudes in and around

the site. Using these T values along with altitude, past and present sea-level CO_2 record (p1) (CO_2 Now website, https://www.CO_2.earth/), and other parameters in Equation 2.2-1, CO_2 (p2) of each spot could be calculated. Next, the calibration curve between stomatal frequencies and CO_2 for *Quercus gilva* was constructed using SigmaPlot v.12.5.

2.2.3.4 Palaeo-CO_2 calculation

For cuticle analysis, I used five fossilized *Quercus gilva* leaves that are stored in the Graduate School of Horticulture, Chiba University (Ito et al., 2017). I first treated them with 20% HCl for about 6 h to remove calcareous materials, and then washed them until they were neutralized. I enclosed each leaf in glycerin on a glass slide, with the lower epidermis facing up, and observed the same portion that I observed for extant materials under a fluorescence microscope (Nikon Optiphot-2) linked to a digital camera. Five cuticular fields (0.08 mm^2) were photographed for each fossil leaf and the number of stomata in the field was counted to calculate the stomatal density (SD, the number of stomata per mm^2 of leaf). Stomatal index (SI) is not available because of the preservation of the fossilized leaves. Using the stomatal density of our fossil materials in the established correlation, I estimated the sea-level palaeo-CO_2 of the Sayama Formation.

2.2.3.5 Palaeo-temperature reconstruction

From the Sayama Formation leaf bed, 39 woody angiosperm species identified by Ito et al. (2017) were used for LMA (Table 2.2-1). I classified them into entire- and toothed-margin leaves, and then calculated the percentage of species with entire margin leaves to estimate the mean annual temperature (MAT). I classified lobed leaves without serration and spinose leaves as entire margin leaves. Different negative correlations between the percentage of entire margin leaf species in woody dicot flora and MAT have been estimated for different regions (Wolfe, 1979; Wilf, 1997; Jacobs, 1999; Gregory-Wodzicki, 2000; Greenwood et al., 2004; Spicer et al., 2004; Traiser et al., 2005; Su et al., 2010), and here, I used the equation for East Asia (Wolfe, 1979) because its sampling area

covers the entire area of Honshu, Japan. The standard error (SE) of estimated MAT was calculated following Miller et al. (2006).

MAT(°C) = 1.141 + 30.6×p

Equation 2.2-2

$$SE = b \times \sqrt{[1 + \varphi(n-1)p(1-p)] \times \frac{p(1-p)}{n}}$$

Equation 2.2-3

p: proportion of woody dicot species with entire leaves

b: slope of the equation; here, 30.6

φ: over dispersion factor, with a value of 0.052 from Miller et al. (2006);

n: total number of woody dicot species among the flora

2.2.4 Results

2.2.4.1 Palaeo-CO_2 reconstruction

Based on the cuticular images of the extant materials (Figure 2.2-2), I calculated their SD data, which showed a significant negative linear relationship (p<0.0001) with estimated CO_2 at each of the sampling sites (Figure 2.2-3).

The average SD value of fossilized *Quercus gilva* leaves was 669.5±42.1 mm^{-2}. Plugging this value into the SD-CO_2 relationship based on extant materials, palaeo-CO_2 was estimated as 36.41±2.58 pa (359±25 ppmv).

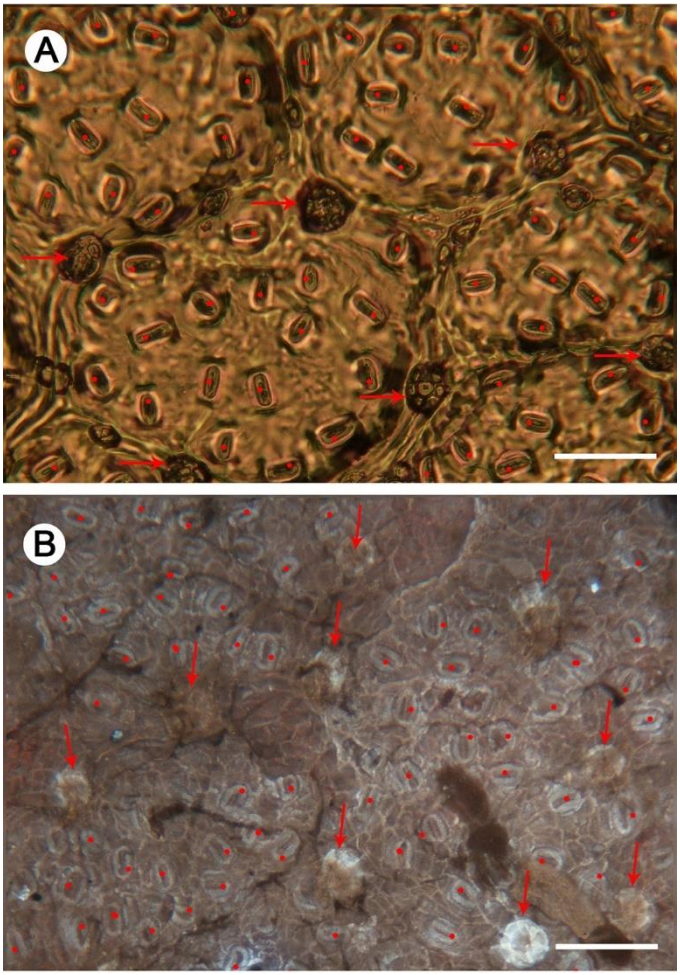

Figure 2.2-2 Cuticular images of modern (A) and fossil (B) *Quercus gilva*. Stomata are marked by red dots, and arrows indicate hair bases. Error bar = 50 μm.

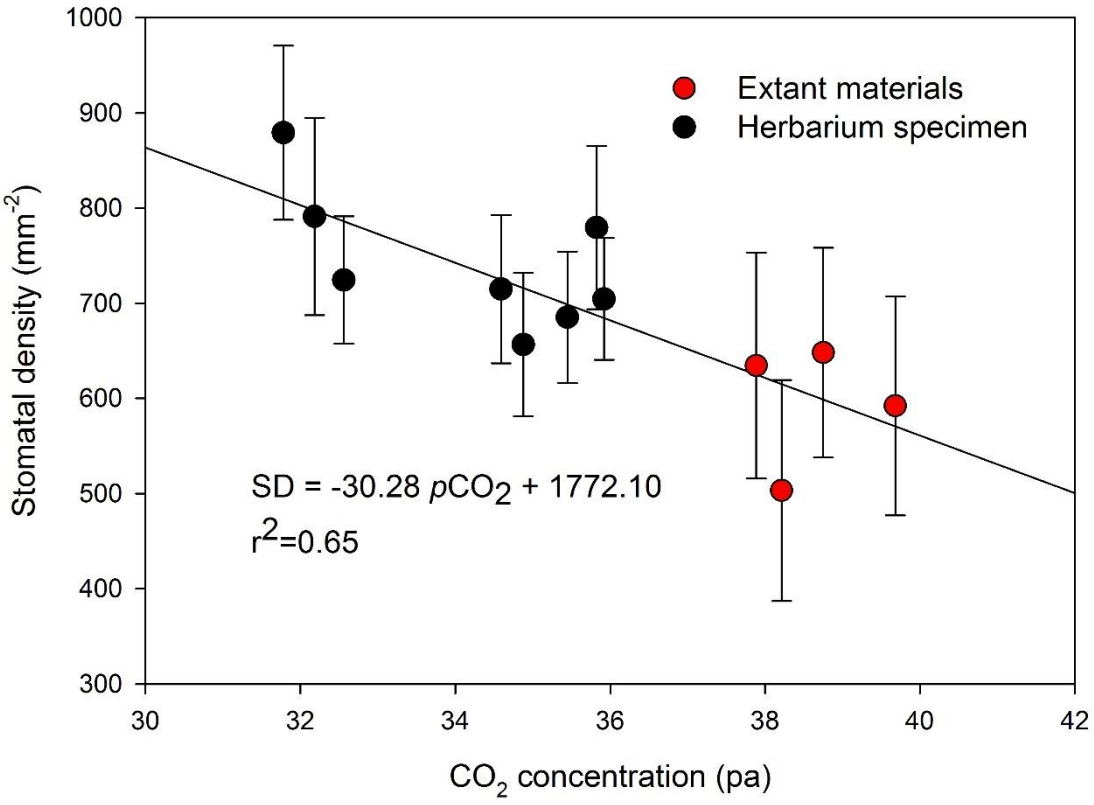

Figure 2.2-3 Relationship between CO_2 and stomatal density based on the extant sun leaves of *Quercus gilva* (error bar = 1σ).

2.2.4.2 Palaeo-temperature reconstruction

Among the 39 dicots (Figure 2.2-4 and Table 2.2-1), 12 species have entire leaf margin (scored as 1), while the leaves of *Fagus japonica* include both toothed and entire margins (scored as 0.5). Thus, the percentage of species with entire leaf margins (P) was calculated as 32%. The calculated MAT based on the East Asian equation (Equation 2.2-2) was 11.0 °C and the SE was ±2.67 °C (Equation 2.2-3).

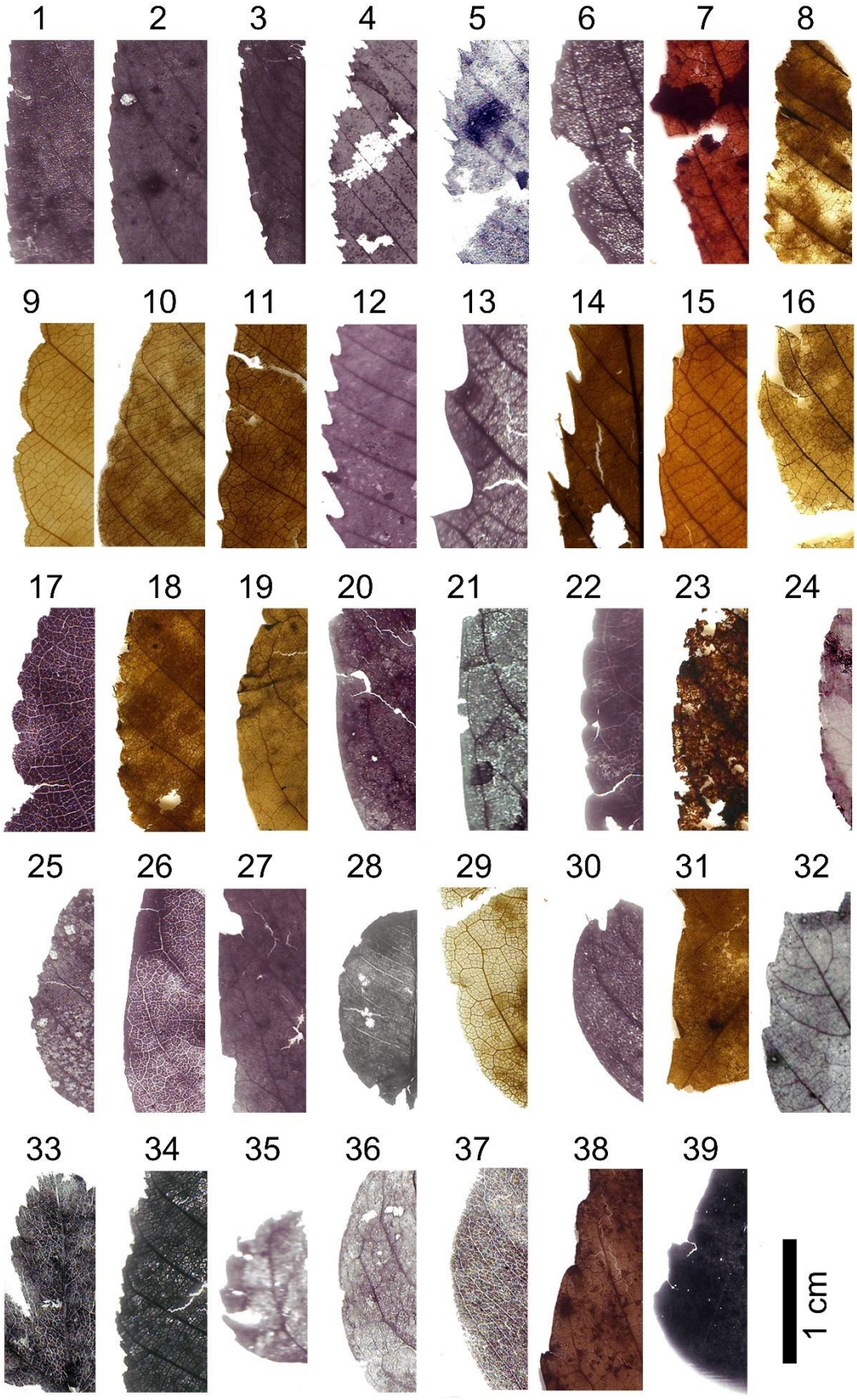
1
2
3
4
5
6
7
8
9
10
11
12
13
14
15
16
17
18
19
20
21
22
23
24
25
26
27
28
29
30
31
32
33
34
35
36
37
38
39
1 cm

Figure 2.2-4 Leaf margins of fossil leaves for leaf margin analysis (LMA) from the Sayama Formation. 1. *Salix subfragilis* Andersson; 2. *Salix sieboldiana* Blume; 3. *Salix gilgiana* Seemen; 4. *Carpinus laxiflora* (Siebold et Zucc.) Blume; 5. *Carpinus tschonoskii* Maxim.; 6. *Alnus* cf. *japonica* (Thunb.) Steud.; 7. *Ostrya* cf. *japonica* Sarg.; 8. *Betula grossa* Siebold et Zucc.; 9. *Fagus crenata* Blume; 10. *Fagus japonica* Maxim.; 11. *Fagus stuxbergi* (Nathorst) Tanai; 12. *Quercus serrata* Murray; 13. *Quercus* sect. *Prinus* sp.; 14. *Quercus acutissima* Carruth.; 15. *Quercus gliva* Blume; 16. *Zelkova serrata* (Thunb.) Makino; 17. *Celtis sinensis* Pers.; 18.*Ulmus davidiana* Planch.var. *japonica* (Rehder) Nakai; 19. *Lindera umbellata* Thunb.; 20. *Cinnamomum camphora* (L.) J.Presl; 21. *Cinnamomum tenuifolium* (Makino) Sugim. ex H. Hara; 22. *Cercidiphyllum* cf. *japonicum* Siebold et Zucc. ex Hoffm. et Schult.; 23. *Liquidambar formosana* Hance; 24. *Sorbus* cf. *commixta* Hedl.; 25. *Rosa* cf. *multiflora* Thunb.; 26. *Albizia kalkora* (Roxb.) Prain; 27. *Wisteria floribunda* (Willd.) DC.; 28. *Lespedeza cyrtobotrya* Miq.; 29. *Cercis chinensis* Bunge; 30. Leguminosae (Fabaceae) spp; 31. *Acer pictum* Thunb.; 32. *Acer diabolicum* Blume ex K.Koch; 33. *Acer palmatum* Thunb.; 34. *Aesculus turbinata* Blume; 35. *Tilia* sp.; 36. *Lagerstroemia indica* L.; 37. Ericaceae sp.; 38. *Fraxinus japonica* Blume ex K. Koch; 39. *Smilax china* L..

Table 2.2-1 List of dicotyledonous fossil species in the Sayama Formation (Ito et al., 2017).

Family	Fossil species	Score for LMA
Salicaceae	*Salix gilgiana* Seemen	0
	S. sieboldiana Blume	0
	S. subfragilis Andersson	0
Betulaceae	*Alnus* cf. *japonica* (Thunb.) Steud.	0
	Betula grossa Siebold et Zucc.	0
	Carpinus laxiflora (Siebold et Zucc.) Blume	0
	C. tschonoskii Maxim.	0
	Ostrya cf. *japonica* Sarg.	0
Fagaceae	*Fagus crenata* Blume	0
	F. japonica Maxim.	**0.5**
	F. stuxbergi (Nathorst) Tanai	0
	Quercus acutissima Carruth.	0
	Q. serrata Murray	0
	Q. sect. Prinus sp.	0
	Q. gliva Blume	0
Ulmaceae	*Celtis sinensis* Pers.	0
	Ulmus davidiana Planch.var. japonica (Rehder) Nakai	0
	Zelkova serrata (Thunb.) Makino	0
Lauraceae	*Cinnamomum camphora* (L.) J.Presl	**1**
	C. tenuifolium (Makino) Sugim. ex H. Hara	**1**
	Lindera umbellata Thunb.	**1**
Cercidiphyllaceae	*Cercidiphyllum* cf. *japonicum* Siebold et Zucc.ex Hoffm. et Schult.	0
Hamamelidaceae	*Liquidambar formosana* Hance	0
Rosaceae	*Sorbus* cf. *commixta* Hedl.	0
	Rosa cf. *multiflora* Thunb.	0
Leguminosae	*Albizia kalkora* (Roxb.) Prain	**1**
	Cercis chinensis Bunge	**1**
	Lespedeza cyrtobotrya Miq.	**1**
	Wisteria floribunda (Willd.) DC.	**1**
	Leguminosae (Fabaceae) spp.	**1**
Aceraceae	*Acer diabolicum* Blume ex K.Koch	0
	A. palmatum Thunb.	0
	A. pictum Thunb.	**1**

Hippocastanaceae	*Aesculus turbinata* Blume	0
Tiliaceae	*Tilia* sp.	0
Lythraceae	*Lagerstroemia indica* L.	**1**
Ericaceae	Ericaceae sp.	**1**
Oleaceae	*Fraxinus japonica* Blume ex K. Koch	0
Liliaceae	*Smilax china* L.	**1**

2.2.5 Discussion

2.2.5.1 Relationships between stomatal density and CO_2

The negative correlation of SD values of the extant leaves with CO_2 (Figure 2.2-3) indicate the sensitivity of the leaves to CO_2 change. SD is generally believed to be less reliable for palaeo-CO_2 reconstruction than the stomatal index (SI), which is calculated as the number of stomata divided by the number of epidermal cells. Compared with SI, SD generally exhibits a lower correlation coefficient with CO_2 (Bai et al., 2015; Hu et al., 2015), possibly owing to the changes induced by leaf expansion, which is susceptible to other environmental factors (Salisbury, 1928; Woodward, 1987; Kürschner et al., 1996; Kürschner, 1997; Kouwenberg et al., 2007). However, the high correlation coefficient (r^2=0.65) obtained in this study demonstrates the reliability of using SD in atmospheric CO_2 reconstruction based on *Quercus gilva* leaves.

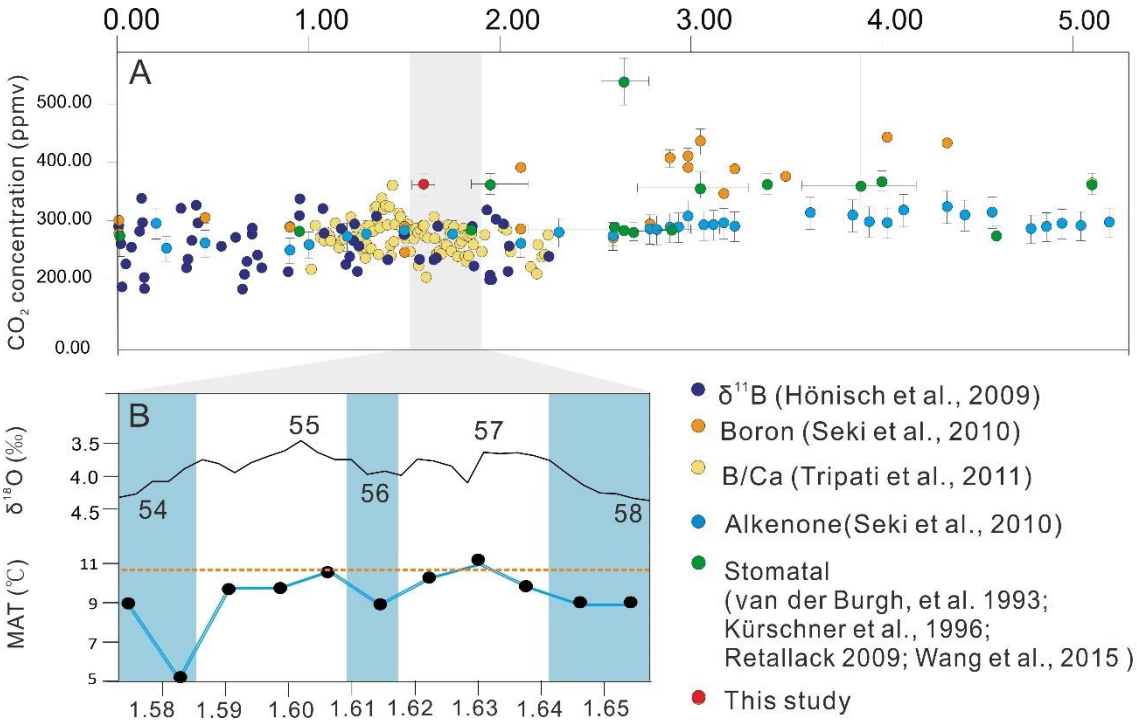

Figure 2.2-5 (A) Palaeo-CO_2 data derived from different proxies since 5 Ma. (B) Mean annual temperature (MAT) curve based on the Early Pleistocene Uonuma Group

(Momohara et al., 2017) compared with the $\delta^{18}O$ record (Lisiecki and Raymo, 2005). The orange broken line indicates the palaeo-temperature reconstructed from the Sayama leaf bed.

Besides *Quercus gilva*, which was used in this study, *Fagus crenata* leaves from the same fossil assemblage have been used to reconstruct palaeo-CO_2 in our previous study (Wang et al., 2018). Based on the SD of *Fagus crenata*, sea-level palaeo-CO_2 was estimated at more than 36.41±2.58 pa (359±25 ppmv) (Wang et al., 2018), consistent with the data based on the SD of *Quercus gilva* obtained in this study, i.e., 36.41 pa (359 ppmv). However, the sea-level palaeo-CO_2 based on the SI of *Fagus crenata* was estimated at more than 39.60 pa (391 ppmv) (Wang et al., 2018), higher than the estimated palaeo-CO_2 value obtained in this study.

The cross-checking of palaeo-CO_2 data from two species confirms that the sea-level palaeo-CO_2 (over 359 ppmv) in the study area was higher than most of the previous results obtained based on marine materials during the early Pleistocene (Figure 2.2-5). Boron and alkenone data of foraminifera from the Ocean Drilling Program site 999A indicated a CO_2 concentration of around 277 ppmv between 1.5 and 1.65 Ma (Seki et al., 2010). Palaeo-CO_2 data based on B/Ca data (Tripati et al., 2011) and $\delta^{11}B$ (Hönisch et al., 2009) vary between 200–300 ppmv during 1.5–1.7 Ma. A similar high CO_2 level of ca. 360 ppmv was recorded by B/Ca (Tripati et al., 2011) at around 1.44 Ma: an age that is a little younger than the age of our data. Although the Pleistocene CO_2 results derived from different proxies are relatively consistent with each other compared with the records in the Neogene, most of the results still vary from ca. 190 ppmv to ca. 360 ppmv (Beerling and Royer, 2011).

Compared with the published CO_2 data based on stomatal method applied to the last 5 Ma (Van Der Burgh et al., 1993; Kürschner et al., 1996; Retallack, 2009; Wang et al., 2015), I can see a stable CO_2 level at around 350 ppmv between 3–4 Ma, corresponding to the middle Pliocene warming (Dowsett et al., 1996; Haywood et al., 2016).

Subsequently, decreased palaeo-CO_2 levels of around 300 ppmv were recorded for the latest Pliocene cooling phase between 2.8 and 2.5 Ma, except for some extraordinary data showing more than 500 ppmv at 2.6 Ma (Bai et al., 2015), which may be affected by the abnormal emission of CO_2 from wetlands. In addition, high-resolution CO_2 data based on ice core analysis indicates a noticeable difference in CO_2 level between glacial and interglacial stages during the Pliocene: 180 ppmv in the glacials and 280-300 ppmv in the interglacials (Jouzel et al., 2007; Lüthi et al., 2008). Early Pleistocene CO_2 levels varied between ca. 280–360 ppmv, and a record of ca. 360 ppmv in 1.9 Ma (Kürschner et al., 1996) indicates a similar high CO_2 level to our data.

2.2.5.2 Relationships between palaeo-CO_2 and palaeotemperature

Consistent with this relatively high CO_2 level recorded, the palaeo-temperature reconstructed on the basis of LMA was also high. Momohara et al. (2017) reconstructed the palaeotemperature for the same timebased on the coldest limiting temperature of thermophilous taxon using plant megafossil assemblages of the Uonuma Group, central Japan (Figure 2.2-5, B). The MAT of interglacials peak in MIS 57 (11.0 °C) and MIS 55 (10.6 °C) (Momohara et al., 2017), which is almost equivalent to our contemporaneous palaeo-temperature data. The assemblage composition of the Sayama leaf bed is characterized by evergreen broad-leaved trees including *Actinodaphne, Cinnamomum*, and *Quercus* subgen. *Cyclobalanopsis* (Ito et al., 2017). Based on the study in 3.1, stomatal analysis of fossilized *Fagus crenata* leaves from the same assemblage clarified that altitudinal transportation of leaves before burial was greater than 1000 m. This altitudinal transportation caused a mixture of different climate elements in the Sayama Formation: cool-temperate elements such as *Betula glossa*, *Cercidiphyllum japonicum*, and *Aesculus turbidata*; warm-temperate elements such as *Ginkgo biloba*, *Cercis chinensis*, *Liquidambar formosana,* and *Cunninghamia lanceolata* var. *konishii*; and subtropical elements such as *Quercus gilva*, *Cinnamomum yabunikkei*, *Albizzia kalkora*, and *Lagerstroemia indica* (Ito et al., 2017). Because cool temperate elements from higher altitude tend to be serrated, LMA based on a leaf assemblage that includes high altitude

plants will produce a cooler MAT result. Based on our palaeo-temperature and palaeo-CO_2 results, the fossil assemblage undoubtedly indicates a warm, interglacial environment, which is also confirmed by the position of the leaf bed just below the marine transgressive horizon (Ito et al., 2017). Thus, our results indicate a warm climate under high CO_2 level during an interglacial stage of the early Pleistocene.

Many studies have documented a coupled relationship between CO_2 and temperature during the Pleistocene. Atmospheric CO_2 level change based on fossil *Metasequoia* needles from Japan exhibits a similar decreasing trend with palaeo-temperature since the late Miocene to early Pleistocene (Wang et al., 2015). Research on Antarctic ice cores has also demonstrated a positive relationship between palaeo-CO_2 and palaeo-temperature (Jouzel et al., 2007; Lüthi et al., 2008) during the Middle and Late Pleistocene. Evidences from other geological times also shows that atmospheric CO_2 levels have played an important role in global climate change (Petit et al., 1999; Bijl et al., 2010; Pagani et al., 2011). Our research provides evidence to support the coupling of high palaeo-CO_2 and high palaeo-temperature episodes during the early Pleistocene, based on a terrestrial plant assemblage. However, it is important to carry out stomatal studies together with palaeo-temperature reconstruction for other interglacial stages as well, which could help to reveal the role of atmospheric CO_2 in relation to global temperature changes in the early Pleistocene.

3 Extended application of stomatal analysis: reconstruction of altitudinal transportation range of leaves before fossilization

3.1 An example of the Early Pleistocene *Fagus* leaf fossils from the Sayama Formation, central Japan

3.1.1 Introduction

The transportation of plant organs before their burial (Astorga et al., 2016; Steart et al., 2006) is an important process in the formation of fossil assemblage. It can affect the composition of fossil flora, which complicates the reconstruction of paleoclimates and paleovegetation. To increase the resolution of quantitative paleoclimate analysis (Mosbrugger and Utescher, 1997; Spicer et al., 2009; Su et al., 2010; Wilf, 1997), a better understanding of plant transportation in ancient times become necessary.

Transportation of plant organs has been recognized in modern sedimentation of leaf, fruit/seed, and pollen assemblages by comparison with the positions of their mother plants. Investigations of the taphonomical process of modern subfossil leaf assemblages from their source forests often indicate significant differences in their composition, which are caused mainly by wind/water-aided transportation (Astorga et al., 2016; Ozaki, 1969). Water currents transport fruits and seeds into the areas far from their mother plants (Gee, 2005; Sims and Cassara, 2009; Vassio and Martinetto, 2012), while winged seeds are transferred for an extended distance by wind (Zheng et al., 2004). Pollen transportation has been studied for a long time, in relation to the pollen source area and sedimentary basin size. The pollen assemblage commonly includes pollen that is transported between 2 and 100 km away (Prentice, 1985; Prentice et al., 1987; Sugita, 1994); Pinaceae pollen is transported for more than 500 km (Dyakowska, 1947; Szczepanek et al., 2017).

Assemblages in ancient times also exhibit evidence of the long-distance transportation of plant organs. Holocene leaf fossil assemblages in the crevasse-splay deposits in an

Alabama delta show that most of the plant remains cannot be assigned to the local flora and were transported long distances from the plant communities growing on the upper delta plains (Gastaldo et al., 1987). The possibility of plant transportation from a higher altitude is presumed from the composition of Cenozoic fossil floras with a mixture of subtropical evergreen trees (e.g., *Cyclobalanopsis*, *Actinodaphne*, *Cinnamomum*) and cool temperate and/or subarctic trees (e.g., *Abies, Picea*, and *Betula*), which inhabit different climate conditions (e.g. Huzioka, 1963). The altitudinal transportation might be estimated from the temperature difference between the distribution limits of the most thermophilous and the most cold-loving elements in assemblage components (e.g., Momohara et al., 2017). However, the altitudinal limit of plant distribution is decided by plural temperature parameters, along with the other environmental factors, such as precipitation, wind, snow depth, and geology (Cantón et al., 2004; Ozaki, 1969; Takahashi, 1962; Wolfe, 1993; Woodward and Williams, 1987). Therefore, proxy changing at a constant rate along altitude is necessary to estimate the altitudinal transportation of plant organs.

To clarify the altitudinal transportation of a leaf, I considered the stomatal frequency variation of leaves of one species as a possible proxy of the CO_2 level decreasing with altitude. The stomatal frequency of fossil leaves has been used as a proxy of paleo-CO_2 for a long time (e.g. Bai et al., 2015; Hu et al., 2015; Wang et al., 2015; Royer, 2003; Beerling and Royer, 2002; Rundgren and Beerling, 1999; Kürschner, 1997), while many reports suggest the potential of altimetry by using stomatal frequency that is sensitive to the CO_2 change with altitude (Kouwenberg et al., 2007; McElwain, 2004). If one species of fossil leaves in an assemblage demonstrates a variation of stomatal frequency larger than that observed in its modern population at the same altitude, I can estimate the altitudinal transportation range of leaves based on the predictable decrease in CO_2 with altitude.

In this research, I studied the altitudinal change of stomatal frequency in modern *Fagus crenata* leaves to clarify the altitudinal transportation of leaves from a Lower

Pleistocene Sayama Formation fossil assemblage. The detected altitudinal transportation can be used to explain the co-existence of elements that have different climatic requirements in the fossil assemblage (Ito et al., 2017).

3.1.2 Materials

3.1.2.1 Modern materials

Fagus crenata is a dominant element of the cool temperature forest in Japan and is distributed in a wide altitudinal range between ca. 600 and 2000 m a.s.l. in central Japan (Takahashi, 1962). For the present study, the extant, mature leaves of *Fagus crenata* were collected from 120 individuals at different elevations ranging from 250 to 1980 m a.s.l. in eight localities. In most of the localities, five individuals were collected at an altitudinal interval of 100 m (Figure 3.1-1). As sun and shade leaves have different stomatal frequencies (Kouwenberg et al., 2007; Kürschner et al., 1996; McElwain, 2004; Royer et al., 2001), I collected sun and shade leaves from different portions of the trees. Sun leaves were collected from the surface in the top or southern side of the canopy, while shade leaves were collected from the shoots under the canopy. To represent the stomatal frequency within one individual tree (Beerling and Royer, 2002; Poole, 1999), ten sun leaves were collected from each tree. To observe the differences between sun and shade leaves, ten shade leaves were collected from 17 randomly selected trees at the eight localities where the sun leaves were collected.

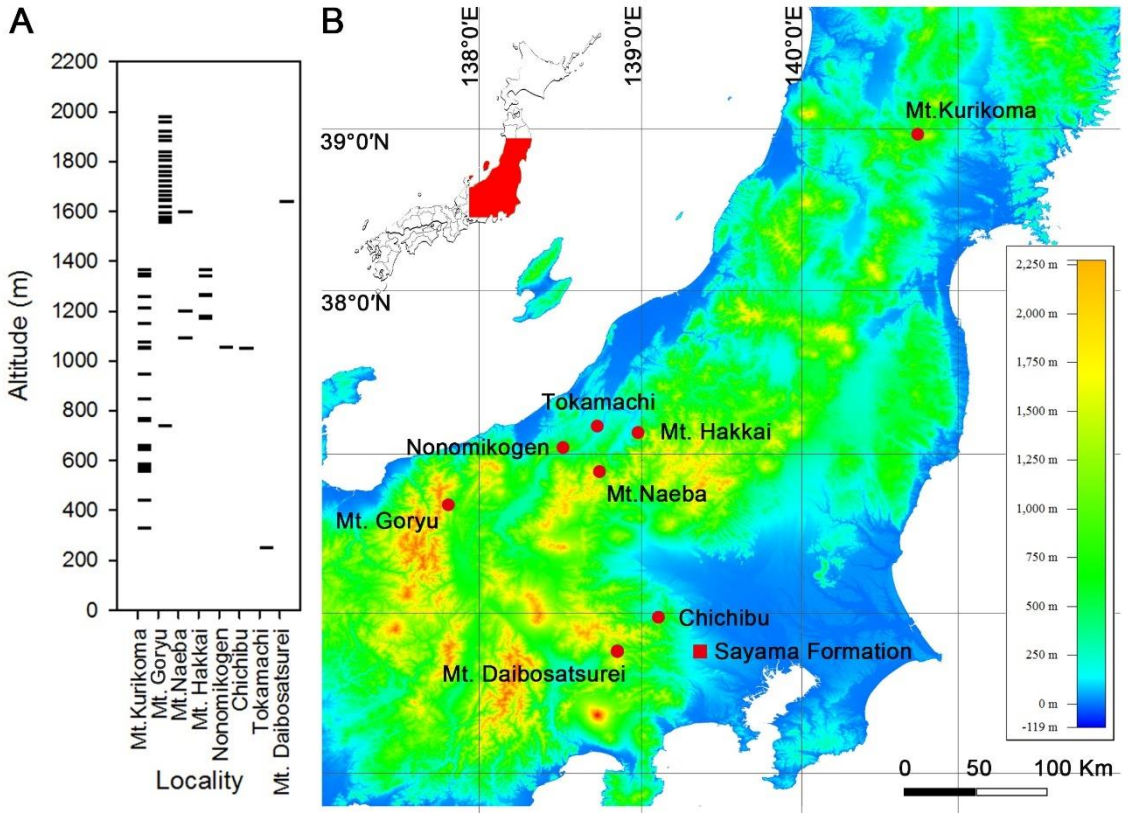

Figure 3.1-1 Map showing the sampling sites for extant and fossil leaves of *Fagus crenata*. (A) Altitude information of modern sampling sites from eight localities. (B) Eight localities where extant leaves of *Fagus crenata* were collected (circles) and one fossil site of the Lower Pleistocene Sayama Formation in Sayama Hill where fossil leaves of *Fagus crenata* were collected (square). The original map was downloaded from Consortium for Spatial Information (CGIAR-CSI; http://www.cgiar-csi.org/).

3.1.2.2 Fossil materials

I selected 30 fossil leaves of *Fagus crenata* from the same leaf fossil bed with the fossil *Quercus gilva* leaves I used in section 2.1 from the Lower Pleistocene (Calabrian) Sayama Formation in the Sayama Hills, western Tokyo (Figure 3.1-1), which has been introduced in 2.2.2. The age of these fossil leaves is constrained to between 1.55 and 1.65 Ma. All the *Fagus crenata* fossil leaves were collected within the thickness of 10 cm in the sediment showing rapid and continuous fluvial sedimentation. Thus I considered that

our fossil materials came from the same age.

3.1.3 Method

3.1.3.1 Cuticular photography

I treated the fossil leaves of *Fagus crenata* (Figure 3.1-2) with 20% HCl for about six hours to remove calcareous matters. Then, the leaves were washed until they became neutral. For each leaf, I cut a small piece roughly along the midvein and two adjacent, secondary veins in the central part of the leaf. I then moved the piece onto a glass slide with the lower epidermis facing up and enclosed it with glycerin. I observed the slide under a confocal laser microscope (Zeiss LSM510) linked to a Zeiss camera (AxioCam HRc). Five cuticular fields (0.086 mm^2) were photographed of each fossil leaf under fluorescence (DAPI).

I chose mature, extant leaves of *Fagus crenata* for cuticular photography and cut a small piece for each leaf in the same manner as for the cuticular examination of fossil leaves. I macerated the cut pieces of leaves using a 1:1 solution of 36% CH_3COOH and 30% H_2O_2 for approximately 6 hours. After washing them with water, I made slides following the same method used for the fossil leaves and then observed the slides under a fluorescence microscope (Zeiss Axioplan 2). Three cuticle fields from each leaf were captured by a Zeiss AxioCam camera linked to the microscope. The size of each image was 0.038 mm^2.

3.1.3.2 Sorting of sun and shade leaves in the fossil assemblage

According to former studies, the stomatal frequency of sun leaves is commonly higher than shade leaves (Kürschner, 1997; Kouwenberg et al., 2007; Lake et al., 2002). Because the difference of stomatal frequency between sun and shade leaves significantly affects CO_2 reconstruction, it is necessary to distinguish sun and shade leaves in the fossil leaf samples. Previous studies proved that the undulation of epidermal cells can be used to

distinguish sun and shade leaves (Kürschner, 1997; Metcalfe and Chalk, 1979). Undulation index (UI) (Kürschner, 1997; Metcalfe and Chalk, 1979) is used to describe the pattern of anticlinal walls of epidermal cells as follows:

$$UI = \frac{Ce}{Co} = \frac{Ce}{2 \times \pi \times \sqrt{\frac{Ae}{\pi}}}$$

Equation 3.1-1

UI (dimensionless) represents the undulation index, while Ce (μm) the circumference of the cell, Co (μm) the circumference of the circle with the same area as the cell, and Ae (μm^2) the area of the cell. The UI is the ratio of the measured epidermal cell circumference and the circumference of a standard geometrical object, a circle with the same area as the cell (Kürschner, 1997). For both sun and shade leaves, 17 trees of different altitudes from the eight sampling sites, ten leaves for each tree, and one cell representative of each leaf were examined. A total of 340 cells were measured to calculate UI by using the software package "ZEN lite" to clarify the difference between sun and shade morphotypes.

3.1.3.3 Stomatal frequency calculation

For both extant and fossil leaves, stomatal density and stomatal index were calculated based on the captured cuticular images. Stomatal density (SD) is the number of stomata per mm^2 on the leaf surface, and stomatal index (SI) is the proportion of stomata to the total number of epidermal cells (Salisbury, 1928) (Equation 2.1-1 in 2.1.2.3). Stomatal and epidermal cells were counted using the software package "ZEN lite" based on the cuticular images. For modern samples, the SD and SI for each tree were calculated as the mean of 30 counts per tree.

3.1.3.4 Calibration curves between stomatal frequency and CO_2

To build the correlation between stomatal frequency of *Fagus crenata* and CO_2, the CO_2 of each sampling spot was calculated by using Equation 2.2-1 in 2.2.3.3 (Jones, 1992). To get the accurate T data of each site, relationships between altitude and temperature of

each modern sampling locality are necessary. Based on 1 km mesh climate data (1980 to 2010) from National Land Numerical Information (http://nlftp.mlit.go.jp/ksj/,), I built relationships between altitude and temperature of different modern sites. Based on these relationships, the mean annual temperature of sea level and of the different spots of eight sites can be calculated. The CO_2 (p2) of each spot can be calculated by applying these T results, altitude, present CO_2 (p1) (41.4 pa, see https://www.CO_2.earth/), and other parameters into Equation 2.2-1. The calculated atmospheric CO_2 was believed to reflect the true atmospheric pCO_2 in the field (McElwain, 2004). Then, calibration curves between stomatal frequencies and pCO_2 for *Fagus crenata* can be constructed based on extant samples by SigmaPlot v.12.5.

3.1.3.5 Paleo-CO_2 and vertical transportation of fossils

The stomatal frequency of the fossil materials was analyzed and applied to the calibration curves prepared using the extant field materials to estimate paleo-CO_2 variation range. The estimated paleo-CO_2 variation range along with the paleotemperature derived from LMA (284 K, unpublished data) will be applied into Equation 2.2-1 in 2.2.3.3 to estimate the paleoaltitude difference (H), which is the vertical transportation distance of fossil leaves.

3.1.4 Results

3.1.4.1 Criterion for separating sun and shade leaves

For modern *Fagus crenata* leaves, the anticlinal walls of epidermal cells in sun leaves are straight to slightly curved, and those in shade leaves are characterized by a U-shaped undulation with shallow to deep amplitude (Figure 3.1-2Fig. 3.1-2). Our results indicate that shade leaves have a higher undulation index than sun leaves. Shade leaves have a UI of over 0.9, while sun leaves have a UI of below 0.7, and both leaf types share a UI of 0.7-0.9 as a transitional zone (Figure 3.1-3). Most of our fossil leaves yielded a UI lower

than 0.7, indicating the dominance of sun leaves. Since shade leaves occur rarely in the fossil assemblage and mixed use both of sun and shade leaves causes a large error in estimating paleo-CO_2, I excluded shade leaves from this research. I chose fossil leaves with a UI less than 0.7 for stomatal frequency analysis to compare with modern sun leaves. Fossil leaves with a Ul of more than 0.7 and those without obscure anticlinal walls were excluded. Finally, thirty fossil sun leaves were used for detecting stomatal frequency variation.

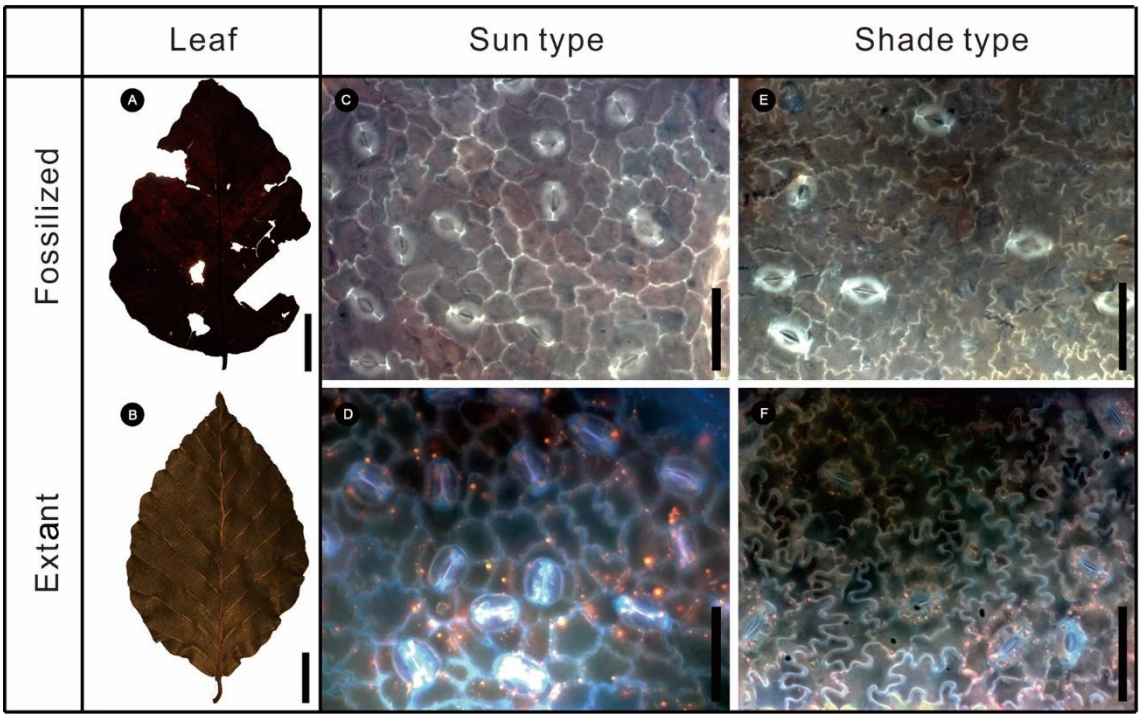

Figure 3.1-2 Leaves (bar = 1 cm) and cuticular images (bar = 0.05 mm) of extant and fossil *Fagus crenata*

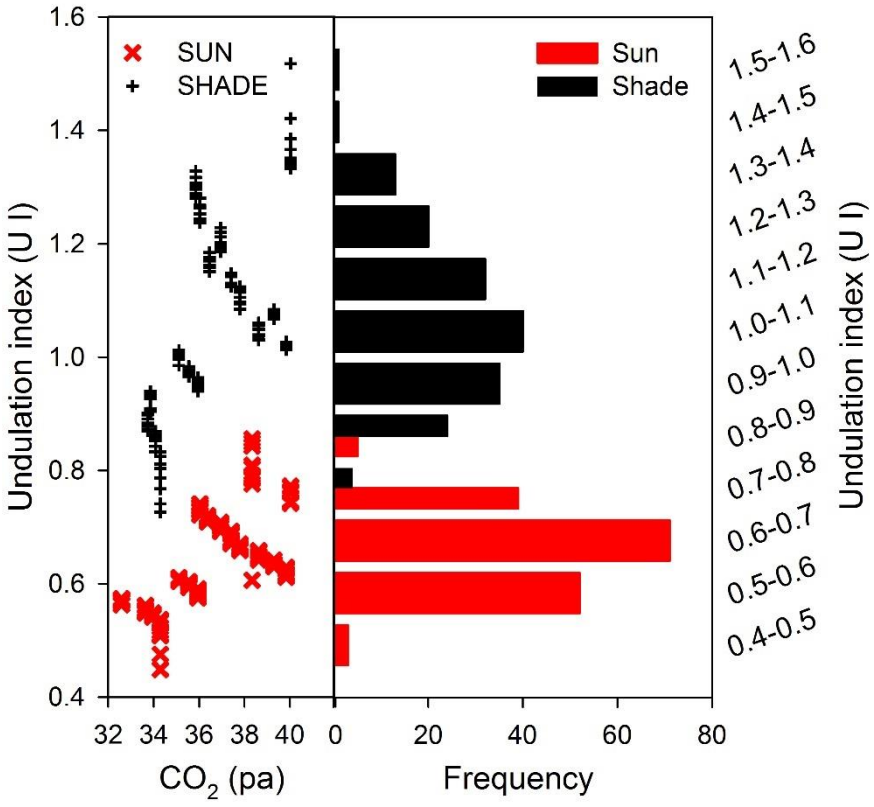

Figure 3.1-3 UI results of modern sun and shade leaves of *Fagus crenata*.

3.1.4.2 Temperature calculation of different sampling sites for modern materials

The relationships between temperature and altitude of each modern sampling sites (p<0.0001) are shown in Figure 3.1-4. The CO_2 of each sampling sites can be calculated from the altitude information of the sampling sites (Figure 3.1-1) from different localities.

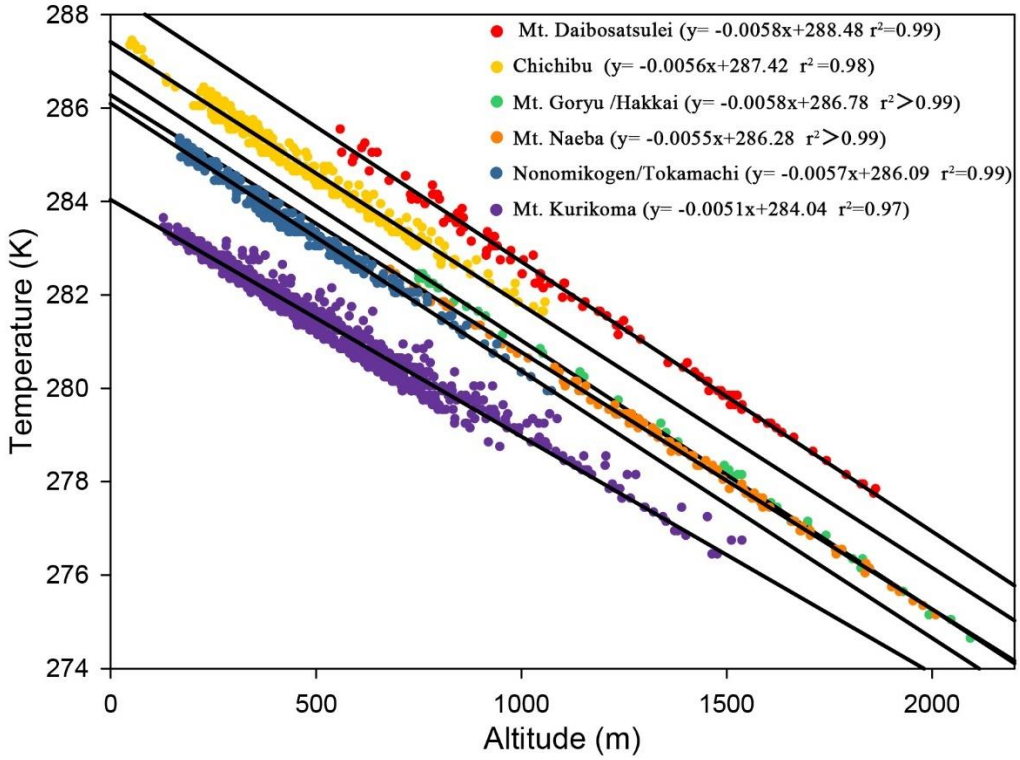

Figure 3.1-4 Relationship between temperature and altitude of eight sites for extant materials

3.1.4.3 Relationship between stomatal frequency and CO_2

I plotted the average value with standard deviation of stomatal frequency from each modern tree at the CO_2 value of its sampling site and then drew the linear regression curves for three (average, maximum, and minimum) values of stomatal frequency, respectively (Figure 3.1-5;Table 3.1-1). All of the curves showed a significant negative linear relationship ($p < 0.0001$).

Table 3.1-1 Relationships between CO_2 and various stomatal frequency based on extant sun leaves of *Fagus crenata*

		Equation	No.	r^2
SI	Max	SI = -0.61×CO_2+ 33.76	Equation 3.1-2	0.53
	Average	SI = -0.61×CO_2+ 30.89	Equation 3.1-3	0.62
	Min	SI = -0.55×CO_2+ 28.10	Equation 3.1-4	0.57
SD	Max	SD = -24.05×CO_2+ 1214.46	Equation 3.1-5	0.39
	Average	SD = -23.21×CO_2+1134.79	Equation 3.1-6	0.46
	Min	SD =-21.45×CO_2+ 1027.427)	Equation 3.1-7	0.45

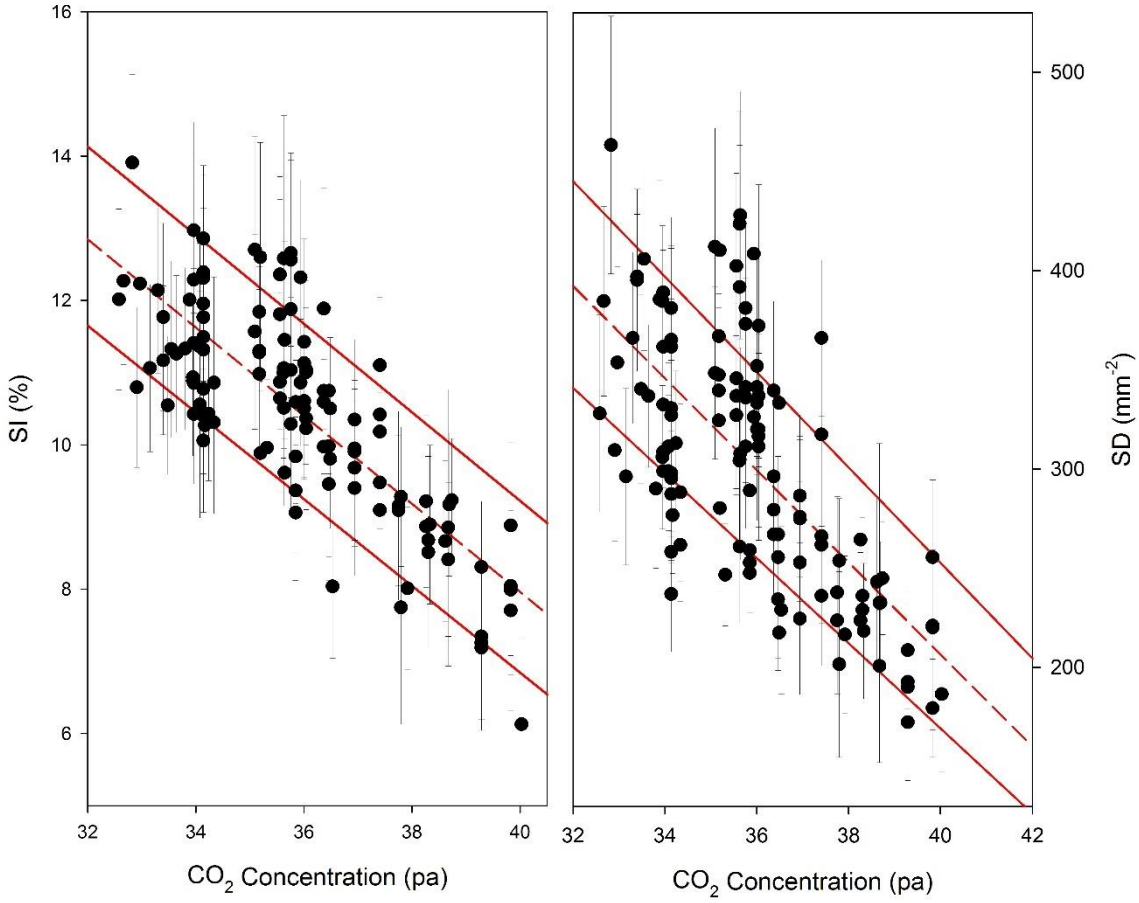

Figure 3.1-5 Relationships between CO_2 and various stomatal frequencies based on extant sun leaves of *Fagus crenata* (Error bar = 1σ). Upper solid line: maximum stomata frequency; dash line: average stomata frequency; lower solid line: minimum stomata frequency.

3.1.4.4 Stomatal frequency of fossil leaves

The calculated SI of fossil leaves varies from 7.12% to 12.41%, with an average of 8.20%, and the calculated SD of fossil leaves varies from 234.9 mm^{-2} to 448.84 mm^{-2}, with an average of 251.7 mm^{-2} (Figure 3.1-6, Table 3.1-1).

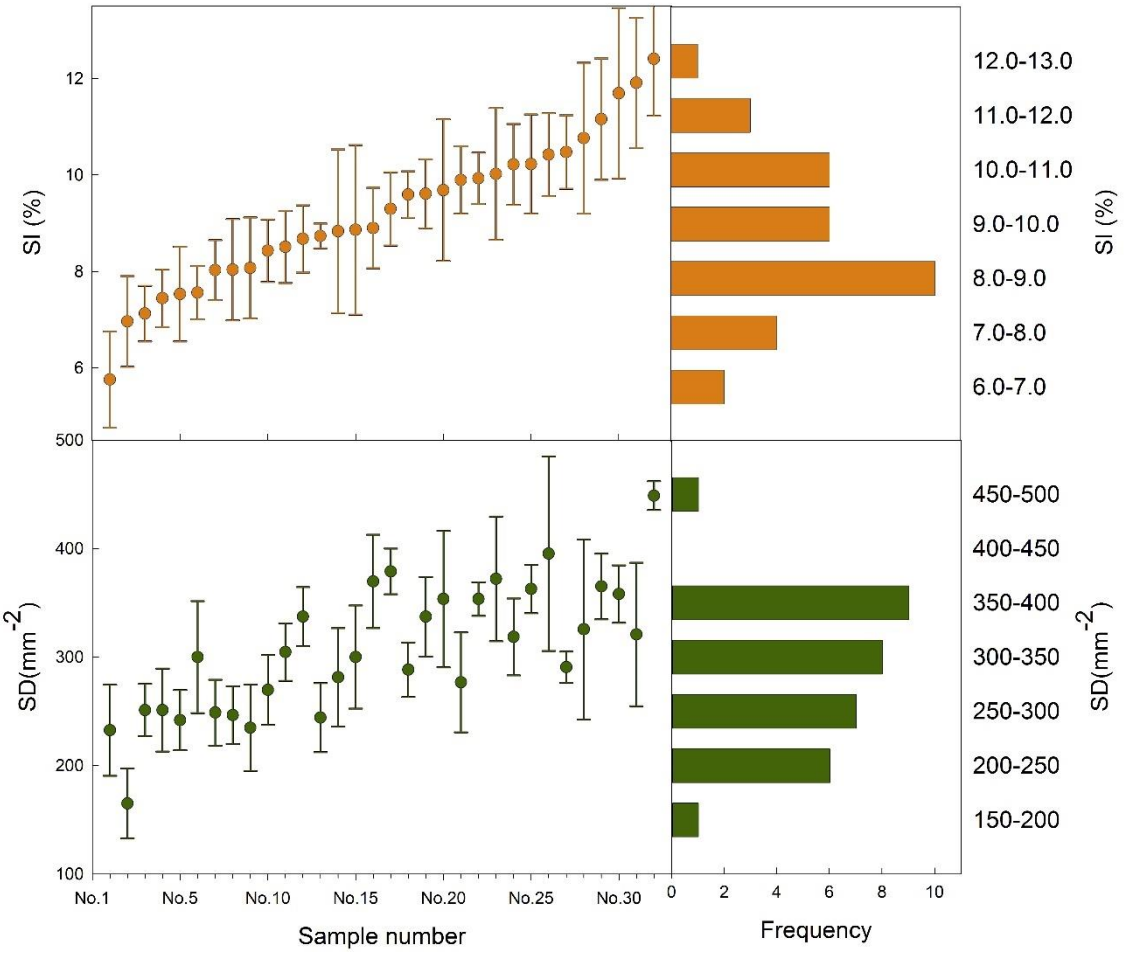

Figure 3.1-6 SI and SD of fossilized *Fagus crenata* from the Sayama Formation along with their frequency distribution histogram (error bar = 1σ)

3.1.4.5 Reconstructed paleo-CO_2 and altitudinal transportation range of fossil materials

I inserted the maximum stomatal frequency values of our fossil materials into Equation 3.1-2 and Equation 3.1-5 (Table 3.1-1) and the minimum stomatal frequency values of our

fossil materials into Equation 3.1-4 and Equation 3.1-7 for CO_2 variation range estimation. I did not use Equation 3 and 6 because they were derived from the average values of ten leaves of each individual while our fossil data were based on a single leaf. Applying the maximum and minimum values into Equation 2.2-1 in 2.2.3.3 and 6 may cause an overestimation of CO_2 variation range because the minimum and maximum values may deviate from the average level. Thus, I used Equation 3.1-2, Equation 3.1-4, Equation 3.1-5,Equation 3.1-7 in this research to estimate CO_2 variation range. CO_2 partial pressure was translated to CO_2 concentration (ppmv) using Equation 3.1-8 (Kürschner et al., 2008) as follows.

CO_2 concentration (ppmv) = (CO_2 partial pressure/101325) × 10^6

Equation 3.1-8

Based on the stomatal data of our fossil materials, the CO_2 range was calculated as 35.00-39.60 pa (345-390 ppmv) based on SI data and 31.83-36.95 pa (314-364 ppmv) based on SD data. Applying the results of CO_2 variation range along with other parameters into Equation 2.2-1, the range of altitudinal transportation was calculated as 1028 m and 1234 m, for SI and SD data respectively.

3.1.5 Discussion

3.1.5.1 Sun leaf versus shade leaf

As aforementioned, distinguishing sun leaves from shade leaves is necessary when using stomatal frequency as the proxy for paleo-CO_2 estimation (Hu et al., 2015; Kürschner, 1997). Epidermal anticlinal wall pattern is an important key characteristic that can be used to distinguish sun and shade leaves (Dilcher, 1974; Kürschner, 1997). Our observations on modern leaves indicated that the anticlinal walls of epidermal cells in sun leaves were straight to slightly curved while those in shade leaves had a U-shaped undulation of shallow to deep amplitude (Figure 3.1-2). These features are consistent with previous results based on *Quercus* (Hu et al., 2015; Kürschner, 1997). By using UI as the

indicator of leaf type, most of our fossil materials have been classified as sun leaves. Such dominance of sun leaves in a fossil assemblage has also been observed in a former study of fossilized oak leaves (Kürschner et al., 1996), which showed only 10% of the fossilized leaves represent distinct shade leaves. This dominance of sun leaves may be caused by two advantages of sun leaves in the process of forming leaf assemblages. First, the selective transport by wind favors the preservation of sun leaves, while shade leaves tend to be trapped within the trunk space of the forest diminishing their dispersal and chances for fossilization. Second, the thicker mesophyll and cuticle in sun leaves delay their bacterial degradation (Roth and Dilcher, 1978; Spicer, 1981).

3.1.5.2 Relationships between stomatal frequency and CO_2

To calculate the CO_2 level, I need to establish a relationship between stomatal frequency and CO_2 of the nearest living relative of a fossil taxon (Beerling and Royer, 2011; Royer, 2003). As our studied fossil leaves show a close similarity of morphology and venation architecture with modern *Fagus crenata* (Ito et al., 2017), modern stomatal frequency data is applied to our fossil leaves. Our results indicated that the leaf stomatal frequency of *Fagus crenata* responds sensitively to the CO_2 gradient (Figure 3.1-5), which exhibits a linear relationship between stomatal frequency and CO_2 (Royer, 2003; Rundgren and Beerling, 1999; Woodward and Williams, 1987).

In this study, both SI and SD of *Fagus crenata* showed a negative relationship with CO_2 change, which is consist with the results derived from the seedlings grown study of *Fagus crenata* at different CO_2 levels (Hirano et al.).However, the lower correlation coefficient (r^2) of the SD-CO_2 relationship (Figure 3.1-5) indicated it might be affected by the other factors. The lower r^2 may ascribe dependence of SD on the size and/or spacing of epidermal cells during leaf expansion, which is affected by water stress, temperature, and irradiance level, as well as air humidity, while SI is less affected by environmental factors other than atmospheric CO_2 (Kürschner, 1997; Kouwenberg et al., 2007; Kürschner et al., 1996; Salisbury, 1928; Woodward and Williams, 1987). For this

reason, the paleo-CO_2 derived from SI is more promising (Hu et al., 2015; Kouwenberg et al., 2007). However, if SI cannot be measured due to the poor quality of the fossil cuticle and the inability to recognize the epidermal cells clearly, the paleo-CO_2 reconstructed from SD data will also be instructive (Kouwenberg et al., 2007).

3.1.5.3 Paleo-CO_2 during the Early Pleistocene

The variation ranges of SI and SD for our fossil leaves are 7.1-12.4% and 234.9-448.8 mm^{-2}, respectively. Because such large ranges are not observed in our modern leaf samples collected from the same CO_2 level (Figure 3.1-7), I can presume that the fossil leaf assemblage includes leaves which developed under different CO_2 levels. The maximum CO_2 level reconstructed from our fossil leaves does not always represent sea-level CO_2, this is because it is uncertain whether the lowermost distribution of *Fagus crenata* was at the altitude of fossil deposition and situated in the sedimentary basin along the coast. Thus, the past sea-level CO_2 is assumed to be almost the same or higher than the CO_2 reconstructed from our fossil leaves.

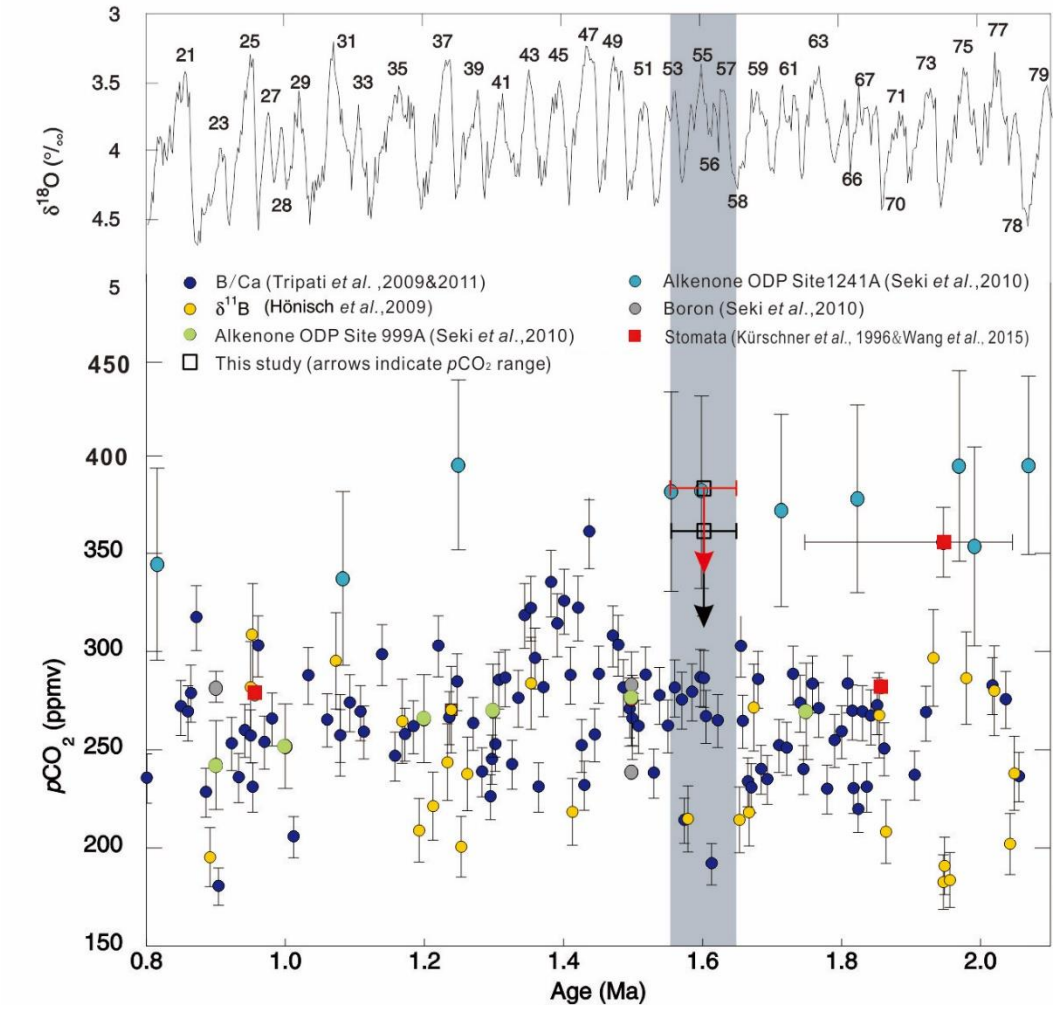

Figure 3.1-7 Reconstructed paleo-CO_2 during the Early Pleistocene compared with the marine $\delta^{18}O$ record (Lisiecki and Raymo, 2005). Vertical error bar = 1σ; horizon error bar = age range; arrows represent the variation range of our CO_2 data.

Our paleo-CO_2 result is higher than most of the previous ones reconstructed by different methods for the same age (Figure 3.1-7). Boron and Alkenone data of foraminifera from ODP site 999A indicates stable CO_2 around 277 ppmv during 1.5 to 1.65 Ma, while the results from ODP site 1241A are around 433 ppmv (Seki et al., 2010), which is comparable to our data. However, because of the position of site 1241A within the upwelling cell of the eastern equatorial Pacific, the high values at site 1241A relative to Site 999A was ascribed to a contribution of upwelled deeper water with higher aqueous

CO_2 (Seki et al., 2010). The paleo-CO_2 based on B/Ca data (Tripati et al., 2011) and $\delta^{11}B$ (Hönisch et al., 2009) varies between 200-300 ppmv during 1.5-1.7 Ma.

The stomatal index of oak leaves (Kürschner et al., 1996) yields a CO_2 level of 358 ppmv at 1.8-2.0 Ma, while the *Metasequoia* leaves at around 1.85 Ma and 0.95 Ma from Japan indicate a 280 ppmv level similar to the preindustrial level (Wang et al., 2015). Comparing to these published studies, CO_2 data of this research may indicate a relatively high CO_2 level during a transient period in the Early Pleistocene. The position of the fossil leaf bed below a marine bed suggests a marine transgression and rich evergreen broadleaved tree elements in the leaf assemblage together indicate an interglacial environment. Thus, our high CO_2 result during 1.66-1.54 Ma can be correlated with the transient interglacial phases namely MIS 57, MIS 55, or MIS 53 recorded by the marine $\delta^{18}O$ (Lisiecki and Raymo, 2005) (Figure 3.1-5).

3.1.5.4 Vertical transportation of fossil leaves

The paleo-CO_2 variation estimated from the fossil leaves indicated altitudinal transportation of 1028 m based on SI data and 1234 m based on SD data. The distribution of modern *Fagus crenata* leaves along the riverbed of a mountain in central Japan demonstrated their altitudinal transportation from the areas at least 600 m higher than the place of deposition (Ozaki, 1969). Our results showed a larger altitudinal transportation range than this record, which may have been controlled by factors such as steep slope and strong current beneficial to the altitudinal transport of plant organs (Steart et al., 2006; Teodoridis et al., 2017). Figure 3.1-6 showed that the SI distribution of the fossilized leaves has a peak around 8.0% to 9.0%, which skews to the lower altitude than the median (9.21%). This difference may indicate that the fossil assemblage consisted mainly of the leaves from trees near the place of fossil deposition, whereas a small sample of leaves was transported from a higher altitude. However, the distribution of SD from fossilized *Fagus crenata* did not show as clear a regularity as SI distribution, and some samples with lower SI value (around 10%) indicated a higher SD value (350-400 mm^2) (Figure

3.1-6). This difference suggests fossilized SD data may be affected by the other factors, which is consistent with the lower r^2 of the SD-CO_2 relationship derived from modern materials (Figure 3.1-5).

Fossil taxa which occurred together with *Fagus crenata* represent different climate types, including cool-temperate elements such as *Betula glossa*, *Cercidiphyllum japonicum*, and *Aesculus turbidata*; warm-temperate elements such as *Ginkgo biloba*, *Cercis chinensis*, *Liquidambar formosana* and *Cunninghamia lanceolata* var. *konishii*; and subtropical elements such as *Quercus gilva*, *Cinnamomum yabunikkei*, *Albizzia kalkora*, and *Lagerstroemia indica* (Ito et al., 2017). This mixture of different elements in the fossil assemblage indicates they may have originated from different altitudes with different temperatures. Moreover, pollen grains recognized from the same sedimentary layer include abundant *Picea* (Nirei and Takegoshi, 2007), which is distributed over 1000 m a.s.l. in central Japan (Takahashi, 1962), suggesting its transportation from a higher altitude to the basin.

Based on our results of leaf transportation, during the Early Pleistocene, the paleoaltitude of the Kanto Mountains, which provided sediments into the Sayama Formation, was over 1000 m a.s.l. According to previously published studies, mountain ranges with 2,000 to 3,200 m peaks in central Japan, e.g., the Echigo Mountains (Kazaoka, 1986) and the Hida Mountains (Oikawa, 2003), began to uplift during the late Pliocene, while the Akaishi and the Kiso Mountains began to uplift in the late Early Pleistocene (Suganuma et al., 2003). The pebble-cobble layers frequently interfingered in the Sayama Formation (Ueki and Sakai, 2007) indicate the Kanto Mountains at the west of Sayama Hill continued to uplift during the Late Pliocene and Early Pleistocene. All of these studies support the assumption that a mountain higher than 1000 m a.s.l. existed along the sedimentary basin, and that some elements in the Sayama Formation fossil assemblage has experienced altitudinal transportation. Research on the process of mountain uplift have been based mainly on lithological changes in the surrounding sedimentary basin and the dating of minerals within the mountain body. Because the

altitudinal change of mountain was difficult to detect, our results demonstrate the potential availability of stomatal evidence as an altimeter to clarify the process of mountain uplift.

3.1.5.5 Implications for paleoclimate interpretation

Paleoclimate has been reconstructed through fossil flora based on an assumption in that all the taxa composing the fossil flora had coexisted at the same altitude (Mosbrugger and Utescher, 1997; Spicer et al., 2009; Wilf, 1997; Wing and Greenwood, 1993). However, our study certified that a fossil assemblage includes taxa that might be transported downwards from much different altitudes. Those taxa from the higher elevation obviously represent a cooler climate than the others.

This phenomenon has been realized in paleovegetation reconstructions based on pollen assemblages with nearly indistinguishable local and regional pollen (Prentice, 1985; Prentice et al., 1987; Sugita, 1994). However, plant macrofossil assemblages have commonly been believed to be relatively autochthonous, so the possibility of long-distance transportation was ignored (Cappers, 1993; Ferguson, 1995). This belief can sometimes cause problems when applying the coexistence approach (Mosbrugger and Utescher, 1997) for paleoclimate reconstruction. In this approach, taxa with climatic requirement ranges exceeding the coexistence interval of most assemblage components were excluded from paleoclimatic reconstruction as “outliers” (Jacques et al., 2011; Mosbrugger and Utescher, 1997). These outliers are ascribed to misidentification, inaccuracy of modern climate references, and/or the change of distribution (e.g., relicts) through geological time (Mosbrugger and Utescher, 1997). Results of our research suggest that such cold-loving outliers were possibly transported from higher altitudes than the altitudinal range of coexistence of the other assemblage components. Meanwhile, thermophilous outliers with their colder limit of distribution at a warmer condition than the coexistence range are often excluded from the paleotemperature reconstruction. However, these outliers should indicate a more accurate paleotemperature at altitude near

the place of fossil deposition than the area of coexistence range, which changes depending on the components transported from a higher altitude. Leaf margin analysis can also be affected by the altitudinal transportation of leaves because toothed species are more common in higher altitudes (Momohara, 1997). Results may be affected in both paleotemperature reconstruction and paleo-CO_2 reconstruction. Paleo-CO_2 data based on the stomatal frequency of *Quercus guyavifolia* (late Pliocene, south-western China) were lower than the data estimated from other proxies, which can be explained by the high paleoaltitude of the living environment of fossil leaves (Hu et al., 2015). With this data in mind, Momohara et al. (2017) have reconstructed the paleotemperature based on the most thermophilous taxon among the fossil assemblage components, which are believed to inhabit only the lowermost altitude near the site of fossil deposition and can avoid the effect of transportation from a higher elevation. Therefore, further efforts for crosscheck by the stomatal frequency of plural taxa are necessary to understand the effect from leaf transportation and achieve more accurate and reliable estimations of temperature gradients in the altitudinal range of habitats of fossil assemblage components.

3.2 **Middle and Late Holocene altitudinal distribution limit changes of *Fagus crenata* forest indicated by stomatal evidence**

3.2.1 Introduction

The influence of present climate changes on forest ecosystems is a major public concern (Canziani, 2001; Walker et al., 1999). Numerous studies suggested the migration of major canopy tree species to northern and/or higher altitude areas under the present climate scenarios (Altman et al., 2018; Coops et al., 2016; Huntley et al., 1995; Sykes et al., 1996; Uchijima, 1992). Sensitivity of plant distribution to millennium-scale climatic fluctuations of the Holocene has been demonstrated by the reconstruction of timberline

fluctuations (Avnaim-Katav et al., 2019; Bakker et al., 2017; Feurdean et al., 2016; Kearney and Luckman, 1983; Marsicek et al., 2018; Mayewski et al., 2004; Tinner and Kaltenrieder, 2005). Among the Holocene climate stages, the mid-Holocene is well known for a climate warmer than the present, which can provide evidence of plant distribution changes as an analog in the near-future climate conditions with the present global warming. Sensitivity of plant distribution to millennium-scale climatic fluctuations of the Holocene has been demonstrated by the reconstruction of timberline fluctuations (Avnaim-Katav et al., 2019; Bakker et al., 2017; Feurdean et al., 2016; Kearney and Luckman, 1983; Marsicek et al., 2018; Mayewski et al., 2004; Tinner and Kaltenrieder, 2005). Among the Holocene climate stages, the mid-Holocene is well known for a climate warmer than the present, which can provide evidence of plant distribution changes as an analog in the near-future climate conditions with the present global warming.

In this study, I conducted an initial attempt at detecting the change of altitudinal distribution limit of *Fagus crenata* forest in a fossil locality during the Middle to Late Holocene, using stomatal analysis. This can help understand the response of *Fagus crenata* to climate fluctuations. Although the distribution change of *Fagus crenata* forests has been investigated using pollen analysis (Kito and Takimoto, 1999; Tsukada, 1982), its altitudinal changes have been difficult to detect based on airborne pollen, even comparing data at different altitudes (Morita and Fujiki, 1997). Thus, I collected fossilized *Fagus crenata* leaves from different horizons of a Holocene fossil locality in northern Japan, located near the upper distribution limit of modern *Fagus crenata* in the region. Based on stomatal analysis of these fossil leaves, I reconstructed atmospheric paleo-CO_2 concentration and evaluated variation trend of the altitudinal distribution range of *Fagus crenata*. According to the results, I discussed the climate factors that constrained the altitudinal distribution of *Fagus crenata* during the Middle to Late Holocene.

3.2.2 Materials and methods

3.2.2.1 Geological setting

Mt. Kurikoma (1627 m a.s.l.) is a volcanic mountain in the central part of the Ou Mountains in the northern Honshu Island, Japan, where the major volcanic activities ceased at ca. 0.1 Ma (Fujinawa et al., 2001). Mountain zone between ca. 300 and 1300 m a.s.l. in Mt. Kurikoma is occupied by a broadleaved deciduous forest dominated by *Fagus crenata*, while higher altitudes, between ca. 1300 m a.s.l. to the top of the mountain are occupied by subalpine shrubs dominated by *Quercus crispula* and *Menziesia multiflora*are. *Fagus crenata* is distributed up to 1367 m a.s.l. in northwestern ridge of Mt. Magusadake, a west peak of Mt. Kurikoma (Wang et al., 2018a). Our fossil locality (38°58'25.9"N, 140°45'18.2"E, 1080 m a.s.l) is an outcrop of peaty sediment, approximately 5 m in thickness, which has deposited in a peat bog on the northwestern slope of Mt. Kurikoma (Figure 3.2-1). The profile of the peaty sediments comprises mainly undecomposed bryophyte (*Drepanocladus fluitans*) (Wakamatsu and Kiguchi, 2006), occasionally including silt, and sandy peaty silt layers, which are dominant in the upper part of the profile. Three tephra layers are included in the profile, and the uppermost one is To-a tephra dated as AD 915 (Figure 3.2-2) (Wakamatsu and Kiguchi, 2006).

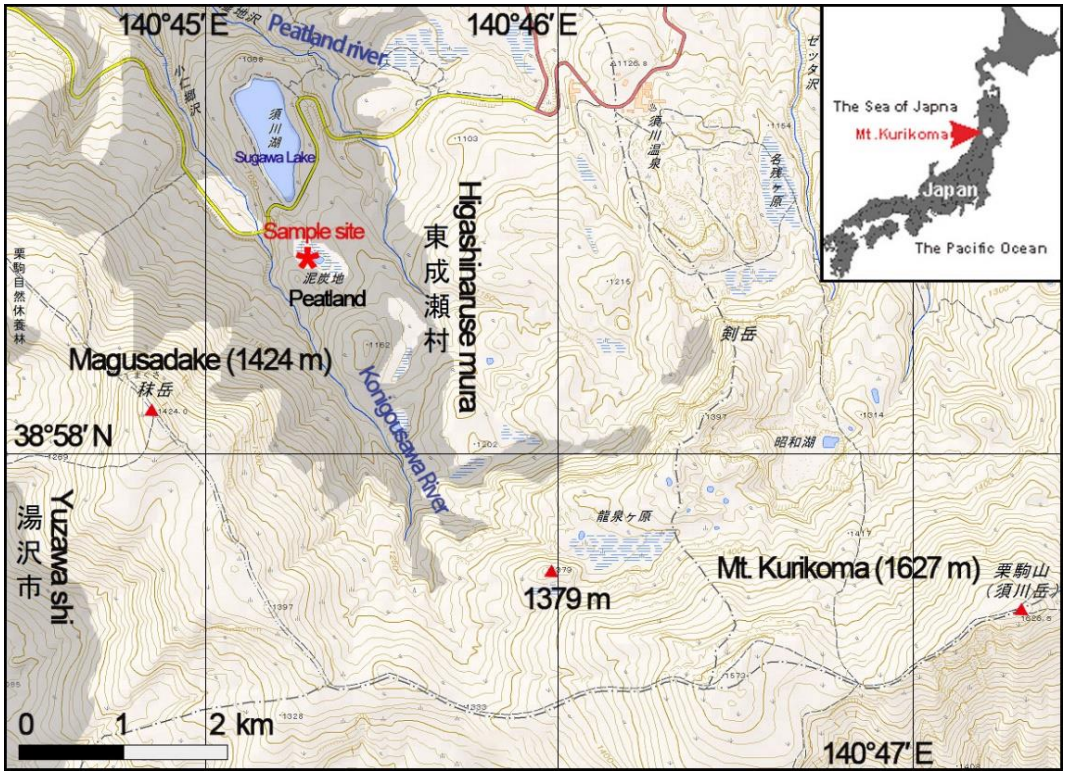

Figure 3.2-1 Geographical position of the sampling site in Mt. Kurikoma, northern Japan. Shaded area in the map shows the distribution area of *Fagus crenata* forest around our fossil site (Report of Vegetation Survey on National Basic Survey on Natural Environment; http://www.biodic.go.jp/). The map is adapted from Geospatial Information Authority of Japan (http://gis.biodic.go.jp/webgis/index.html).

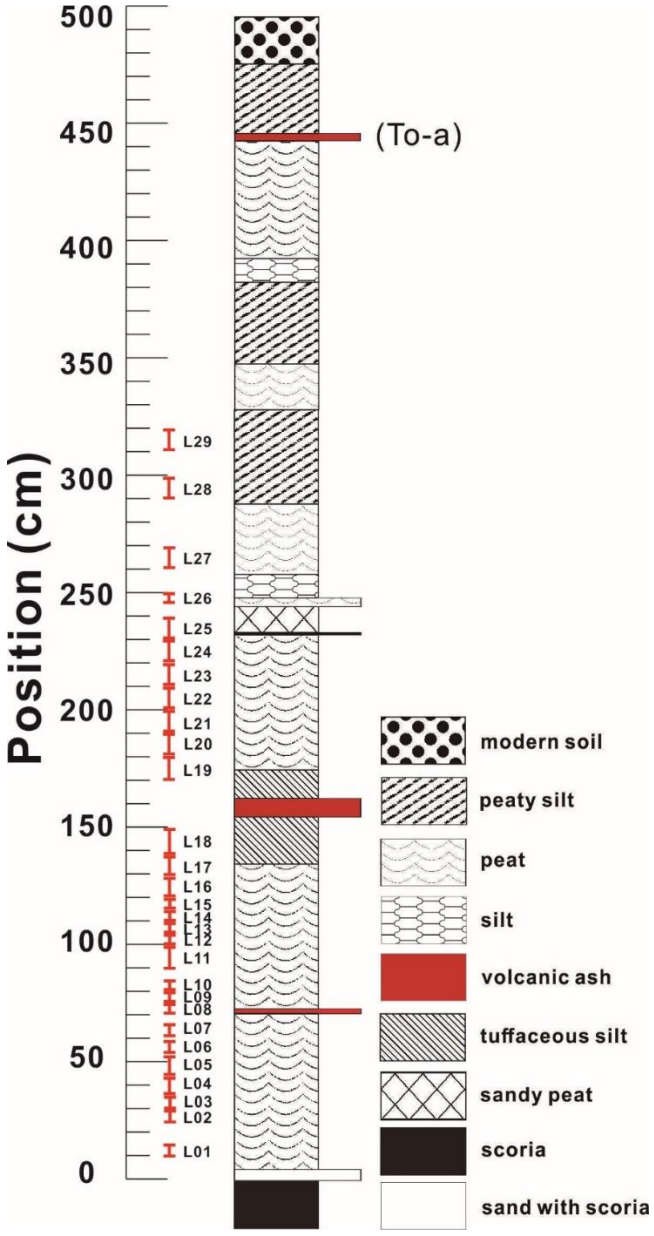

Figure 3.2-2 Geological profile of the sampling site in Mt. Kurikoma, northern Japan.

3.2.2.2 Fossil *Fagus crenata* leaves and age dating

The fossil leaves of *Fagus crenata* were taken from 29 horizons (L01 – L29 inFigure 3.2-2). From each horizon, a block of approximately 50×30 cm^2 with a thickness between 5 and 10 cm was taken, in which 50-150 fossil *Fagus crenata* leaves were included. Fossils from the upper part of the profile were not used for this study because it was not possible to obtain well-preserved fossil leaves. The fossil *Fagus crenata* leaves from L01,

L11, L15, L17, L23 and L29 were dated by accelerator mass spectrometry (AMS) in the Laboratory of Radiocarbon Dating (The University Museum, The University of Tokyo), and calibrated by using the OxCAL4.2 calibration program (Ramsey, 2009) and IntCal13 Radiocarbon Age Calibration Curves (Reimer et al., 2013).

3.2.2.3 Cuticular observation

The collected fossil leaves were washed clean by water. For each leaf, I cut a small piece roughly between two secondary veins in the central part of the leaf, and then sealed it with water, with the lower epidermis facing up. For each fossil leaf, five cuticular fields (0.086 mm^2) were photographed under a fluorescence microscope (DAPI).

For paleo-CO_2 reconstruction, it is necessary to distinguish between the sun leaves and shade leaves in the fossil leaf samples as they present different SI values under the same CO_2 level (Kürschner et al., 2008; Wang et al., 2018a). Sun leaves of *Fagus crenata* are generally dominant in fossil assemblages and can be distinguished easily from the shade leaves based on its less developed undulation of anticlinal walls and noncircular shape of epidermal cells (Wang et al., 2018a). Undulation index (UI, Metcalfe and Chalk, 1979) is used to measure curvature of cell wall and roundness of cell (Equation 3.1-1 in 3.1.3.2). Base on the results of section 3.1.4.1, the UI of modern shade leaves of *Fagus crenata* is over 0.7 (Wang et al., 2018a), I identified fossil leaves with UI below 0.7 as sun type leaves. I selected 17-53 sun type leaves from each layer according to the availability of materials for the stomatal analysis (Table 3.2-1).

Based on the captured cuticular images, the software package “ZEN lite” was used to determine the number of epidermal cells and stomatal complexes (stomatal pore with guard cells) (Equation 2.1-1 in 2.1.2.3). SD was not included in this study because it is more susceptible to other climate factors in addition to CO_2 concentration.

3.2.2.4 SI Variation range of modern *Fagus crenata* leaves

To estimate the altitudinal range of *Fagus* trees that have provided leaves into fossil

assemblage of each horizon, I calculated variation ranges of the SI values of modern *Fagus crenata* sun leaves when leaves from higher altitudes are included. I used SI data based on the study of Wang et al. (2018a) where modern *Fagus crenata* leaves were collected from 14 sites at each ca. 100 m altitudinal interval between 300 and 1400 m a.s.l. in Mt. Kurikoma. The SI variation range that was formed via a combination of SI data from a range of altitudinally different sites provides analogue of fossil leaf assemblage including leaves transported from higher altitude areas. I then established a regression line between the altitudinal range and the corresponding SI range of modern leaves along with prediction interval bands and 95% confidence interval by SigmaPlot (version 14.0), to estimate past altitudinal distribution ranges of *Fagus crenata* based on SI variation ranges in fossil leaf assemblage.

3.2.2.5 Paleo-CO_2 concentration estimation

The stomatal frequency of the fossil materials was analyzed and applied to the published calibration curves (Equation 3.2-1) to calculate the paleo-CO_2 partial pressure (pa) (Wang et al., 2018a), and translated to CO_2 concentration (ppmv) using Equation 3.1-8 (Kürschner et al., 2008) as follows.

$$CO_2\ (pa) = 50.64 - 1.64 \times SI \qquad r^2 = 0.62 \qquad p < 0.001$$

Equation 3.2-1

3.2.3 Results

3.2.3.1 Chronology of the sample layers

Based on age modeling, the median date of our materials was estimated to be between 5298 cal BP and 2530 cal BP, a time span ranging from the late Middle to the early Late Holocene (Figure 3.2-3, Table 3.2-1).

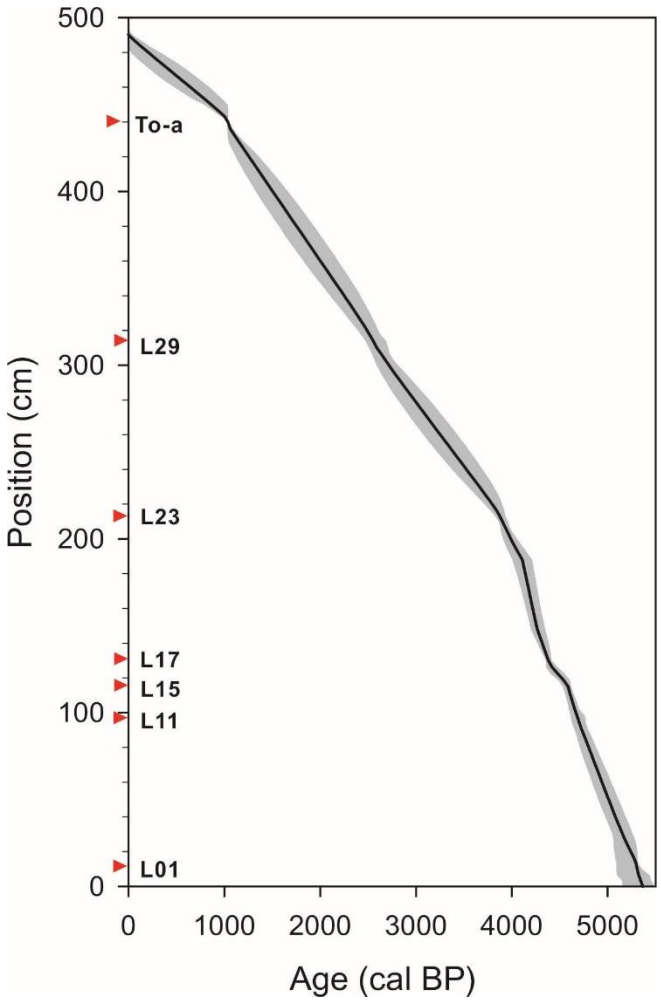

Figure 3.2-3 Time–depth curve based on calibrated ages of fossil *Fagus crenata* leaves (solid line) dated by accelerator mass spectrometry (AMS) and tephra (To-a). The shaded area in the curve indicates 1σ (68% confidence ranges) of calibrated ages. Triangles indicate horizons of fossil leaves dated by AMS.

3.2.3.2 SI variation of modern sun leaves by combining data from different altitudinal ranges

The SI variation of modern *Fagus crenata* leaves at each site is between 3.2% and 5.2%, with an average of 4.1%. I can deduce the possibility of leaf transportation from a higher altitude when the SI variation of a fossil leaf assemblage excess is over 4.1%. The regression line between altitudinal range and the corresponding SI range of modern *Fagus crenata* sun leaves is expressed as follows (Figure 3.2-4):

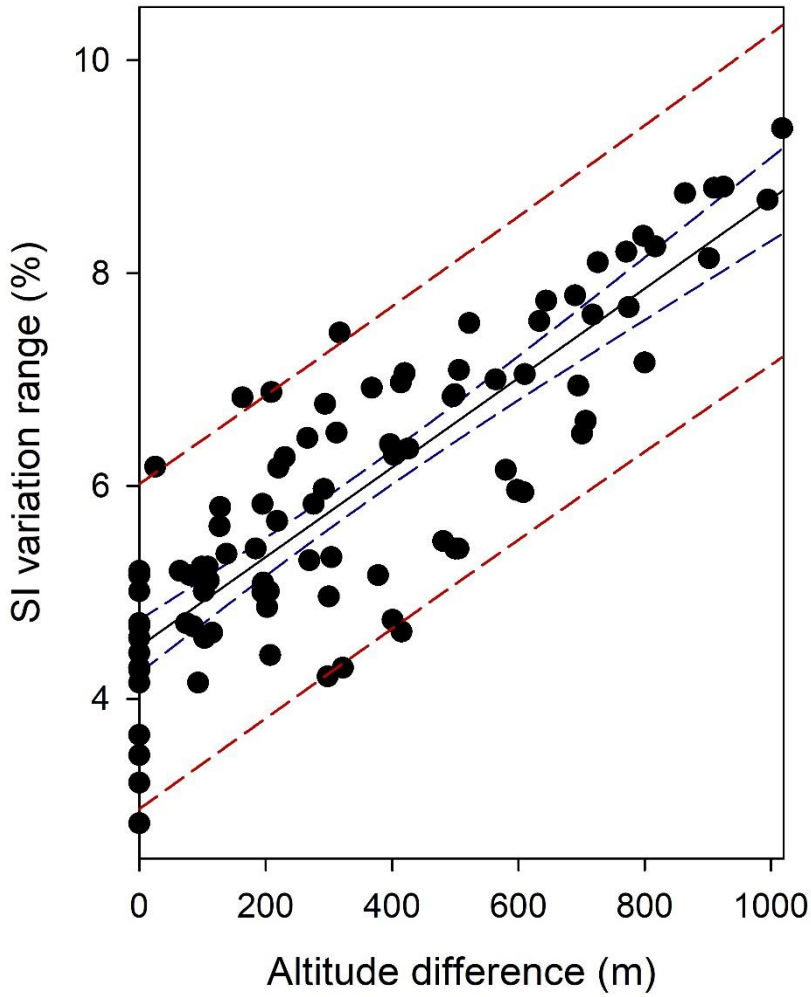

Figure 3.2-4 SI variation range of modern *Fagus crenata* sun leaves mixed from different altitudinal range with liner regression line (black solid line), prediction interval bands (red dash line) and 95% confidence interval (blue dash line).

SI variation range= 0.0042×altitudinal range+4.49 $p<0.0001$ $r^2= 0.72$

Equation 3.2-2

The upper and lower boundaries of prediction interval (Figure 3.2-4) are expressed as follows:

SI variation range= 0.0042×altitudinal range+5.99

Equation 3.2-3

SI variation range= 0.0042×altitudinal range+2.98

Equation 3.2-4

3.2.3.3 SI data of fossil leaves and paleo-CO_2 reconstruction

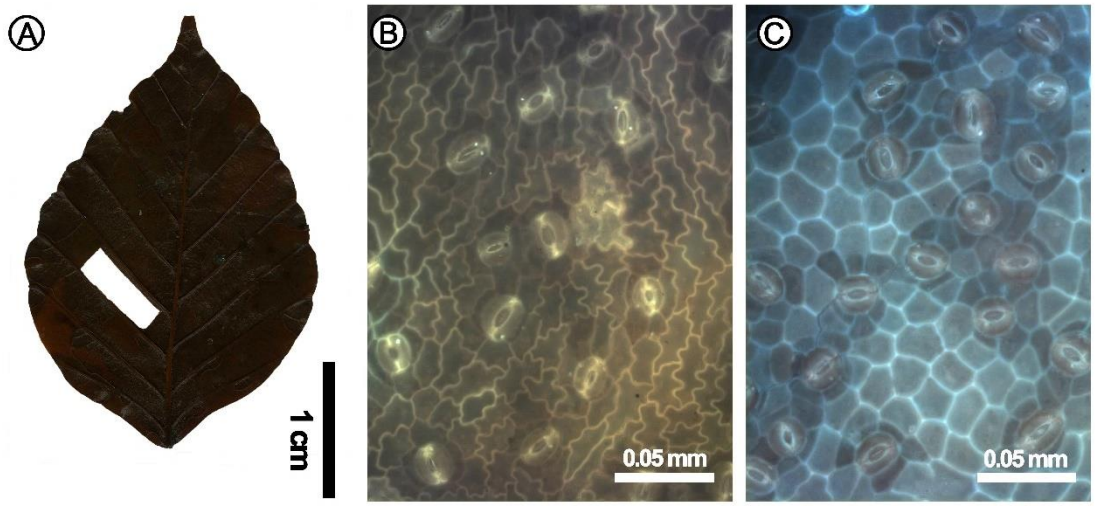

Figure 3.2-5 Leaves and cuticular images of fossil *Fagus crenata*. (A) Cleaned fossil leaf, the incised part is for cuticle observation; (B) Cuticular image of a shade type fossil leaf; (C) Cuticular image of a sun type fossil leaf.

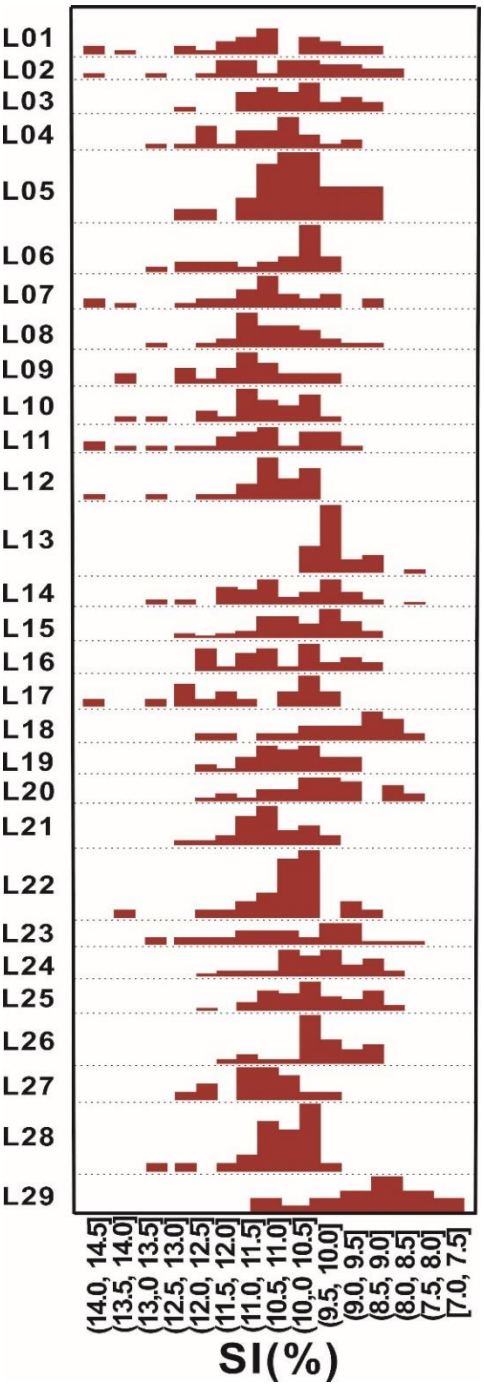

Figure 3.2-6 Frequency of SI data of fossil *Fagus crenata* leaves from each layer.

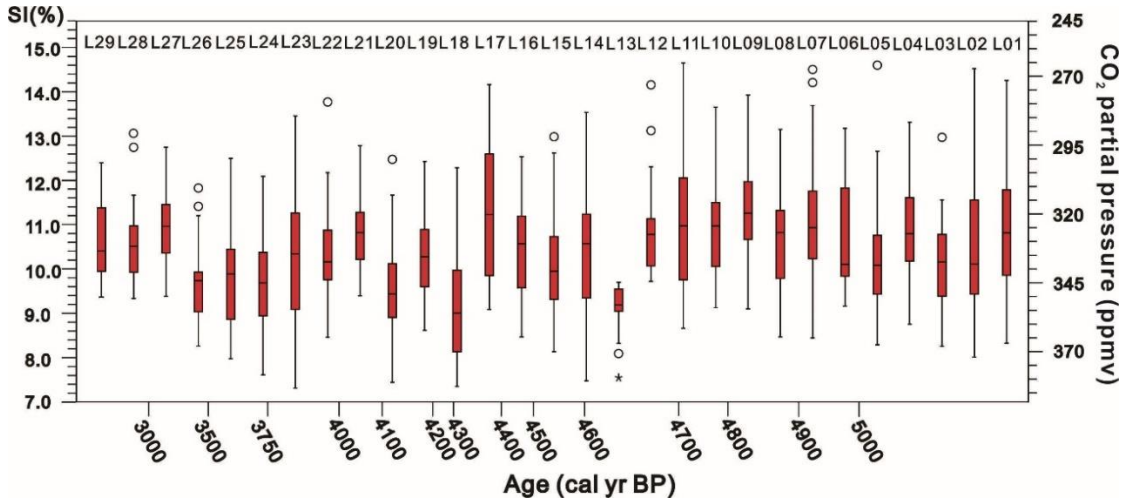

Figure 3.2-7 Turkey boxplot of the SI results of fossil *Fagus crenata* leaves along with the corresponding paleo-CO_2 estimations of each layer. Open circle and asterisk indicate mild and extreme outliers, respectively.

SI values were distributed in the range 7.25-14.59, and the distribution of each assemblage was skewed to the higher SI range than the median (Figure 3.2-6). The average SI of each layer fluctuated between 9.11 (L18) and 11.29 (L09), which is equivalent of the reconstructed paleo-CO_2 level between 317 and 352 ppmv (Figure 3.2-7, Table 3.2-1). SI data of L20 (4142-4092 cal BP), L18 (4339-4257 cal BP), L13 (5638-4612 cal BP) showed significantly low values (p<0.05) than most of the other horizons, indicating higher CO_2 level. Clearer fluctuation of reconstructed paleo-CO_2 level is recorded between 4700-4000 cal BP than before and after this period.

The variation ranges of SI data of each layer ranged between 2.15 % (L13) and 6.51 % (L02) (Figure 3.2-8, C; Table 3.2-1), which is equivalent to the altitudinal transportation ranges from limited to 480 m based on Equation 3.2-2 and from limited to 800 m based on Equation 3.2-3 and Equation 3.2-4. The SI variation range fluctuated visibly and was frequently in excess of 6 % before ca 3800 cal BP; it also exhibited a decreasing trend form older to younger ages (p<0.01). The SI variation range of each layer was not influenced significantly by sample size (p=0.12) and was significantly correlated with the maximum values of SI (p<0.001).

Table 3.2-1 Mean, Minimum and Maximum values of SI and SD results of each sample layer along with the corresponding CO_2 estimation

Layer number	Position (cm)	Age range (cal yr BP)	Age range (yr)	Sample size (n)	SI (%)				SI-based CO_2 (ppmv)			Altitudinal transportation (m) based on Equation 3.2-2	Altitudinal transportation range (m) based on Equation 3.2-3 and Equation 3.2-4
					Mean*±σ	Min	Max	Variation range	Mean*±σ	Min	Max		
L29	310-320	2592-2468	124	18	10.59±0.92	9.30	12.34	3.04	328±15	300	349	Limited**	<13
L28	290-300	2848-2718	130	23	10.31±0.60	9.28	13.00	3.72	333±10	312	349	Limited	<176
L27	260-270	3253-3097	156	16	10.92±0.91	9.32	12.69	3.37	323±15	294	349	Limited	<92
L26	245-250	3459-3389	70	25	9.45±0.75	8.20	11.77	3.57	347±12	320	367	Limited	<140
L25	230-240	3662-3526	136	43	9.58±0.98	7.91	12.44	4.53	345±16	316	372	10	<370
L24	220-230	3795-3661	134	42	9.56±1.10	7.55	12.03	4.48	345±18	305	378	Limited	<358
L23	210-220	3903-3795	108	35	10.19±1.47	7.25	13.40	6.15	335±24	288	383	395	37-759
L22	200-210	4008-3902	106	24	10.12±0.93	8.40	13.71	5.31	336±15	304	364	195	<557
L21	190-200	4091-4007	84	27	10.75±0.84	9.34	12.72	3.38	326±14	294	348	Limited	<94
L20	180-190	4142-4090	52	32	9.39±1.14	7.38	12.42	5.04	348±19	312	380	130	<492
L19	170-180	4181-4141	40	35	10.25±1.02	8.55	12.37	3.82	334±16	300	361	Limited	<200
L18	137-150	4339-4257	82	18	9.11±1.42	7.29	12.22	4.93	352±23	302	382	105	<466
L17	130-137	4382-4338	44	17	11.11±1.57	9.03	14.11	5.08	320±25	271	353	140	<502
L16	120-130	4519-4381	138	28	10.39±1.29	8.41	12.48	4.07	332±21	298	364	Limited	<260
L15	115-120	4588-4518	70	53	9.93±1.02	8.08	12.93	4.85	339±17	297	369	86	<447
L14	110-115	4613-4587	26	51	10.21±1.22	7.42	13.47	6.05	335±20	288	380	371	13-743

L13	105-110	4638-4612	26	26	9.19±0.36	7.49	9.64	2.15	351±6	343	365	Limited	Limited
L12	100-105	4669-4637	32	23	10.58±0.69	9.66	14.10	4.44	329±11	302	343	Limited	<349
L11	90-100	4732-4668	64	29	11.17±1.65	8.60	14.59	5.99	319±27	264	360	357	<720
L10	80-85	4805-4767	38	24	10.94±1.09	9.07	13.59	4.52	323±18	280	353	7	<368
L09	75-80	4838-4804	34	25	11.29±1.22	9.04	13.86	4.82	317±20	275	353	79	<440
L08	70-75	4871-4837	34	30	10.62±1.05	8.41	13.09	4.68	328±17	288	364	45	<406
L07	60-66	4940-4892	48	26	10.62±1.13	8.38	14.44	6.06	328±18	291	364	374	16-737
L06	52-60	5005-4939	66	24	10.55±1.15	9.10	13.12	4.02	329±19	294	352	Limited	<248
L05	45-52	5046-5004	42	29	9.98±1.06	8.23	14.54	6.31	338±17	296	367	433	74-797
L04	35-45	5119-5045	74	28	10.79±1.09	8.70	13.26	4.56	325±18	294	359	17	<377
L03	30-35	5147-5119	28	26	9.98±0.93	8.20	12.91	4.71	338±15	314	367	52	<413
L02	25-30	5195-5147	48	30	10.28±1.57	7.95	14.46	6.51	333±25	265	371	480	121-844
L01	10-15	5310-5286	24	28	10.91±1.57	8.27	14.20	5.93	323±25	270	364	343	<705

* Outliers in Figure 3.2-5 are excluded in mean value calculation

** Altitudinal range is limited to be detected by Equation 3.2-2, Equation 3.2-3 or Equation 3.2-4

3.2.4 Discussion

3.2.4.1 Holocene atmospheric CO_2 concentration changes based on stomatal data

The CO_2 data from Mt. Kurikoma exhibit higher and more fluctuated values than the atmospheric CO_2 concentration data from ice cores in Greenland and Antarctic (Indermühle et al., 1999; Leuenberger et al., 1992; Monnin et al., 2001) (Figure 3.2-8, b), which are considered to be the most reliable and precise reconstruction of atmospheric paleo-CO_2. Although the ice core records are accepted widely as a stable CO_2 concentration at a level lower than the pre-industrial level throughout the Holocene, the stomatal-based CO_2 data generally indicate more fluctuated and/or higher CO_2 concentration. For example, *Betula pubescens* and *B. pendula* from Denmark (Wagner et al., 2002) and northeastern Netherlands (Wagner et al., 1999) indicate fluctuating CO_2 patterns during the Early and Middle Holocene and the values are generally 20-60 ppmv higher than CO_2 records from the Antarctic Taylor Dome ice core (Indermühle et al., 1999). SI of *Dryas integrifolia*, *Picea mariana*, *Picea glauca* and *Larix laricina* from Atlantic Canada also indicate a fluctuated CO_2 level between 230 and 320 ppmv just before the Younger Dryas stadial (10400-11500 cal BP), and excess 300 ppmv after the stadial (Mcelwain et al., 2002), which is about 30-40 ppmv higher than CO_2 measurements in the Dome Concordia core (Monnin et al., 2001). Whereas, a CO_2 curve for the last 9000 cal BP based on *Salix herbacea* leaves (Rundgren and Beerling, 1999) from northern Sweden (999 m) exhibits a generally similar CO_2 level with that of ice-core (Indermühle et al., 1999), but it records variation of more than 50 ppmv within several hundred years. A curve based on *Tsuga heterophytta* from North America (1311 m a.s.l.) (Kouwenberg et al., 2005) also indicates a fluctuant CO_2 trend for AD 800–2000, with peaks of up to 50-80 ppmv higher than that of Antarctic Taylor Dome ice cores (Indermühle et al., 1999). Not only stomatal parameters of fossil plants, but carbon isotope of south American fossil mosses and sedges also indicate a CO_2 peak of ca. 320

ppmv at ca. 4000 cal BP (Figge and White, 1995), which is not recorded in ice cores.

Compared with flat ice core CO_2 curves, remarkable correlations are revealed between the stomatal-based CO_2 concentration and paleo-temperature based on various kinds of proxies. The Early Holocene CO_2 variation trend based on *Betula* leaves is in harmony with North Atlantic sea-surface temperatures (Wagner et al., 1999) and $\delta^{18}O$ profile for the Younger Dryas-Holocene transition in the Greenland GISP2 ice core (Grootes et al., 1993; Stuiver et al., 1995). *Dryas integrifolia*, *Picea mariana*, *Picea glauca,* and *Larix laricina* from Atlantic Canada share a similar variation trend with the summer surface-water temperatures reconstructed from chironomid remains of the same fossil site in the lake (Levesque et al., 1994). *Tsuga*-based CO_2 data also present a clear covariation between CO_2 and global temperature, particularly concerning the timing of the warm periods and the CO_2 maxima at ca. AD 950 and AD 1300 (Mann and Jones, 2003). These correlations between stomatal-based CO_2 and temperature imply that a number of short-term CO_2 fluctuations recorded by using the stomatal methods cannot be detected in ice cores. The stability of ice core CO_2 value is explained by gradual trapping of air into bubbles within ice of low accumulation rates which induces an averaged ice core CO_2 concentration relative to the actual temporal variations (Trudinger et al., 2003). According to Neftel et al. (1988), CO_2 fluctuation in ice core with a duration of less than twice the bubble enclosure time cannot be detected.

This CO_2 data visibly fluctuate before 4000 cal BP (L21-L01), especially between 4700 and 4000 cal BP (L15-L21) (Figure 3.2-8, B). Fluctuation is generally consistent with alkenone-based sea surface temperature (SST) of Mutsu Bay situated at ca. 300 km north of Mt. Kurikoma, which was higher than the present temperature (22 ºC) in the Middle and Early Late Holocene (Figure 3.2-8, A) (Kawahata et al., 2009). The SST of Mutsu Bay is determined mainly by the intensity of the Tsugaru Warm Current, a branch of the Tsushima Warm Current (Kawahata et al., 2009). SST changes the solubility of CO_2 in ocean making it, for example, approximately two times more soluble in the cold surface waters in polar regions than in the warm surface waters near the equator

(Houghton, 2007). In addition, a higher SST decreases surface water density and stabilizes the water column without mixing surface and deeper waters, which also prevents oceanic uptake of atmospheric CO_2 (Houghton, 2007). In this study, the high CO_2 levels at L05, L13, L18 and L 20 are correlated with the peaks of SST records (Figure 3.2-8). Thus, the CO_2 level changes in our fossil site are possibly related to the shift in oceanic CO_2 uptake capacity affected by the strength of Tsushima Warm Current in the Sea of Japan.

Local volcanic CO_2 gas emission is another factor that may also affect CO_2 results from Mt. Kurikoma. Although the last major volcanic activities ceased at ca. 0.1 Ma (Fujinawa et al., 2001), further volcanic activity, such as phreatic eruptions and earthquakes were documented (Disaster Prevention Office of Iwate Prefectural Government, 2008), and emission of volcanic volatiles, including CO_2, may have occurred after the main period of volcanism in Mt. Kurikoma. According to Figure 2, there are three tephra layers in the profile between L1 and L29, corresponding to three minor eruption. Among the tephra layers, the middle one at 160 cm from the base of the outcrop (4339-4257 cal BP) is the thickest one, which indicated eruption that was the largest and/or nearest to the fossil locality. L18, a layer within a tuffaceous sediment adjacent to this tephra, includes leaves showing the lowest SI and the highest CO_2 values. This record may have been affected by local volcanic CO_2 emission besides oceanic CO_2 uptake capacity controlled by SST. Another conspicuous peak with the lowest SI variation range at L13 indicates possibility of local CO_2 emission event in spite of absence of tephra. van Hoof et al. (2008) also found that changes in CO_2 radiative forcing based on stomatal analysis of *Quercus robur* (English oak) from the Netherlands are of a magnitude similar to variations of volcanic activity. We suppose oceanic CO_2 uptake capacity affected by SST and volcanic CO_2 emission together contributed to the higher CO_2 record in this study than ice-core records. The occurrence of local volcanic actives can be evidenced by CO_2 records.

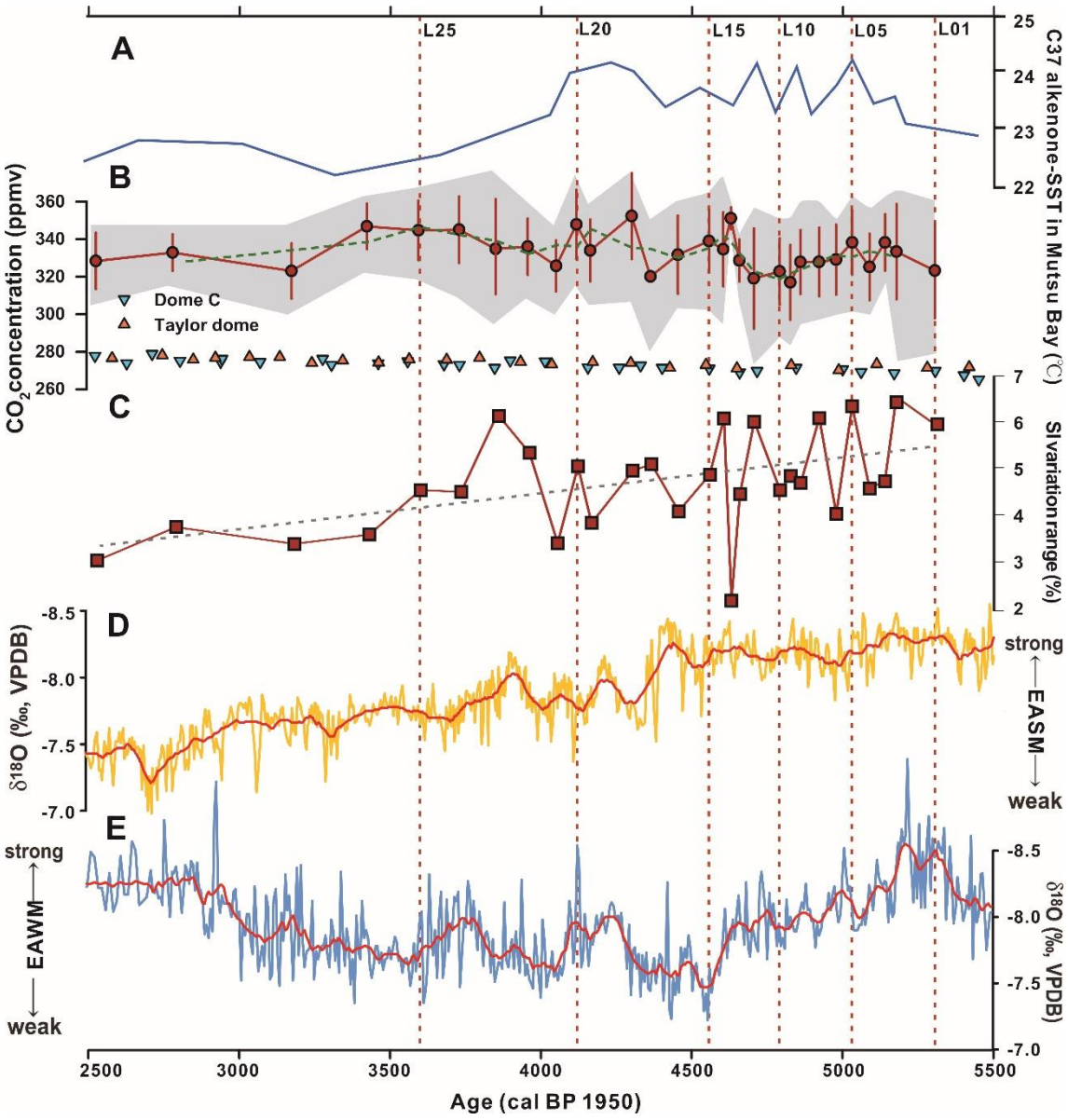

Figure 3.2-8 Stomatal analysis of *Fagus crenata* compared with previously published climate data. (A) Alkenone-base sea surface temperature (SST) of Mutsu Bay (Kawahata et al., 2009); (B) Average CO_2 concentration curve of this study (Error bar = 1σ, shade indicates the range between the maximum and the minimum in our data), along with ice-core records from Dome C (Monnin et al., 2001) transferred on AICC2012 chronology (Veres et al., 2013) and Taylor Dome (Indermühle et al., 1999); (C) Changes of the SI

variation range with respective altitudinal transportation range of each layer based on Equation 3.2-2 with a dash line showing the decreasing trend; (D) $\delta^{18}O$ data from Dongge Cave, China (Wang et al., 2005), showing intensity of East Asian Summer Monsoon (EASM); (E) $\delta^{18}O$ data from Fukugaguchi Cave, Japan (Sone et al., 2013), indicating intensity of East Asian Winter Monsoon (EAWM).

3.2.4.2 Upper distribution limit changes of *Fagus* population

Our SI results exhibit large CO_2 variation ranges (Figure 3.2-8, C), compared with previously published stomatal-based CO_2 data in which the SI variation was often ascribed to the individual difference within a population at a given altitude (e.g. Hu et al., 2015; Royer et al., 2001; Wang et al., 2018b; Wang et al., 2015). Meanwhile, the altitudinal transportation of leaves before fossilization also causes a more considerable SI variation than that observed in a modern population at an altitude (Wang et al., 2018a). Transportation of plant organs from higher altitudes is a common phenomenon in mountainous areas and the macrofossil assemblages are composed of a mixture of plants from a wide altitudinal range (Huzioka, 1963; Vassio and Martinetto, 2012). The altitudinal transportation of modern *Fagus crenata* leaves is reported as more than 600 m along the river of a mountain in central Japan (Ozaki, 1969). In addition, based on the SI variation of fossil *Fagus crenat*a leaves from the lower Pleistocene Sayama Formation in central Japan, an even larger altitudinal transportation range of more than 1000 m was estimated (Wang et al., 2018a). Fossil leaf assemblages of several horizons in our fossil site exhibit SI variation ranges are larger than those observed in a modern population at the same altitude. In addition, SI distribution in the most horizons skews to the value lower than the median (Figure 3.2-6), and almost all of outliers of SI values constituted the highest part of the SI ranges (Figure 3.2-7). These features indicate that the leaves from higher altitude areas under lower atmospheric CO_2 conditions flew down into the

fossil site and mixed with the leaf assemblages from population surrounding the fossil deposition site.

The fluctuated and higher SI variation range before 4600 cal BP (Figure 3.2-8) indicates frequent inflows of leaves from higher altitudes before fossilization. An exception is the assemblage of L13 which implied a leaf assemblage originated only from the forest surrounding the fossil deposition site by a high SI and lowest SI variation range. Based on the SI variation of fossil leaves before 3,800 cal BP, the transportation ranges of the fossil leaves before fossilization were estimated as several hundreds to limited (Table 3.2-1), which indicates a possibility that altitudinal distribution limit of *Fagus* population was situated at an altitude higher than the present limit at 1367 m a.s.l. (Figure 3.2-1).

Meanwhile, the continuous low-level SI variation in assemblages from L26 to L29 demonstrates a ceasing of *Fagus crenata* leaves inflow from altitude higher than the forest surrounding the fossil deposition site since 3500 cal BP. However, the generally decreasing trend of SI variation range from the base to top of the profile cannot be explained by the decrease of fluvial activity to transport leaves from higher altitudes as the coarsening upward sedimentary facies of the profile indicates increasing fluvial activity to younger assemblages (Figure 3.2-2). The lower part of bryophyte peat with little inorganic materials indicates a lacustrine environment with low fluvial inflow, while the sandy and silty sediments including assemblages upper than L25 exhibit supply of inorganic materials from upper reaches of the river by increased fluvial activity. SI variation decrease despite active fluvial activity possibly demonstrates downfall of distribution limit of *Fagus crenata* to the altitude around the fossil deposition site.

3.2.4.3 Climate factors controlling the altitudinal distribution of *Fagus crenata*

Among the factors controlling the distribution limit of a species, climate plays a significant role (Austin and Van Niel, 2011; Hamann and Wang, 2006; Hara, 2010; Pearson and Dawson, 2003), while biotic factors such as species interactions, and seed

dispersal are also crucial to determining the distribution of species (Hampe, 2004; Hara, 2010; Pearson and Dawson, 2003; Svenning et al., 2008). However, the fossil assemblages in our study including the presence of very few leaves except for *Fagus crenata* indicate that the influence of the competition with other species (Bradshaw et al., 2010) is assumed to be limited in the forest around the study site. The decreasing SI variation trend follows the declining curve of the Mutsu Bay SST (Kawahata et al., 2009) and East Asian Summer Monsoon intensity (Wang et al., 2005), which demonstrates that downward shift of altitudinal distribution limit of *Fagus crenata* is ascribed to climatic deterioration, which was represented by cooler and dryer summers. From this viewpoint, the low values of the SI variation range between 4300 and 4100 cal BP are associated with the cooling events at the Middle and Late Holocene boundary, which have been shown in East Asian Summer Monsoon curve (Figure 3.2-8), coral reef oxygen isotope record in Ryukyu Islands of Japan (Abram et al., 2001), loess-paleosol sequence in China (Huang et al., 2010), lacustrine isotope record from southern Sweden (Jessen et al., 2005) and ice core records from Greenland (Johnsen et al., 2001).

The intensity of winter monsoon may have also influenced altitudinal distribution of *Fagus crenata* because the combination of stronger winter monsoon and warmer sea surface temperature in the Sea of Japan produced heavier snow conditions, which promoted the regeneration and spread of *Fagus crenata* (Fujita, 1987; Fukushima et al., 1995; Hara, 2010; Homma, 1997; Homma et al., 1999). Modern *Fagus crenata* is more dominant in forests and more widespread in areas under lower temperature conditions in the heavy snow region facing the Sea of Japan than the Pacific side of Japan (Fujita, 1987; Fukushima et al., 1995). This phenomenon is ascribed to the tolerance of *Fagus crenata* to snow pressure, which prevents the growth of the other tree species (Hara, 2010). In addition, the thick snow cover can reduce the chance for rodents finding seeds in winter (Homma et al., 1999), and also reduce the water stress on *Fagus crenata* in winter and spring. Stalagmite oxygen isotope record from Fukugaguchi Cave, Itoigawa, ca. 400 km southwest of our study site, provided proxy of winter precipitation, snowfall, during the

Holocene (Figure 3.2-8) (Sone et al., 2013), and the declining trend of snowfall from 5300 cal BP to 4500 cal BP is consistent with the decreasing SI variation range of *Fagus crenata* leaves in our study site. However, this coupling was broken since 4500 cal BP, which may imply the altitudinal distribution limit of *Fagus crenata* was more strongly constrained by mean annual temperature and summer precipitation than winter precipitation during the Late Holocene.

4 Main findings of this study

During the Paleogene, the Earth experienced a significantly warm and humid environment, which is referred as a greenhouse climate (Bowen et al., 2004; Hansen et al., 2008; Beerling and Royer, 2011). Stomatal analysis of fossil leaves, as a popular method for paleo-CO_2 reconstruction, however, have provided limited data for the Paleogene. This study provided four new stomatal-based CO_2 data for this period using fossil *Metasequoia* needles to fill this gap. The extensive and frequent occurrence of *Metasequoia* fossils in time and space (LePage et al., 2005) make it an ideal material for long-term CO_2 reconstruction, but *Metasequoia*-based CO_2 data for the early Cenozoic are rare. This study makes it possible to depict a detailed CO_2 curve throughout the Cenozoic by combining with former published late Cenozoic *Metasequoia*-based CO_2 data. This CO_2 evolution curve is based on one species by using same methods, thus can avoid the noise derived from using different kinds of proxies. Besides, this study also includes the oldest CO_2 level data based on the stomatal analysis of *Metasequoia* needles to date.

Stomatal-based CO_2 data have been compared with paleo-temperature reconstructed from marine oxygen isotope, which might show some deviation from terrestrial temperature at the place where fossil leaves have grown. Thus, for an Early Pleistocene fossil locality, I estimated both palaeo-temperature and palaeo-CO_2 using fossil leaves from a fossil assemblage, which was the first trial toprovide a direct comparison between terrestrial CO_2 and temperature. The palaeo-CO_2 was estimated to have been at a higher level than previously reported, and the according mean annual paleo-temperature was almost equivalent to the contemporaneous data from the Uonuma Group, central Japan, which is an interglacial warm period during the Pleistocene. This result indicates a warm climate under high CO_2 level in an interglacial stage of the early Pleistocene, demonstrating the vital role of CO_2 level in controlling the early Pleistocene interglacial temperature.

The altitudinal transportation of plant organs before their burial (Gastaldo et al., 2016; Steart et al., 2006) is an important process in the formation of fossil assemblage, which cannot be ignored in reconstruction of paleoenvironment. Although transportation of fossil pollen and fruits/seeds has been studied by many researches, researches of leaf transportation before fossilization is limited. This study estimated the altitudinal transportation range of *Fagus crenata* leaves before fossilization for the first time, and indicated that the altitudinal transportation range of leaves before burial is large enough to affect the accuracy of paleo-environment reconstruction by paleobotany method, such as leaf morphology-based paleoclimate data and stomal-based paleo-CO_2 data. On the other hand, this research indicates that estimated leaf transportation range before fossilization can be a potential indicator of paleoaltitude, and can reflect altitudinal distribution range of a species, which are important in understanding the floral and geomorphological evolution in ancient times. On this basis, for a Holocene fossil locality in Mt. Kurikoma, based on the stomatal analysis of fossil *Fagus crenata* leaves from fossil assemblages between ca. 5000 and ca. 2500 cal BP, I reconstructed the temporal changes of its altitudinal distribution limit, this is the first result in that stomata analysis of fossil leaves is contributed on reconstruction of altitudinal changes of plant distribution, which provided a new method in detecting plant reaction to climate change in ancient times.

5 Conclusions

In this study, based on the fossil *Metasequoia* needles, I reconstructed CO_2 for four time periods during the early and middle Paleocene and middle Eocene. In the early and middle Paleocene (63–60 Ma), CO_2 was estimated at 300–400 ppmv, which is a little lower than the present level. During the middle Eocene, CO_2 was estimated at 473 ppmv in 47.5–41.3 Ma and 706 ppmv in 41–40 Ma. The CO_2 values estimated by stomatal index from fossil *Metasequoia* leaves are consistent with those based on *Ginkgo*, which demonstrates the excellence of *Metasequoia* for use as a proxy to demonstrate paleo-CO_2 levels, along with its common and frequent occurrence through the whole Cenozoic. During the Paleogene, climate change under the thermal environment cannot merely be explained by variations in CO_2; other factors, such as paleogeography, high latitude vegetation feedbacks, increased polar stratospheric clouds, and increased latent heat transport, may be complementary warming mechanisms. This means that CO_2 played a less crucial role in these ancient epochs.

However, unlike the early Cenozoic, CO_2 level played a vital role in controlling the late Cenozoic temperature based on our study on the Sayama Formation, central Japan. I reconstructed the palaeo-CO_2 and palaeo-temperature during an interglacial stage in MIS 57 or 55 (1.66–1.55 Ma), based on a leaf bed in the Sayama Formation. According to the stomatal density exhibited by leaves of *Quercus gilva*, the palaeo-CO_2 was estimated to have been 36.41±2.58 pa (359±25 ppmv), which is at a higher level than previously reported. Based on the leaf margin analysis of woody dicots in the fossil assemblage, the mean annual temperature was estimated at 11.0 °C, which is almost equivalent to the contemporaneous data from the Uonuma Group, central Japan. This result indicates a warm climate under high CO_2 level in an interglacial stage of the early Pleistocene, demonstrating the vital role of CO_2 level in controlling the early Pleistocene interglacial temperature.

I also conducted an initial attempt at detecting leaf transportation before fossilization

by using SI variation of fossil *Fagus crenata* from the late Early Pleistocene Sayama Formation. Although Cenozoic plant fossil records can imply the possibility of altitudinal transportation from higher altitude before fossilization by the mixture of elements from different climate zones within one fossil assemblage, there is a shortage of direct evidence for this hypothesis. In paleoclimates and paleovegetation reconstruction work, cool elements transported from higher altitudes will cause an underestimated result. The first step to eliminate this disturbance is to quantitatively estimate the transport range of plant organs before fossilization and check if this transport range is large enough to hinder paleoenvironment reconstruction. Our data showed an altitudinal transportation range of over 1000 m, which is large enough to affect the accuracy of paleoclimates and paleovegetation reconstruction. However, as transportation efficiency is different among various organs of different species, more detailed studies of many species, both fossil and modern, is required to minimize the effect of this taphonomic bias on paleoenvironment reconstruction.

For another fossil locality in Mt. Kurikoma that also include fossil leaves of *Fagus crenata* from 29 deposition layers, differences of the SI variation range among the fossil assemblages from different horizons indicate the temporal changes of altitudinal distribution limit of the species. The Holocene paleo-CO_2 estimated from *Fagus crenate* in this study showed a higher and more fluctuant record than the ice core record, which may have been affected by the strength of Tsushima warm current. Thus, paleo-CO_2 data from this research should be considered as a regional level data rather than global. Large variation of SI data from one deposition layer was detected as a proxy for the altitudinal distribution range of *Fagus crenata*. I found that from ca. 5000 to ca. 2500 cal BP, the upper limit of *Fagus crenata* distribution moved down from the altitude similar to or higher than the present to the areas surrounding the fossil site under climate deterioration with a cooling event happened at ca. 4000 cal BP and drier growing seasons caused by the decrease of East Asian Summer Monsoon. This study demonstrates the potential of stomata analysis of fossil leaves for detecting the altitudinal distribution of species, which

can help provide a better understanding of forest evolution under climate change in the past.

References

Abram, N., Webster, J., Davies, P., Dullo, W., 2001: Biological response of coral reefs to sea surface temperature variation: evidence from the raised Holocene reefs of Kikai-jima (Ryukyu Islands, Japan). *Coral Reefs* 20, 221-234.

Ahn, J., Brook, E.J., 2008. Atmospheric CO_2 and climate on millennial time scales during the last glacial period. *Science* 322, 83-85.

Altman, J., Ukhvatkina, O.N., Omelko, A.M., Macek, M., Plener, T., Pejcha, V., Cerny,T., Petrik, P., Srutek, M., Song, J.-S., Zhmerenetsky, A.A., Vozmishcheva, A.S., Krestov, P.V., Petrenko, T.Y., Treydte, K., Dolezal, J., 2018: Poleward migration of the destructive effects of tropical cyclones during the 20th century. *PNAS* 115, 11543-11548.

Astorga, G.A., Jordan, G.J., Brodribb, T., 2016. Towards understanding the fossil record better: Insights from recently deposited plant macrofossils in a sclerophyll-dominated subalpine environment. *Review of Palaeobotany and Palynology* 233, 1-11.

Austin, M.P., Van Niel, K.P., 2010: Improving species distribution models for climate change studies: variable selection and scale. *Journal of Biogeography* 38, 1-8.

Avnaim-Katav, S., Almogi-Labin, A., Schneider-Mor, A., Crouvi, O., Burke, A.A., Kremenetski, K.V., MacDonald, G.M., 2019: A multi-proxy shallow marine record for Mid-to-Late Holocene climate variability, Thera eruptions and cultural change in the Eastern Mediterranean. *Quaternary Science Reviews* 204, 133-148.

Bai, Y.J., Chen, L.Q., Ranhotra, P.S., Wang, Q., Wang, Y.F., Li, C.S., 2015. Reconstructing atmospheric CO_2 during the Plio-Pleistocene transition by fossil Typha. *Global Change Biology* 21, 874-881.

Bakker, P., Clark, P.U., Golledge, N.R., Schmittner, A., Weber, M.E., 2017: Centennial-scale Holocene climate variations amplified by Antarctic Ice Sheet discharge. *Nature* 541, 72-76.

Beerling D.J., 1999. Stomatal density and index: Theory and application In: Jones TP, Rowe NP, editors. *Fossil plants and spores: modern techniques*. London: Geological Society of London. 251–256.

Beerling, D.J., Royer, D., 2002. Reading a CO_2 signal from fossil stomata. *New Phytologist* 153, 387-397.

Beerling, D.J., Fox, A., Anderson, C.W., 2009. Quantitative uncertainty analyses of ancient atmospheric CO_2 estimates from fossil leaves. *American Journal of Science* 309, 775-787.

Beerling, D.J., Royer, D.L., 2002. Fossil Plants as Indicators of the Phanerozoic Global Carbon Cycle. *Annual Review of Earth and Planetary Sciences* 30, 527-556.

Beerling, D.J., Royer, D.L., 2011. Convergent Cenozoic CO_2 history. *Nature Geoscience* 4, 418-420.

Beerling, D.J., Woodward, F.I., 1996. Palaeo-ecophysiological perspectives on plant responses to global change. *Trends in Ecology & Evolution* 11, 20-23.

Berner, R.A., 1994. GEOCARB II: A revised model of atmospheric CO_2 over Phanerozoic time. *American Journal of Science* 301, 182-204.

Berner, R.A., 2006. GEOCARBSULF: A combined model for Phanerozoic atmospheric O_2 and CO_2. *Geochimica et Cosmochimica Acta* 70, 5653-5664.

Berner, R.A., Kothavala, Z., 2001. GEOCARB III: a revised model of atmospheric CO_2 over Phanerozoic time. *American Journal of Science* 301, 182-204.

Bijl, P.K., Houben, A.J.P., Schouten, S., Bohaty, S.M., Sluijs, A., Reichart, G.-J., Sinninghe Damsté, J.S., Brinkhuis, H., 2010. Transient Middle Eocene atmospheric CO_2 and temperature variations. *Science* 330, 819-821.

Bohaty, S.M., Zachos, J.C., Florindo, F., Delaney, M.L., 2009. Coupled greenhouse warming and deep-sea acidification in the middle Eocene. *Paleoceanography* 24, PA2207.

Bowen, G.J., Beerling, D.J., Koch, P.L., Zachos, J.C., Quattlebaum, T., 2004. A humid climate state during the Palaeocene/Eocene thermal maximum. *Nature* 432, 495.

Bradshaw, R.H.W., Kito, N., Giesecke, T., 2010: Factors influencing the Holocene history of Fagus. *Forest Ecology and Management* 259, 2204-2212.

Cantón, Y., Del Barrio, G., Solé-Benet, A., Lázaro, R., 2004. Topographic controls on the spatial distribution of ground cover in the Tabernas badlands of SE Spain. *Catena* 55, 341-365.

Canziani, O.F., 2001: *Climate change 2001: impacts, adaptation, and vulnerability: contribution of Working Group II to the third assessment report of the Intergovernmental Panel on Climate Change.* 1005 pp. Cambridge University Press, Cambridge.

Cappers, R., 1993. Seed dispersal by water: a contribution to the interpretation of seed assemblages. *Vegetation History and Archaeobotany* 2, 173-186.

Coops, N.C., Waring, R.H., Plowright, A., Lee, J., Dilts, T.E., 2016: Using Remotely-Sensed Land Cover and Distribution Modeling to Estimate Tree Species Migration in the Pacific Northwest Region of North America. *Remote Sense* 8, 65.

Dickens, G.R., Castillo, M.M., Walker, J.C., 1997. A blast of gas in the latest Paleocene: Simulating first-order effects of massive dissociation of oceanic methane hydrate. *Geology* 25, 259-262.

Dilcher, D.L., 1974. Approaches to the identification of angiosperm leaf remains. The Botanical Review 40, 1-157.

Doria, G., Royer, D.L., Wolfe, A.P., Fox, A., Westgate, J.A., Beerling, D.J., 2011. Declining atmospheric CO_2 during the late Middle Eocene climate transition. *American Journal of Science* 311, 63-75.

Dowsett, H., Barron, J., Poore, R., 1996. Middle Pliocene sea surface temperatures: a global reconstruction. Marine Micropaleontology 27, 13-25.

Dyakowska, J., 1947. The pollen rain on the sea and on the coast of Greenland. *Bulletin international de l'Académie des sciences de Cracovie.* BI, 25-33.

Eberle, J.J., Greenwood, D.R., 2012. Life at the top of the greenhouse Eocene world — A review of the Eocene flora and vertebrate fauna from Canada's High Arctic. *Bulletin* 124, 3-23.

Ehleringer J.R., Cerling T.E., 1995. Atmospheric CO_2 and the ratio of intercellular to ambient CO_2 concentrations in plants. *Tree Physiology*, 15, 105-111.

Ekart, D.D., Cerling, T.E., Montanez, I.P., Tabor, N.J., 1999. A 400 million year carbon isotope record of pedogenic carbonate: implications for paleoatmospheric carbon dioxide. *American Journal of Science* 299, 805-827.

Ferguson, D., 1995. Plant part processing and community reconstruction. *Eclogae Geologicae Helvetiae* 88, 627-641.

Feurdean, A., Gałka, M., Tanţău, I., Geantă, A., Hutchinson, S.M., Hickler, T., 2016: Tree and timberline shifts in the northern Romanian Carpathians during the Holocene and the responses to environmental changes. *Quaternary Science Reviews* 134, 100-113.

Figge, R.A., White, J.W.C., 1995: High-resolution holocene and late glacial atmospheric CO_2 record: variability tied to changes in thermohaline circulation. *Global Biogeochemical Cycle* 9, 391-403.

Fletcher, B.J., Brentnall, S.J., Anderson, C.W., Berner, R.A., Beerling, D.J., 2008. Atmospheric carbon dioxide linked with Mesozoic and early Cenozoic climate change. *Nature Geoscience* 1, 43.

Flora of China Editorial Committee, 1994. *Flora of China*. Science Press, Beijing, China and Missouri Botanical Garden Press, St. Louis, Missouri.

Franks, P.J., Beerling, D.J., 2009. Maximum leaf conductance driven by CO_2 effects on stomatal size and density over geologic time. *Proceedings of the National Academy of Sciences* 106, 10343-10347.

Freeman, K.H., Hayes, J., 1992. Fractionation of carbon isotopes by phytoplankton and estimates of ancient CO_2 levels. *Global Biogeochemical Cycles* 6, 185-198.

Fujinawa, A., Fujita, K., Takahashi, M., Umeda, K., Hayashi, S., 2001: Development History of Kurikoma Volcano, Northeast Japan. *Volcano* 46, 269-284. (in Japanese, with English abstract)

Fujita, N., 1987: One-sided distribution of the component species of the Japanese beech forest along either the Pacific or the Japan Sea. *Acta Phytotaxonomica et Geobotanica* 38, 311–329. (in Japanese, with English abstract)

Fukushima, T., Takasuna, H., Matsui, T., Nishio, T., Kyan, Y., Tsunetomi, Y., 1995: New phytosociological classification of beech forests in Japan. *Japanese Journal Ecology* 45, 79-98. (in Japanese, with English abstract)

Gastaldo, R.A., Douglass, D.P., McCarroll, S.M., 1987. Origin, characteristics, and provenance of plant macrodetritus in a Holocene crevasse splay, Mobile Delta, Alabama. *Palaios*, 229-240.

Gee, C.T., 2005. The genesis of mass carpological deposits (bedload carpodeposits) in the Tertiary of the Lower Rhine Basin, Germany. *Palaios* 20, 463-478.

Gray, J.E., Holroyd, G.H., Van Der Lee, F.M., Bahrami, A.R., Sijmons, P.C., Woodward, F.I., Schuch, W., Hetherington, A.M., 2000. The HIC signalling pathway links CO_2 perception to stomatal development. *Nature* 408, 713.

Greenwood, D.R., Scarr, M.J., Christophel, D.C., 2003. Leaf stomatal frequency in the Australian tropical rainforest tree Neolitsea dealbata (Lauraceae) as a proxy measure of atmospheric pCO_2. *Palaeogeography, Palaeoclimatology, Palaeoecology* 196, 375-393.

Greenwood, D.R., Wilf, P., Wing, S.L., Christophel, D.C., 2004. Paleotemperature estimation using leaf-margin analysis: is Australia different? *Palaios* 19, 129-142.

Greenwood, D.R., Wing, S.L., 1995. Eocene continental climates and latitudinal temperature gradients. *Geology* 23, 1044-1048.

Gregory-Wodzicki, K.M., 2000. Relationships between leaf morphology and climate, Bolivia: implications for estimating paleoclimate from fossil floras. *Paleobiology* 26, 668-688.

Grein M, Oehm C, Konrad W, Utescher T, Kunzmann L, Roth-Nebelsick A. Atmospheric CO_2 from the late Oligocene to early Miocene based on photosynthesis data and fossil leaf characteristics. *Palaeogeography, Palaeoclimatology, Palaeoecology*. 2013; 374: 41-51.

Grootes, P.M., Stuiver, M., White, J.W.C., Johnsen, S., Jouzel, J., 1993: Comparison of oxygen isotope records from the GISP2 and GRIP Greenland ice cores. *Nature* 366, 552-554.

Hamann, A., Wang, T., 2006: Potential effects of climate change on ecosystem and tree species distribution in British Columbia. *Ecology* 87, 2773–2786.

Hampe, A., 2004: Bioclimate envelope models: what they detect and what they hide. *Global Ecology and Biogeography* 13, 469-476.

Hansen, J., Sato, M., Kharecha, P., Beerling, D., Berner, R., Masson-Delmotte, V., Pagani, M., Raymo, M., Royer, D.L., Zachos, J.C., 2008. Target atmospheric CO_2: Where should humanity aim? *Open Atmospheric Science Journal* 2, 217-231.

Hara, M., 2010: Climatic and historical factors controlling horizontal and vertical distribution patterns of two sympatric beech species, *Fagus crenata* Blume and *Fagus japonica* Maxim., in eastern Japan. *Flora - Morphology, Distribution, Functional Ecology of Plants* 205, 161-170.

Hasegawa, H., Suzuki, N., Saito, H., 2009. Coal-bearing succession of the middle Eocene Ishikari Group in Sanbi Coal Mine, central Hokkaido. *The Journal of the Geological Society of Japan* 115, 15-16.

Haworth M., Heath J., McElwain J.C., 2010. Differences in the response sensitivity of stomatal index to atmospheric CO_2 among four genera of Cupressaceae conifers. *Annals of Botany* 105, 411-418.

Haywood, A.M., Dowsett, H.J., Dolan, A.M., 2016. Integrating geological archives and climate models for the mid-Pliocene warm period. *Nature communications* 7, 10646.

Higgins, J.A., Schrag, D.P., 2006. Beyond methane: towards a theory for the Paleocene–Eocene thermal maximum. *Earth and Planetary Science Letters* 245, 523-537.

Hirano A., Hongo I., Koike T., 2012. Morphological and physiological responses of Siebold's beech (Fagus crenata) seedlings grown under CO_2 concentrations ranging from pre-industrial to expected future levels. Landscape Ecology Eng DOI 10.1007/s11355-011-0149-0Hönisch, B., Hemming, N.G., Archer, D., Siddall, M., McManus, J.F., 2009. Atmospheric carbon dioxide concentration across the mid-Pleistocene transition. *Science* 324, 1551-1554.

Homma, K., 1997: Effects of snow pressure on growth form and life history of tree species in Japanese beech forest. *Journal of Vegetation Science* 8, 781-788.

Homma, K., Akashi, N., Abe, T., Hasegawa, M., Harada, K., Hirabuki, Y., Irie, K., Kaji, M., Miguchi, H., Mizoguchi, N., Mizunaga, H., Nakashizuka, T., Natume, S., Niiyama, K., Ohkubo, T., Sawada, S., Sugita, H., Takatsuki, S., Yamanaka, N., 1999: Geographical variation in the early regeneration process of Siebold's Beech (*Fagus crenata* Blume) in Japan. *Plant Ecology* 140, 129-138.

Hönisch, B., Hemming, N.G., Archer, D., Siddall, M., McManus, J.F., 2009. Atmospheric carbon dioxide concentration across the mid-Pleistocene transition. *Science* 324, 1551-1554.

Horiuchi, J., Uemura, K., 2017. Paleocene occurrence of *Pseudotorellia* Florin (Ginkgoales) from Northeast Japan and the Meso–Cenozoic history of *Pseudotorellia* and *Torellia*. *Review of Palaeobotany and Palynology* 246, 146-160.

Houghton, J., Ding, Y., Griggs, D., Noguer, M., van der Linden, P., Dai, X., Maskell, K., Johnson, C., 2001. *IPCC Climate Change: the Scientific Basis*. Cambridge University Press, Cambridge, 881 pp.

Houghton, R.A., 2007: Balancing the Global Carbon Budget. *Annual Review of Earth and Planetary Sciences* 35, 313-347.

Hu, J.J., Xing, Y.W., Turkington, R., Jacques, F.M.B., Su, T., Huang, Y.J., Zhou, Z.K., 2015: A new positive relationship between pCO_2 and stomatal frequency in *Quercus guyavifolia* (Fagaceae): a potential proxy for palaeo-CO_2 levels. *Annals of Botany* 115, 777-788.

Huang, C.C., Pang, J., Zha, X., Zhou, Y., Su, H., Li, Y., 2010: Extraordinary Floods of 4100−4000 a BP recorded at the Late Neolithic Ruins in the Jinghe River Gorges, Middle Reach of the Yellow River, China. *Palaeogeography, Palaeoclimatology, Palaeoecology* 289, 1-9.

Huntley, B., Berry, P.M., Cramer, W., McDonald, A.P., 1995: Special paper: Modelling present and potential future ranges of some European higher plants using climate response surfaces. *Journal of Biogeography* 22, 967-1001.

Huzioka, K., 1963. The Utto flora of northern Honshu. Tertiary floras of Japan, Miocene floras (in Japanese with English abstract). *The Collaborating Association to Commemorate the 80th Anniversary of the Geological Survey of Japan*, 153-216.

Indermühle, A., Stocker, T.F., Joos, F., Fischer, H., Smith, H.J., Wahlen, M., Deck, B., Mastroianni, D., Tschumi, J., Blunier, T., Meyer, R., Stauffer, B., 1999: Holocene carbon-cycle dynamics based on CO_2 trapped in ice at Taylor Dome, Antarctica. *Nature* 398, 121-126.

Ito, A., Momohara, A., Zhou, Z., 2017. Pleistocene fossil leaflets of Albizia kalkora (Roxb.) Prain(Leguminosae subfamily Mimosaceae) from central Honshu, Japan, and its implications for historical biogeography. *Japanese Association of Historical Botany* 26, 10.

Ito, M., Katsura, Y., 1992. Inferred glacio-eustatic control for high-frequency depositional sequences of the Plio-Pleistocene Kazusa Group, a forearc basin fill in Boso Peninsula, Japan. *Sedimentary Geology* 80, 67-75.

Jacobs, B.F., 1999. Estimation of rainfall variables from leaf characters in tropical Africa. *Palaeogeography, Palaeoclimatology, Palaeoecology* 145, 231-250.

Jacques, F.M.B., Guo, S.X., Su, T., Xing, Y.W., Huang, Y.J., Liu, Y.S., Ferguson, D.K., Zhou, Z.K., 2011. Quantitative reconstruction of the Late Miocene monsoon climates of southwest China: A case study of the Lincang flora from Yunnan Province. *Palaeogeography, Palaeoclimatology, Palaeoecology* 304, 318-327.

Jessen, C.A., Rundgren, M., Björck, S., Hammarlund, D., 2005: Abrupt climatic changes and an unstable transition into a late Holocene Thermal Decline: a multiproxy lacustrine record from southern Sweden. *Journal of Quaternary Science* 20, 349-362.

JMA (Japan Meteorological Agency), 2011. Monthly Climatological Normals (1981e2010). http://www.data.jma.go.jp/obd/stats/etrn/index.php.

Johnsen, S.J., Dahl-Jensen, D., Gundestrup, N., Steffensen, J.P., Clausen, H.B., Miller, H., Masson-Delmotte, V., Sveinbjörnsdottir, A.E., White, J., 2001: Oxygen isotope and palaeotemperature records from six Greenland ice-core stations: Camp Century, Dye-3, GRIP, GISP2, Renland and NorthGRIP. *Journal of Quaternary Science* 16, 299-307.

Jones H.G., 1992. *Plants and microclimate: a quantitative approach to environmental plant physiology*. Cambridge, UK: Cambridge University Press.

Jouzel, J., Masson-Delmotte, V., Cattani, O., Dreyfus, G., Falourd, S., Hoffmann, G., Minster, B., Nouet, J., Barnola, J.M., Chappellaz, J., 2007. Orbital and millennial Antarctic climate variability over the past 800,000 years. *Science* 317, 793-796.

Kawahata, H., Yamamoto, H., Ohkushi, K., Yokoyama, Y., Kimoto, K., Ohshima, H., Matsuzaki, H., 2009: Changes of environments and human activity at the Sannai-Maruyama ruins in Japan during the mid-Holocene Hypsithermal climatic interval. *Quaternary Science Reviews* 28, 964-974.

Kazaoka, O., 1986. Stratigraphy and facies of the Uonuma Group in the Uonuma district, Niigata Prefecture, central Japan (in Japanese with English abstract). *The Journal of the Geological Society of Japan* 92, 829-853.

Kearney, M.S., Luckman, B.H., 1983: Holocene Timberline Fluctuations in Jasper National Park, Alberta. *Science* 221, 261-263.

Kito, N., Takimoto, F., 1999: Population growth and migration rate of *Fagus crenata* during the Holocene in Southwestern Hokkaido, Japan. *The Quaternary Research* 38, 297-311. (in Japanese, with English abstract)

Kleidon, A., 2004. Optimized stomatal conductance of vegetated land surfaces and its effects on simulated productivity and climate. *Geophysical Research Letters* 31, L21203.

Koch, P.L., Zachos, J.C., Gingerich, P.D., 1992. Correlation between isotope records in marine and continental carbon reservoirs near the Palaeocene/Eocene boundary. *Nature* 358, 319-322.

Koike, F., 1989. Foliage-crown development and interaction in *Quercus gilva* and *Q. acuta*. *The Journal of Ecology*, 92-111.

Kouwenberg, L.L.R., Kürschner, W.M., McElwain, J.C., 2007. Stomatal Frequency Change Over Altitudinal Gradients: Prospects for Paleoaltimetry. *Reviews in Mineralogy and Geochemistry* 66, 215-241.

Kouwenberg, L.L.R., Wagner, R., Kürschner, W.M., Visscher, H., 2005: Atmospheric CO_2 fluctuations during the last millennium reconstructed by stomatal frequency analysis of *Tsuga heterophylla* needles. *Geology* 33, 33-36.

Kump, L.R., Arthur, M.A., 1999. Interpreting carbon-isotope excursions: carbonates and organic matter. *Chemical Geology* 161, 181-198.

Kürschner, W., Wagner, F., Dilcher, D.L., Visscher, H., 2001. Using fossil leaves for the reconstruction of Cenozoic paleoatmospheric CO_2 concentrations. *Geological Perspectives of Global Climate Change* 47, 169-189.

Kürschner, W.M., 1997. The anatomical diversity of recent and fossil leaves of the durmast oak (*Quercus petraea* Lieblein/*Q. pseudocastanea* Goeppert) — implications for their use as biosensors of palaeoatmospheric CO_2 levels. Review of Palaeobotany and Palynology 96, 1-30.

Kürschner, W.M., Kvacek, Z., Dilcher, D.L., 2008. The impact of Miocene atmospheric carbon dioxide fluctuations on climate and the evolution of terrestrial ecosystems. *Proceedings of the National Academy of Sciences* 105, 449-453.

Kürschner, W.M., Van der Burgh, J., Visscher, H., Dilcher, D.L., 1996. Oak leaves as biosensors of late Neogene and early Pleistocene paleoatmospheric CO_2 concentrations. Marine Micropaleontology 27, 299-312.

Lambers H., Chapin F.S., Pons T.L., 1998. *Plant Physiological Ecology*. Springer, New York.

Lake, J.A., Woodward, F.I., Quick, W.P., 2002. Long-distance CO_2 signalling in plants. *Journal of Experimental Botany* 53, 183-193.

LePage, B.A., Williams, C.J., Yang, H., 2005. *The Geobiology and Ecology of Metasequoia*. Springer, Dordrecht, 434 pp.

Leuenberger, M., Siegenthaler, U., Langway, C., 1992: Carbon isotope composition of atmospheric CO_2 during the last ice age from an Antarctic ice core. *Nature* 357, 488-490.

Levesque, A.J., Cwynar L.C., Walker I.R., 1994: A multiproxy investigation of Late-Glacial climate change and vegetation change at Pine Ridge Pond, Southwest, New Brunswick, Canada. *Quaternary Research* 42, 316–327.

Lisiecki, L.E., Raymo, M.E., 2005. A Pliocene-Pleistocene stack of 57 globally distributed benthic $\delta^{18}O$ records. *Paleoceanography* 20.

Lüthi, D., Le Floch, M., Bereiter, B., Blunier, T., Barnola, J.-M., Siegenthaler, U., Raynaud, D., Jouzel, J., Fischer, H., Kawamura, K., 2008. High-resolution carbon dioxide concentration record 650,000–800,000 years before present. *Nature* 453, 379.

Mann, M. E., Jones, P. D., 2003: Global surface temperatures over the past two millennia. *Geophysical Research Letters* 30, 1820.

Markwick, P.J., 1998. Fossil crocodilians as indicators of Late Cretaceous and Cenozoic climates: implications for using palaeontological data in reconstructing palaeoclimate. *Palaeogeography, Palaeoclimatology, Palaeoecology* 137, 205-271.

Marsicek, J., Shuman, B.N., Bartlein, P.J., Shafer, S.L., Brewer, S., 2018: Reconciling divergent trends and millennial variations in Holocene temperatures. *Nature* 554, 92-96.

Martinetto, E., Momohara, A., Bizzarri, R., Baldanza, A., Delfino, M., Esu, D., Sardella, R., 2017. Late persistence and deterministic extinction of "humid thermophilous plant taxa of East Asian affinity" (HUTEA) in southern Europe. *Palaeogeography, Palaeoclimatology, Palaeoecology* 467, 211-231.

Masson-Delmotte, V., Schulz, M., Abe-Ouchi, A., Beer, J., Ganopolski, A., González Rouco, J., Jansen, E., Lambeck, K., Luterbacher, J., Naish, T., 2013. Information from paleoclimate archives. In: Stocker, T.F., Qin, D., Plattner, G.K., Tignor, M., Allen, S.K., Boschung, J., Nauels, A., Xia, Y., Bex, V., Midgley, P.M. (Eds.), *Climate Change 2013: The Physical Science Basis. Contribution of Working Group I to the Fifth Assessment Report of the Intergovernmental Panel on Climate Change*. Cambridge University Press, Cambridge, New York, pp. 383-464.

Maxbauer, D.P., Royer, D.L., LePage, B.A., 2014. High Arctic forests during the middle Eocene supported by moderate levels of atmospheric CO_2. *Geology* 42, 1027-1030.

Mayewski, P.A., Rohling, E.E., Stager, J.C., Karlén, W., Maasch, K.A., Meeker, L.D., Meyerson, E.A., Gasse, F., van Kreveld, S., Holmgren, K., Lee-Thorp, J., Rosqvist, G., Rack, F., Staubwasser, M., Schneider, R.R., Steig, E.J., 2004: Holocene climate variability. *Quaternary Research* 62, 243-255.

McElwain, J.C., 1998. Do fossil plants signal palaeoatmospheric carbon dioxide concentration in the geological past? *Philosophical Transactions of the Royal Society B: Biological Sciences* 353, 83-96.

McElwain, J.C., 2004: Climate-independent paleoaltimetry using stomatal density in fossil leaves as a proxy for CO_2 partial pressure. *Geology* 32, 1017-1020.

McElwain, J.C., Mayle, F.E., Beerling, D.J., 2002: Stomatal evidence for a decline in atmospheric CO_2 concentration during the Younger Dryas stadial: a comparison with Antarctic ice core records. *Journal of Quaternary Science* 17, 21-29.

Meinshausen, M., Smith, S.J., Calvin, K., Daniel, J.S., Kainuma, M.L.T., Lamarque, J.-F., Matsumoto, K., Montzka, S.A., Raper, S.C.B., Riahi, K., Thomson, A., Velders,

G.J.M., van Vuuren, D.P.P., 2011. The RCP greenhouse gas concentrations and their extensions from 1765 to 2300. *Climatic Change* 109, 213.

Metcalfe, C., Chalk, L., 1979: *Anatomy of the Dicotyledons. Vol 1. Systematic Anatomy of the Leaf and Stem.* 276 pp. Oxford Science Publishers, Oxford.

Momohara, A., 1997. Cenozoic history of evergreen broad-leaved forest in Japan. Nat. Hist. Res. 4, 141-156.

Momohara, A., 2016. Stages of major floral change in Japan based on macrofossil evidence and their connection to climate and geomorphological changes since the Pliocene. Quat. Int. 397, 92-105.

Momohara, A., Ueki, T., Saito, T., 2017. Vegetation and climate histories between MIS 63 and 53 in the Early Pleistocene in central Japan based on plant macrofossil evidences. *Quaternary International* 455, 149-165.

Monnin, E., Indermühle, A., Dällenbach, A., Flückiger, J., Stauffer, B., Stocker, T.F., Raynaud, D., Barnola, J.-M., 2001: Atmospheric CO_2 concentrations over the last glacial termination. *Science* 291, 112-114.

Morita, Y., Fujiki, T., 1997: Vegetation History during Last 50,000 Years in Southern Tohoku District, Japan. *Japanese Journal of Palynology* 43, 75-86. (in Japanese, with English abstract)

Mosbrugger, V., Utescher, T., 1997. The coexistence approach — a method for quantitative reconstructions of Tertiary terrestrial palaeoclimate data using plant fossils. Palaeogeography, Palaeoclimatology, Palaeoecology 134, 61-86.

Mudelsee, M., Raymo, M.E., 2005. Slow dynamics of the Northern Hemisphere glaciation. *Paleoceanography* 20, PA4022.

Muramatsu, T., 2008. Fission Track age of volcanic ash distributed over the Moroyama and Kaji hill in Saitama Prefecture (in Japanese with English abstract). *Fission Track Newsletter* 21, 3.

Neftel A., Oeschger H., Staffelbach T., Stauffer, B., 1988: CO_2 record in the Byrd ice core 50,000–5,000 years BP. *Nature* 331, 609.

Nirei, T., Takegoshi, S., 2007. Fossilpollen assemblages of Lower Pleistocene Sayama formation, Kazusa group,in western partof Kanto plain, central Japan (in Japanese with English abstract). *Bulletin of the Saitama Museum of Natural History* 1, 18.

Nordt, L., Atchley, S., Dworkin, S., 2002. Paleosol barometer indicates extreme fluctuations in atmospheric CO_2 across the Cretaceous–Tertiary boundary. *Geology* 30, 703-706.

Oikawa, T., 2003. The spatial and temporal relationship between uplifting and magmatism in the Hida mountain range, central Japan (in Japanese with English abstract). *The Quaternary Research* 42, 141-156.

Ozaki, K., 1969: Observation of transportation of some plant leaves in the Rivers Haya and Sakawa. *Science reports of the Yokohama National University, Section II, Biology and geology science* 15, 95-108. (in Japanese, with English abstract)

Pagani, M., 1999. Late Miocene atmospheric CO_2 concentrations and the expansion of C4 grasses. *Science* 285, 876-879.

Pagani, M., Arthur, M.A., Freeman, K.H., 1999. Miocene evolution of atmospheric carbon dioxide. *Paleoceanography* 14, 273-292.

Pagani, M., Huber, M., Liu, Z., Bohaty, S.M., Henderiks, J., Sijp, W., Krishnan, S., DeConto, R.M., 2011. The role of carbon dioxide during the onset of Antarctic glaciation. *Science* 334, 1261-1264.

Pagani, M., Zachos, J.C., Freeman, K.H., Tipple, B., Bohaty, S., 2005. Marked decline in atmospheric carbon dioxide concentrations during the Paleogene. *Science* 309, 600-603.

Pancost, R.D., Steart, D.S., Handley, L., Collinson, M.E., Hooker, J.J., Scott, A.C., Grassineau, N.V., Glasspool, I.J., 2007. Increased terrestrial methane cycling at the Palaeocene–Eocene thermal maximum. *Nature* 449, 332-335.

Pearson, P.N., Foster, G.L., Wade, B.S., 2009. Atmospheric carbon dioxide through the Eocene–Oligocene climate transition. *Nature* 461, 1110.

Pearson, P.N., Palmer, M.R., 2000. Atmospheric carbon dioxide concentrations over the past 60 million years. *Nature* 406, 695-699.

Pearson, R.G., Dawson, T.P., 2003: Predicting the impacts of climate change on the distribution of species: are bioclimate envelope models useful? *Global Ecology & Biogeography* 12, 361-371.

Petit, J.-R., Jouzel, J., Raynaud, D., Barkov, N.I., Barnola, J.-M., Basile, I., Bender, M., Chappellaz, J., Davis, M., Delaygue, G., 1999. Climate and atmospheric history of the past 420,000 years from the Vostok ice core, Antarctica. *Nature* 399, 429.

Polley H.W., Johnson H.B., Marino B.D. Mayeux H.S., 1993. Increase in C_3 plant water-use efficiency and biomass over Glacial to present CO_2 concentrations. *Nature* 361, 61-64.

Poole, I., 1999. Stomatal density and index. The practice. In: *Fossil plants and spores: modern techniques*. The Geological Society, London 408 pp.

Popescu, S.M., Biltekin, D., Winter, H., Suc, J.-P., Melinte-Dobrinescu, M.C., Klotz, S., Rabineau, M., Combourieu-Nebout, N., Clauzon, G., Deaconu, F., 2010. Pliocene and Lower Pleistocene vegetation and climate changes at the European scale: Long pollen records and climatostratigraphy. *Quaternary International* 219, 152-167.

Prentice, I.C., 1985. Pollen representation, source area, and basin size: toward a unified theory of pollen analysis. *Quaternary Research* 23, 76-86.

Prentice, I.C., Berglund, B.E., Olsson, T., 1987. Quantitative forest-composition sensing characteristics of pollen samples from Swedish lakes. *Boreas*, 16, 43-54.

Quan, C., Sun, C., Sun, Y., Sun, G., 2009. High resolution estimates of paleo-CO_2 levels through the Campanian (Late Cretaceous) based on Ginkgo cuticles. *Cretaceous Research* 30, 424-428.

Ramsey, C.B., 2009. Bayesian Analysis of Radiocarbon Dates. *Radiocarbon* 51, 337-360.

Raven J.A., Ramsden H.J., 1988. Similarity of stomatal index in the C4 plant Salsola kali L. in material collected in 1843 and in 1987: relevance to changes in atmospheric CO_2 content. *Transactions-Botanical Society of Edinburgh* 45, 223-233.

Reimer, P.J., Bard, E., Bayliss, A., Beck, J.W., Blackwell, P.G., Ramsey, C.B., Buck, C.E., Cheng, H., Edwards, R.L., Friedrich, M., Grootes, P.M., Guilderson, T.P., Haflidason, H., Hajdas, I., Hatté, C., Heaton, T.J., Hoffmann, D.L., Hogg, A.G., Hughen, K.A., Kaiser, K.F., Kromer, B., Manning, S.W., Niu, M., Reimer, R.W., Richards, D.A., Scott, E.M., Southon, J.R., Staff, R.A., Turney, C.S.M., van der Plicht, J., 2013: IntCal13 and marine13 radiocarbon age calibration curves 0-50,000 years cal BP. *Radiocarbon* 55, 1869-1887.

Retallack, G.J., 2001. A 300-million-year record of atmospheric carbon dioxide from fossil plant cuticles. *Nature* 411, 287.

Retallack, G.J., 2009. Greenhouse crises of the past 300 million years. *Geological Society of America Bulletin* 121, 1441-1455.

Ricketts, B.D., Stephenson, R.A., 1994. The demise of Sverdrup Basin; Late Cretaceous–Paleogene sequence stratigraphy and forward modeling. *Journal of Sedimentary Research* 64, 516-530.

Rohling, E., Foster, G.L., Grant, K., Marino, G., Roberts, A., Tamisiea, M.E., Williams, F., 2014. Sea-level and deep-sea-temperature variability over the past 5.3 million years. *Nature* 508, 477.

Roth, J., Dilcher, D., 1978. Some considerations in leaf size and leaf margin analysis of fossil leaves. *Courier Forschungsinstitut Senckenberg* 30, 165-171.

Roth-Nebelsick, A., Grein, M., Utescher, T., Konrad, W., 2012. Stomatal pore length change in leaves of *Eotrigonobalanus furcinervis* (Fagaceae) from the Late Eocene to the Latest Oligocene and its impact on gas exchange and CO_2 reconstruction. *Review of Palaeobotany and Palynology* 174, 106-112.

Royer, D.L., 2001: Stomatal density and stomatal index as indicators of paleoatmospheric CO_2 concentration. *Review of Palaeobotany and Palynology* 114, 1-28.

Royer, D.L., 2003. Estimating latest Cretaceous and Tertiary atmospheric CO_2 from stomatal indices. *Special Papers – Geological Society of America* 369, 79-93.

Royer, D.L., Berner, R.A., Beerling, D.J., 2001a. Phanerozoic atmospheric CO_2 change: evaluating geochemical and paleobiological approaches. *Earth-Science Reviews* 54, 349-392.

Royer, D.L., Berner, R.A., Montañez, I.P., Tabor, N.J., Beerling, D.J., 2004. CO_2 as a primary driver of Phanerozoic climate. *GSA Today* 14, 4-10.

Royer, D.L., Wing, S.L., Beerling, D.J., Jolley, D.W., Koch, P.L., Hickey, L.J., Berner, R.A., 2001: Paleobotanical evidence for near present-day levels of atmospheric CO_2 during part of the Tertiary. *Science* 292, 2310-2313.

Royer, D.L., Wing, S.L., Beerling, D.J., Jolley, D.W., Koch, P.L., Hickey, L.J., Berner, R.A., 2001b. Paleobotanical evidence for near present-day levels of atmospheric CO_2 during part of the Tertiary. *Science* 292, 2310-2313.

Rundgren, M., Beerling, D., 1999: A Holocene CO_2 record from the stomatal index of subfossil Salix herbacea L. leaves from northern Sweden. *The Holocene* 9, 509-513.

Saitama Research Group & Kanto Quaternary Research Group 1970. Discovery of Metasequoia flora from the Quaternary system in Sayama Hills. *The Journal of the Geological Society of Japan* 76: 315–316 (in Japanese with English abstract).

Sakai, H., Kurokawa, K., 2002. The Tsuike volcanic ash bed of about 1.7 Ma found from the Uonuma Group and the Taira Formation in Niigata Prefecture, central Japan. *Geological society of japan* 108, 123-126.

Salisbury, E.J., 1928: On the causes and ecological significance of stomatal frequency, with special reference to the woodland flora. *Philosophical Transactions of the Royal Society B: Biological Sciences* 216, 1-65.

Seki, O., Foster, G.L., Schmidt, D.N., Mackensen, A., Kawamura, K., Pancost, R.D., 2010. Alkenone and boron-based Pliocene pCO_2 records. *Earth and Planetary Science Letters* 292, 201-211.

Shellito, C.J., Lamarque, J.F., Sloan, L.C., 2009. Early Eocene Arctic climate sensitivity to pCO_2 and basin geography. *Geophysical Research Letters* 36, L09707.

Sims, H.J., Cassara, J.A., 2009. The Taphonomic Fidelity of Seed Size in Fossil Assemblages: A Live-Dead Case Study. *Palaios* 24, 387-393.

Sinha, A., Stott, L.D., 1994. New atmospheric pCO_2 estimates from palesols during the late Paleocene/early Eocene global warming interval. *Global and Planetary Change* 9, 297-307.

Sloan, L.C., Pollard, D., 1998. Polar stratospheric clouds: A high latitude warming mechanism in an ancient greenhouse world. *Geophysical Research Letters* 25, 3517-3520.

Smith, R.Y., Greenwood, D.R., Basinger, J.F., 2010. Estimating paleoatmospheric pCO_2 during the Early Eocene Climatic Optimum from stomatal frequency of Ginkgo, Okanagan Highlands, British Columbia, Canada. *Palaeogeography, Palaeoclimatology, Palaeoecology* 293, 120-131.

Sone, T., Kano, A., Okumura, T., Kashiwagi, K., Hori, M., Jiang, X., Shen, C.-C., 2013: Holocene stalagmite oxygen isotopic record from the Japan Sea side of the Japanese Islands, as a new proxy of the East Asian winter monsoon. *Quaternary Science Reviews* 75, 150-160.

Spicer, R.A., 1981. The sorting and deposition of allochthonous plant material in a modern environment at Sillwood Lake, Sillwood Park, Berkshire, England. *Geological Survey professional paper* 1143, 1-77.

Spicer, R.A., Parrish, J.T., 1990. Late Cretaceous–early Tertiary palaeoclimates of northern high latitudes: a quantitative view. *Journal of the Geological Society* 147, 329-341.

Spicer, R.A., Valdes, P.J., Spicer, T.E.V., Craggs, H.J., Srivastava, G., Mehrotra, R.C., Yang, J., 2009. New developments in CLAMP: Calibration using global gridded meteorological data. P Palaeogeography, Palaeoclimatology, Palaeoecology 283, 91-98.

Spicer, Robert A., Herman, Alexei B., Kennedy, Elizabeth M., 2004. Foliar Physiognomic Record of Climatic Conditions during Dormancy: Climate Leaf

Analysis Multivariate Program (CLAMP) and the Cold Month Mean Temperature. *The Journal of Geology* 112, 685-702.

Steart, D.C., Boon, P.I., Greenwood, D.R., 2006. Overland transport of leaves in two forest types in southern Victoria, Australia and its implications for palaeobotanical studies. *Proceedings-royal society of victoria* 118, 65.

Stocker, T., Qin, D., Plattner, G., Tignor, M., Allen, S., Boschung, J., Nauels, A., Xia, Y., Bex, V., Midgley, P., 2013. *IPCC, 2013: summary for policymakers in climate change 2013: the physical science basis, contribution of working group I to the fifth assessment report of the intergovernmental panel on climate change.* Cambridge University Press, Cambridge, 1523 pp.

Stott, L.D., 1992. Higher temperatures and lower oceanic pCO_2: A climate enigma at the end of the Paleocene Epoch. *Paleoceanography* 7, 395-404.

Stuiver, M., Grootes, P.M., Braziunas, T.F., 1995: The GISP2 $\delta^{18}O$ climate record of the past 16,500 years and the role of the sun, ocean, and volcanoes. *Quaternary Research* 44, 341-354.

Su, T., Xing, Y.W., Liu, Y.S., Jacques, F.M.B., Chen, W.Y., Huang, Y.J., Zhou, Z.K., 2010. Leaf Margin Analysis: A New Equation from Humid to Mesic Forests in China. *Palaios* 25, 234-238.

Suganuma, Y., Suzuki, T., Yamazaki, H., Kikuchi, T., 2003. Chrono-stratigraphy of the Ina Group, Central Japan, based on correlation of volcanic ash layers with Pleistocene widespread tephras (in Japanese with English abstract). *The Quaternary Research* 42, 321-334.

Sugita, S., 1994. Pollen Representation of Vegetation in Quaternary Sediments: Theory and Method in Patchy Vegetation. *Journal of Ecology* 82, 881-897.

Sun B, Ding S, Wu J, Dong C. Carbon isotope and stomatal data of Late Pliocene *Betulaceae* leaves from SW China: implications for palaeoatmospheric CO_2-levels. *Turkish Journal of Earth Sciences*, 2012; 21: 237-250.

Suzuki, T., Obara, M., Aoki, T., Murata, M., Kawashima, S., Kawai, M., Nakayama, T., Tokizane, K., 2011. Identification of Lower Pleistocene tephras under Tokyo and reconstruction of Quaternary crustal movements, Kanto Tectonic Basin, central Japan. *Quaternary International* 246, 247-259.

Svenning, J.-C., Normand, S., Skov, F., 2008: Postglacial dispersal limitation of widespread forest plant species in nemoral Europe. *Ecography* 31, 316-326.

Sykes, M.T., Prentice, I.C., Cramer, W., 1996: A bioclimatic model for the potential distributions of North European tree species under present and future climates. *Journal of Biogeography* 23, 203-233.

Szczepanek, K., Myszkowska, D., Worobiec, E., Piotrowicz, K., Ziemianin, M., Bielec-Bąkowska, Z., 2017. The long-range transport of Pinaceae pollen: an example in Kraków (southern Poland). *Aerobiologia* 33, 109-125.

Takahashi, K., 1962. Studies on vertical distribution of the forest in middle Honshu. Japanese Journal of Ecology 14, 1-171.

Tanai, T., 1979. Late Cretaceous floras from the Kuji District, Norheastern Honshu, Japan. Journal of the Faculty of Science, Hokkaido University (Series 4), *Geology and Mineralogy* 19, 75-136 (in Japanese).

Tanai, T., 1990. Euphorbiaceae and Icacinaceae from the Paleogene of Hokkaido, Japan. *Bulletin of the National Science Museum* (Series C) 16, 91-118.

Teodoridis, V., Bruch, A.A., Vassio, E., Martinetto, E., Kvacek, Z., Stuchlik, L., 2017. Plio-Pleistocene floras of the Vildstejn Formation in the Cheb Basin, Czech Republic - A floristic and palaeoenvironmental review. *Palaeogeography, Palaeoclimatology, Palaeoecology* 467, 166-190.

Tesfamichael, T., Jacobs, B., Tabor, N., Michel, L., Currano, E., Feseha, M., Barclay, R., Kappelman, J., Schmitz, M., 2017. Settling the issue of “decoupling” between atmospheric carbon dioxide and global temperature: [CO_2]atm reconstructions across the warming Paleogene–Neogene divide. *Geology* 45, 999-1002.

Tinner, W., Kaltenrieder, P., 2005: Rapid responses of high-mountain vegetation to early Holocene environmental changes in the Swiss Alps. *Functional Ecology* 93, 936-947.

Traiser, C., Klotz, S., Uhl, D., Mosbrugger, V., 2005. Environmental signals from leaves – a physiognomic analysis of European vegetation. *New Phytologist* 166, 465-484.

Tripati, A.K., Roberts, C.D., Eagle, R.A., Li, G., 2011. A 20 million year record of planktic foraminiferal B/Ca ratios: Systematics and uncertainties in pCO_2 reconstructions. *Geochimica et Cosmochimica Acta* 75, 2582-2610.

Trudinger, C.M., Rayner, P.J., Enting, I.G., Heimann, M., Scholze, M., 2003: Implications of ice core smoothing for inferring CO_2 flux variability. *Journal of Geophysical Research* 108, 4492.

Tsukada, M., 1982: Late-quaternary shift of *fagus* distribution. *Journal of Plant Research* 95, 203-217.

Uchijima, Z., 1992: Probable shift of natural vegetation in Japan due to CO_2-climatic warming. *Ecological Process in Agro-Ecosystems* 1, 189-201.

Ueki, T. & Sakai, A. 2007. Geology of the Ome District. *Quadrangle Series, 1:50,000, Geological Survey of Japan*, AIST, Tsukuba, 189 pp (in Japanese with English abstract)

Ufnar, D.F., González, L.A., Ludvigson, G.A., Brenner, R.L., Witzke, B.J., 2004. Evidence for increased latent heat transport during the Cretaceous (Albian) greenhouse warming. *Geology* 32, 1049-1052.

van der Burgh, J., Visscher, H., Dilcher, D.L., Kürschner, W.M., 1993. Paleoatmospheric signatures in Neogene fossil leaves. *Science*, 1788-1790.

van der Hammen, T., Wijimstra, T.A., Zagwijn, W.H., 1971. The floral record of the late Cenozoic of Europe. In: Turekian, K.K. (Ed.), *Late Cenozoic glacial ages*. Yale University Press, New Haven, pp. 391-424.

Vassio, E., Martinetto, E., 2012. Biases in the Frequency of Fruits and Seeds in Modern Fluvial Sediments in Northwestern Italy: The Key to Interpreting Analogous Fossil Assemblages. *Palaios* 27, 779-797.

Veres, D., Bazin, L., Landais, A., Kele, H.T.M., Lemieux-Dudon, B., Parrenin, F., Martinerie, P., Blayo, E., Blunier, T., Capron, E., Chappellaz, J., Rasmussen, S.O., Severi, M., Svensson, A., Vinther, B., Wolff, E.W., 2013: The Antarctic ice core chronology (AICC2012): an optimized multi-parameter and multi-site dating approach for the last 120 thousand years. *Climate of the Past* 9, 1733-1748.

Wagner F, Bohncke SJ, Dilcher DL, Kürschner WM, Geel B, Visscher H. Century-scale shifts in early Holocene atmospheric CO_2 concentration. *Science*. 1999; 284: 1971-1973.

Wagner, F., Aaby, B., Visscher, H., 2002: Rapid atmospheric CO_2 changes associated with the 8,200-years-B.P. cooling event. *Proceedings of the National Academy of Sciences* 99, 12011-12014.

Wagner, F., Bohncke, S.J., Dilcher, D.L., Kürschner, W.M., van Geel, B., Visscher, H., 1999: Century-scale shifts in early Holocene atmospheric CO_2 concentration. *Science* 284, 1971-1973.

Wakamatsu, N., Kiguchi, T., 2006: Environment factors of isolated stands of *Abies mariesii* forest on Mt.Kurukoma in northeastern Japan. *The Japanese Society of Forest Enviroment* 48, 33-41. (in Japanese, with English abstract)

Walker, B., Steffen, W., Canadell, J., Ingram, J., 1999: *The terrestrial biosphere and global change: implications for natural and managed ecosystems.* 160 pp. Cambridge University Press, Cambridge.

Wang, H., Deng, C., Zhu, R., Qi, W., Hou, Y., Boëda, E., 2005: Magnetostratigraphicdating of the Donggutuo and Maliang Palaeolithic sites in the Nihewan Basin,North China. *Quaternary Research* 64, 1e11.

Wang, Y., Ito, A., Huang, Y.-J., Fukushima, T., Wakamatsu, N., Momohara, A., 2018a. Reconstruction of altitudinal transportation range of leaves based on stomatal

evidence: An example of the Early Pleistocene *Fagus* leaf fossils from central Japan. *Palaeogeography, Palaeoclimatology, Palaeoecology* 505, 317-325.

Wang, Y., Momohara, A., Ito, A., Fukushima, T., Huang, Y.-J., 2018b. Warm climate under high CO_2 level in the early Pleistocene based on a leaf fossil assemblage in central Japan. *Review of Palaeobotany and Palynology* 258, 146-153.

Wang, Y., Momohara, A., Wang, L., Lebreton-Anberree, J., Zhou, Z., 2015. Evolutionary History of Atmospheric CO_2 during the Late Cenozoic from Fossilized *Metasequoia* Needles. *PLoS One* 10, e0130941.

Watson, K.B., 1942. The nature and measurement of musical meanings. *Psychological monographs* 54, i.

Wilf, P., 1997. When are leaves good thermometers? A new case for leaf margin analysis. *Paleobiology* 23, 373-390.

Wing, S.L., Greenwood, D.R., 1993. Fossils and Fossil Climate - the Case for Equable Continental Interiors in the Eocene. *Palaeoclimates and their Modelling* 341, 243-252.

Winguth, A., Shellito, C., Shields, C., Winguth, C., 2010. Climate response at the Paleocene–Eocene thermal maximum to greenhouse gas forcing — a model study with CCSM3. *Journal of Climate* 23, 2562-2584.

Wolfe, A.P., Reyes, A.V., Royer, D.L., Greenwood, D.R., Doria, G., Gagen, M.H., Siver, P.A., Westgate, J.A., 2017. Middle Eocene CO_2 and climate reconstructed from the sediment fill of a subarctic kimberlite maar. *Geology* 45, 619-622.

Wolfe, J.A., 1979. Temperature parameters of humid to mesic forests of Eastern Asia and relation to forests of other regions of the Northern Hemisphere and Australasia: analysis of temperature data from more than 400 stations in Eastern Asia. Geological Survey. Professional paper (USA), 1106, 37.

Wolfe, J.A., 1993, A method of obtaining climatic parameters from leaf assemblages: U.S. *Geological Survey Bulletin* 2040, 71.

Woodward, F.I., Williams, B.G., 1987. Climate and plant distribution at global and local scales. *Vegetatio* 69, 189-197.

Woodward F.I., Bazzaz F.A., 1988. The responses of stomatal density to CO_2 partial pressure. *Journal of Experimental Botany* 39, 1771-1781.

Woodward F.I., Kelly C.K., 1995. The influence of CO_2 concentration on stomatal density. *New Phytologist* 131, 311-327.

Yamakawa, C., Momohara, A., Saito, T., Nunotani, T., 2017. Composition and paleoenvironment of wetland forests dominated by Glyptostrobus and Metasequoia in the latest Pliocene (2.6 Ma) in central Japan. *Palaeogeography, Palaeoclimatology, Palaeoecology* 467, 191-210.

Yang, H., Huang, Y., Leng, Q., LePage, B.A., Williams, C.J., 2005. Biomolecular preservation of Tertiary *Metasequoia* Fossil Lagerstätten revealed by comparative pyrolysis analysis. *Review of Palaeobotany and Palynology* 134, 237-256.

Zachos, J., Pagani, M., Sloan, L., Thomas, E., Billups, K., 2001. Trends, rhythms, and aberrations in global climate 65 Ma to present. *Science* 292, 686-693.

Zheng, J.M., Sang, W.G., Ma, K.P., 2004. Advances in model construction of anemochoric seed long-distance dispersal (in Chinese with English abstract). *Acta Phytoecological Sinica* 28, 414-425.